

Copyright Undertaking

This thesis is protected by copyright, with all rights reserved.

By reading and using the thesis, the reader understands and agrees to the following terms:

- 1. The reader will abide by the rules and legal ordinances governing copyright regarding the use of the thesis.
- 2. The reader will use the thesis for the purpose of research or private study only and not for distribution or further reproduction or any other purpose.
- 3. The reader agrees to indemnify and hold the University harmless from and against any loss, damage, cost, liability or expenses arising from copyright infringement or unauthorized usage.

IMPORTANT

If you have reasons to believe that any materials in this thesis are deemed not suitable to be distributed in this form, or a copyright owner having difficulty with the material being included in our database, please contact lbsys@polyu.edu.hk providing details. The Library will look into your claim and consider taking remedial action upon receipt of the written requests.

DISSECTING THE MOLECULAR MACHINERY FOR TONICITY-DRIVEN NUCLEAR IMPORT OF NFAT5 - ROLE OF KPNB1 AND LIQUID-LIQUID PHASE SEPARATION

ZHANG SHUQI

PhD

The Hong Kong Polytechnic University

2023

The Hong Kong Polytechnic University

Department of Applied Biology and Chemical Technology

Dissecting the molecular machinery for tonicitydriven nuclear import of NFAT5 - role of KPNB1 and liquid-liquid phase separation

ZHANG SHUQI

A thesis submitted in partial fulfilment of the requirements for the degree of Doctor of Philosophy

May 2023

CERTIFICATE OF ORIGINALITY

I

Abstract

Mammalian cells undergo osmoadaptation to maintain cell volume when exposed to an anisotonic environment. Nuclear factor of activated T-cells 5 (NFAT5) is the only transcription factor regulated by hypertonicity. Studies have shown that NFAT5 becomes significantly enriched in the nucleus under hypertonic conditions and activate transcription of target genes like osmolyte transporters to quickly restore intracellular osmolality. NFAT5 contains a leucine-rich canonical nuclear export sequence (NES) and a consensus bipartite nuclear localization signal (NLS) within its N-terminal intrinsically disordered region that is required for isotonicity-driven nucleocytoplasmic shuttling. Four phosphorylation sites, tyrosine 143 (Y143), threonine 135 (T135), serine 155 and 158 (S155 and S158), have been identified as crucial for NFAT5 activity regulation. However, the molecular machinery responsible for NFAT5 nuclear import and its regulation by tonicity are not well understood.

Here we report molecular and structural studies to dissect the tonicity-regulated nucleocytoplasmic shuttling process of NFAT5. We first used siRNA screening to confirm that the nuclear import of NFAT5 under hypertonicity required only karyopherin β1 (KPNB1), but not karyopherin α. We then carried out mapping studies to show that a short segment (residues 199-216) termed canonical NLS (cNLS) is required for KPNB1 binding but insufficient for nuclear import of NFAT5. Instead, a longer segment (residues 171-253) termed the full NLS is required to recapitulate the

tonicity-driven nuclear import of NFAT5.

Given the disordered nature of the full NLS region in NFAT5, we reason it might undergo tonicity-mediated LLPS. We first did *in vitro* biochemical assays to confirm that the full NLS of NFAT5 indeed underwent liquid-liquid phase separation (LLPS) in salt-dependent manner. Under low salt concentration of 100 mM NaCl, the full NLS of NFAT5 formed dynamic liquid droplets. However, these droplets readily disappeared when the salt concentration reached 200 mM. Intriguingly, organic solvents like sorbitol had no such effect. This LLPS phenomenon was also observed for a longer segment that included both the AED domain and the full NLS (residues 132-253).

To validate our *in vitro* findings, we used immunofluorescence imaging studies to assess possible LLPS for NFAT5 *in vivo*. Our imaging studies of HeLa cells showed that endogenous NFAT5 formed distinct puncta in the cytosol under all tonicity conditions. To further confirm these puncta are related to LLPS, we generated a GFP-tagged NFAT5 construct (residues 1-543) and assessed its liquid-like property using FRAP experiments. Our data shows that the puncta formed by GFP-NFAT5-1-543 readily recovered their fluorescence signal after photobleaching, a defining feature of LLPS. Overall, our studies confirm that NFAT5 undergoes LLPS both *in vitro* and *in vivo*.

As LLPS would sequester NFAT5 and renders it not available for nuclear import,

we then investigated how KPNB1 would impact the LLPS of NFAT5. Interestingly, KPNB1 readily disrupted the LLPS of NFAT5 full NLS *in vitro*. Additionally, siRNA knockdown of KPNB1 *in vivo* increased the number of puncta for endogenous NFAT5. Furthermore, mutations that mimic the tonicity-driven phosphorylation events also disrupted LLPS of NFAT5. These results suggest that LLPS of NFAT5 is a key factor to regulate its nuclear import by KPNB1. Under hypo- or isotonic conditions, NFAT5 may undergo LLPS, which impedes its binding to KPNB1 and thus impairs its nuclear import. Under hypertonic conditions, the LLPS level for NFAT5 is reduced, which facilities binding to KPNB1 and promotes nuclear import.

Lastly, we also determined the Cryo-EM structure of KPNB1 in complex with the full NLS of NFAT5 at 4.09 Å resolution. In this structure, KPNB1 adopts a conformation that largely resembles the structure of KPNB1-aIBB. Only small amount of density was visible for the cNLS of NFAT5 while the N- and C-terminal flanking segments were absent. Notably, binding site for cNLS of NFAT5 overlaps with that for RanGTP and IBB of KPNA1. Mutational studies confirm that residues in these two regions are critical for NFAT5 bindings. This overlap explains why the nuclear import of NFAT5 is KPNA-independent as its cNLS competes with the IBB of KPNA1 for KPNB1 binding.

In summary, using a combination of biochemical, structural, and functional studies, my thesis work has delineated the molecular mechanism of tonicity-regulated nuclear

import of NFAT5 with LLPS as a novel critical factor. This finding may have broad implications for the nuclear import process of LLPS-competent cargos.

Publications arising from the thesis

Chris Y. Cheung*, Ting-Ting Huang*, Ning Chow*, **Shuqi Zhang**, Yanxiang Zhao, Mary P. Chau, Wing Cheung Chan, Catherine C. L. Wong, Daniela Boassa, Sebastien Phan, Mark H. Ellisman, John R. Yates, SongXiao Xu, Zicheng Yu, Yajing Zhang, Rui Zhang, Ling Ling Ng, Ben C. B. Ko; Unconventional tonicity-regulated nuclear trafficking of NFAT5 mediated by KPNB1, XPOT and RUVBL2. J Cell Sci 1 July 2022; 135 (13): jcs259280. (* These authors contributed equally to the work.)

Acknowledgements

"In hope of mending the world, as ashes and dust would do, of lightening the darkness with the sparkle of fireflies, and of shining as brightly as the sun and the moon, even when reduced to a mere glimmer."

- CAO Zhi

"冀以塵霧之微,補益山海;螢燭末光,曾輝日月"

—曹植 《求自試表》

First and foremost, I would like to express my utmost gratitude to my supervisor Prof. Yanxiang Zhao, whose invaluable guidance, support, and mentorship have been indispensable throughout my doctoral studies. Her expertise and dedication have shaped the direction of my research, and her patience and kindness have kept me motivated even during the most challenging times. Despite my background in medicinal chemistry, Prof. Zhao provided me with the opportunity to explore this field of biology and has supported me every step of the way. I am grateful for her unwavering kindness, patience, and generosity of time and attention, especially whenever I encountered setbacks or mistakes. Prof. Zhao encourages me to focus on answering scientific questions instead of merely avidly pursuing popular topics or coveting immediate outcomes. Her unconditional belief and encouragement have inspired me to pursue my academic interests and strive for excellence in my work. I am honored and grateful to have had such a supportive supervisor.

I would like to thank my lab teammates, who have been integral to my Ph.D. journey. In particular, I would like to give my heartfelt thanks to Dr. Shuai Wu, a virtuous and highly talented scientist, for enlightening me to pursue a research career through his encouragement, recognition, and admirable suggestions. Dr. Na Li and Dr. Xian Yang, thoughtful and warm-hearted colleagues, guided me in mastering biochemical techniques at the start of my Ph.D. study. Mr. Siqiong Zheng, a low-profile and considerate gentleman, helped me to solve the Cryo-EM structure. Ms. Yingting Yu, an elegant lady with a heart of gold, has provided me with the best emotional support and the most warm-hearted companionship. Ms. Lei Wang, a dependable and genuine lady, gave me a much-needed hug during tough times. Mr. Ming Fai Leung, a wise and understated gentleman, supported me, offering selfless companionship and assistance whenever needed. Dr. Jingyi Chen, a sophisticated and life-loving lady, whose optimistic attitude towards life influenced me. Ms. Yuhui Xia and Ms. Yu Feng, generous and thoughtful colleagues, have been companions in my studies. Ms. Tsoi Pui Yan, an exceptionally dependable, attentive, and quick-learning lady who offered me invaluable assistance during a challenging period when I was overwhelmed with my workload. Thanks, lab members, for dealing with lab routine work. I am appreciative to meet all of you.

I am particularly grateful to our collaborator, Dr. Chi-bun Ko, for his research on the NFAT5 project. Thanks, Dr. Chris Cheung, for teaching me cell culture and immunofluorescence imaging technology. I am also thankful to Dr. Wing Cheung Chan for his outstanding work on NFAT5 project. I want to especially thank Dr. Yajing Zhang, my closest friend, who understands me the best and whose beautiful eyes have always been able to see the essence of things. Without her mental support, encouragement, and technical guidance, I would have lost my passion for overcoming difficulties. I want to thank all the members of Dr. Ko' lab for celebrating my birthday every year in Hong Kong. It has been a privilege to work alongside such talented and supportive individuals.

I am deeply grateful to Prof. Mingjie Zhang (Southern University of Science and Technology) for his invaluable support in my research on phase separation. I consider myself fortunate to have been guided by Dr. Xiandeng Wu in this area of study, as his insightful feedback and suggestions greatly improved the quality of my research and helped me pursue my academic goals. I cherish every conversation I had with him, especially the one where he taught me to pass down what I have learned with wholehearted dedication. He is always there for me whenever I need his assistance; I am genuinely grateful. I would also like to sincerely thank Dr. Yingyi Zhang (HKUST) for her intellectual and technical support in my work on Cryo-EM.

Furthermore, I would like to extend my sincere gratitude to Prof. Wenyu Wen and Prof. Zhenguo Wu, for taking the time out of their busy schedule to serve as an external examiner for my oral examination. Their presence and expertise significantly contributed to the overall quality of the examination process, and I am truly grateful for

the opportunity to benefit from their knowledge and experience. Their guidance has undoubtedly helped me refine my research skills and broaden my intellectual horizons.

Besides, I am grateful to Ms. Josephine for revising my dissertation and providing timely feedback. I also extend my gratitude to administrative staff Ms. Peggy, whose tireless work behind the scenes enabled my studies and research to proceed more smoothly.

I am proud to have met my most trustworthy friend, Dr. Yang Liu, a talented and pretty lady who taught me to be fearless in being myself and to embrace my unique qualities.

Finally, my heartfelt appreciation goes to my family and all my close friends I met during my Ph.D. studies. Specifically, I would like to extend my thanks to **my parents** and my elder cousin Dr. Feng Li. Their love, support, and encouragement have been my source of strength throughout my Ph.D. journey. Their unwavering belief in me has kept me motivated during the most challenging times, and their constant encouragement has inspired me to strive for excellence in my work.

The NFAT5 project, in particular, allows me to find what I love, and I am truly grateful for that.

CONTENT

ERTIFICATE OF ORIGINALITYI
ostractII
ıblications arising from the thesisVI
cknowledgementsVII
st of figuresXIX
obreviationsXXIII
napter 1 Introduction1
1.1 NFAT5 is a tonicity-regulated transcription factor that regulates osmo-
protective genes1
1.1.1 NFAT5 promotes the transcription of osmo-protective genes in
response to hypertonicity1
1.1.2 The structure and functional domains of NFAT5
1.1.3 Regulations of NFAT5 activities
1.2 The molecular machinery of nucleocytoplasmic transport
1.2.1 The nucleocytoplasmic trafficking process transports a variety of
cargo molecules across the nuclear pore complexes (NPCs)
1.2.2 Karyopherin proteins as nucleocytoplasmic transport receptors
(NTRs)9
1.2.3 The molecular machinery of nucleocytoplasmic transport involves
specific cargo recognition by NTRs

1.3	For	rmation of membraneless organelles via phase separation15
	1.3.1	Membraneless stress granule as a well-studied example of LLPS 16
	1.3.2	Bilayer protein clustering is driven by a complex interplay between
	macro	molecular interactions and environmental factors
	1.3.3	LLPS in transcription regulation: RNA polymerase (Pol) II21
	1.3.4	NTRs mediate LLPS of NLSs
1.4	Ob	jectives24
	1.4.1	Identifying the karyopherin members that carry out tonicity-driven
	nuclea	ar import of NFAT524
	1.4.2	Mapping the NLS responsible for NFAT5 nuclear import25
	1.4.3	Characterizing possible tonicity-driven liquid-liquid phase separation
	within	the NLS region of NFAT526
	1.4.4	Evaluating impact of KPNB1 on LLPS of NFAT5-NLS region
	throug	th biochemical studies
	1.4.5	Structural study of the $KPNB1$ - $NFAT5_{NLS}$ complex to delineate the
	molec	ular mechanism of KPNB1-mediated nuclear import of NFAT527
	1.4.6	Structure-based mutational studies to delineate the molecular
	mecha	nism of tonicity-driven nuclear import of NFAT5 by KPNB128
Chapter	2 Me	ethodologies31
2.1	Pla	smid construction
	2.1.1	Polymerase Chain Reaction (PCR)
	2.1.2	DNA digestion

	2.1.3	Insert and linear vector purification	34
	2.1.4	Ligation	34
	2.1.5	Transformation	35
	2.1.6	Mutant generation	35
2.2	Re	combinant protein over-expression in Escherichia coli (E.coli)	36
2.3	Pu	rification	38
	2.3.1	Affinity chromatography	39
	2.3.2	Removal of the fusion tag using protease digestion	42
	2.3.3	Anion exchange chromatography	42
	2.3.4	Size exclusion chromatography (SEC)	43
	2.3.5	Concentration measurement	44
	2.3.6	Storage of protein	44
2.4	Bio	ophysical and biochemical analysis	45
	2.4.1	Light scattering	45
	2.4.2	Mass Spectroscopy (MS)	45
	2.4.3	Pull-down assay	46
	2.4.4	Isothermal titration calorimetry (ITC)	46
2.5	Stru	cture analysis: Single-particle cryo-electron microscopy (Cryo-EM	[) 47
	2.5.1	Biochemical sample preparation	47
	2.5.2	Single-particle cryo-electron microscopy (Cryo-EM)	48
2.6	In ·	vitro Liquid-Liquid Phase Separation (LLPS) assays	49
	2.6.1	Protein labeling using fluorophore and labeling efficiency analysis	s. 50

	2.6.2	In vitro droplet formation assay (DIC imaging and Fluorescence
	imagii	ng)50
	2.6.3	Phase diagram as a function of different influence factors51
	2.6.4	In vitro fluorescence recovery after photobleaching (FRAP) assay and
	analys	is52
	2.6.5	Sedimentation assay
	2.6.6	Turbidity assay
	2.6.7	Quantification and Statistical Analysis
2.7	Ce	ll-based experiments
	2.7.1	Immunocytochemistry (ICC) assay
	2.7.2	Live cell imaging of phase separation behavior on NFAT555
	2.7.3	In vivo FRAP assay
Chapter	3 To	nicity-driven nuclear import of NFAT5 depends only on KPNB157
3.1	NF	AT5 undergoes tonicity-driven nucleocytoplasmic shuttling57
3.2	Nu	clear import of NFAT5 depends exclusively on KPNB158
	3.2.1	Nuclear import of NFAT5 depends only on KPNB1 but not other
	KPNE	3 members
	3.2.2	Nuclear import of NFAT5 does not require KPNA family60
	3.2.3	Reconstituted nuclear import assay confirms that the nuclear impor
	of NF	AT5 only depends on KPNB163
Chapter	4 Bio	ochemical and functional mapping of the full NLS segment in
NFAT5 1	respons	sible for tonicity-driven nuclear import67

4.1	Fur	nctional mapping confirms NFAT5 ₁₇₁₋₂₅₃ as the full NLS for tonicity-
driv	en nucl	ear import67
4.2	Red	constituted nuclear import assay confirms NFAT5 ₁₇₁₋₂₅₃ is sufficient for
toni	city-dri	ven nuclear import71
4.3	Bio	chemical mapping confirms the interaction between the full NLS of
NFA	AT5 and	KPNB1
	4.3.1	Design, expression, and purification of various NFAT5 constructs to
	scan th	nrough the full NLS region75
	4.3.2	Expression and purification of KPNA1 _{ARM} , KPNB1 and its
	constr	ucts
	4.3.3	Pull-down assay shows a direct interaction between full NLS of
	NFAT:	5 and KPNB182
	4.3.4	Isothermal titration calorimetry (ITC) shows that full NLS of NFAT5
	interac	ets with KPNB1 and its N-terminal constructs
Chapter	5	The intrinsically disordered AED+NLS region of NFAT5
undergo	es liqui	d-liquid phase separation (LLPS)89
5.1	The	e N-terminal intrinsically disordered domain of NFAT5 undergoes
phas	se separ	ration in vitro89
	5.1.1	Design, expression, and purification of NFAT5 constructs covering
	the N-	terminal AED+NLS region90
	5.1.2	Turbidity of purified NFAT5 constructs94

	5.1.3	Both NFAT5 full NLS and NFAT5 AED+NLS form condensed liquid-
	like d	roplets95
	5.1.4	Fusion of phase separated NFAT5 constructs possess liquid
	prope	rty97
	5.1.5	LLPS of NFAT5 AED+NLS exhibits rigid interfacial boundaries99
	5.1.6	Sedimentation assay shows molecular compositions of condensed
	NFAT	5 full NLS and NFAT5 AED+NLS100
	5.1.7	Phase diagram of NFAT5 condensates as a function of NaCl indicates
	electro	ostatic interaction-driven self-assembly102
	5.1.8	The crowder sorbitol has no effect on LLPS of NFAT5 constructs at a
	fixed	concentration of 100 mM NaCl
	5.1.9	The dynamics of phase separated NFAT5 AED+NLS and NFAT5 full
	NLS	108
5.2	NF	FAT5 undergoes phase separation in vivo
	5.2.1	Endogenous NFAT5 undergoes LLPS under varying tonicity110
	5.2.2	Fusion of phase separated NFAT5 ₁₋₅₄₃ -AcGFP exhibits liquid-like
	prope	rty
	5.2.3	The liquidity of phase separated NFAT5 ₁₋₅₄₃ -AcGFP was increased
	under	hypotonicity
Chapter	6 KI	PNB1 reduces the liquidity of NFAT5 LLPS to facilitate its nuclear
import	•••	116

	6.1	KPNB1 inhibits LLPS of NFAT5 AED+NLS in a concentration-dependent
	manner	116
	6.2	KPNB1 reduces the liquidity of NFAT5 LLPS in vivo119
Cha	apter 7	Structural study of the KPNB1-NFAT5 _{NLS} complex to delineate
the	molecul	ar mechanism of KPNB1-mediated nuclear import of NFAT5122
	7.1	Sample preparation of KPNB1-NFAT5 complex for Cryo-EM studies122
	7.2	Cryo-EM structure determination of the KPNB1-NFAT5 complex124
	7.3	The KPNB1-NFAT5 structure reveals that the binding site for NFAT5
	overlap	s with that for the IBB domain
	7.4	The KPNB1-NFAT5 structure reveals that the binding site for NFAT5 also
	overlap	s with that for Ran-GTP129
	7.5	NFAT5 adopts a similar binding mode to PTHrP _{ncNLS} 131
Cha	apter 8	Structure-based biochemical studies to delineate the molecular
me	chanism	of tonicity-driven nuclear import of NFAT5134
	8.1	Competitive binding assay confirms that NFAT5 and RanGTP bind to
	overlap	pping sites on KPNB1134
	8.2	The conserved acidic loop in KPNB1 is required for binding to NFAT5 _{cNLS}
	8.3	Key residues that contribute to KPNB1-KPNA1 _{IBB} complex are essential
	for KPI	NB1-NFAT5 _{cNLS} complex138
	8.4	The hydrophobic binding surface in KPNB1 is required for binding to
	NFAT5	cni s

	8.5	NFAT5 LLPS is mediated by positively charged residues within the cNLS
	8.6	NFAT5 LLPS is mediated by multiple residues within the full NLS143
	8.7	NFAT5 LLPS is disrupted by tonicity-driven phosphorylation in the
	AED+	NLS region149
Cha	apter 9	Conclusions and discussions151
	9.1	Nuclear import of NFAT5 depends solely on KPNB1 and a ncNLS 151
	9.2	The KPNB1-NFAT5 structure reveals a unique binding site that overlaps
	with R	anGTP and IBB152
	9.3	The NFAT5 NLS undergoes tonicity-regulated LLPS154
	9.4	Broader implications and plans for future studies
Ref	erences	160

List of figures

Fig. 1.1	Time frame of short-term and long-term adaptation to hypertonic stress
Fig. 1.2	Members of NFAT family and NFAT5 functional domains schematic
Fig. 1.3	Kap-mediated nucleocytoplasmic transport
Fig. 1.4	Scheme presentation of the structure and functional domains of KPNB1
Fig. 1.5	Schematic of the clustering assay, depicting the proteins and their interactions
Fig. 2.1	Timeline for recombinant protein over-expression in <i>E.coli</i>
Fig. 2.2	The workflow for protein purification
Fig. 3.1	Endogenous NFAT5 undergoes nuclear-cytoplasmic shuttling regulated by
	extracellular tonicity
Fig. 3.2	KPNB1 is required for nuclear import of NFAT5
Fig. 3.3	KPNA family is not required for the nuclear import of NFAT5
Fig. 3.4	Nuclear import of NFAT5 was not abolished by Bimax1 and Bimax2
Fig. 3.5	In vitro reconstruction of the nuclear import mechanism of NFAT5
Fig. 4.1	Functional mapping of the minimal required domain for NFAT5 nuclear-
	import function
Fig. 4.2	The determination of nuclear import of His6-tagged NFAT5 fragments with
	C-terminal AcGFP
Fig. 4.3	Mutational analysis of the NFAT5 _{cNLS} (published data)
Fig. 4.4	Purification of NFAT5 constructs

Fig. 4.5 KPNB1 Constructs Design and Purification

- Fig. 4.6 Characterization of KPNA1_{ARM}, KPNB1, and its constructs by SDS-PAGE analysis and Mass spectrometry
- Fig. 4.7 *In vitro* pull-down assay to characterize the interaction between full NLS of NFAT5 constructs and KPNB1
- Fig. 4.8 ITC profiles measuring the binding affinity of NFAT5 fragments including residues 199-216 (cNLS, A), 189-216 (B), 199-226 (C), 151-216 (D) and 171-253 (E) to KPNB1
- Fig. 4.9 ITC profiles measuring the binding affinity of synthetic peptide NFAT5_{cNLS} to N-terminal KPNB1 constructs KPNB1_{H1-H10}, KPNB1_{H1-H11}, and KPNB1_{H1-H12}
- Fig. 4.10 ITC profiles measuring the binding affinity (Kd) of synthetic peptide NFAT5 $_{189-216}$ to N-terminal KPNB1 constructs KPNB1 $_{\rm H1-H10}$, KPNB1 $_{\rm H1-H11}$, and KPNB1 $_{\rm H1-H12}$
- Fig. 4.11 NFAT5 putative NLS region 220-253 (A) and the mutation of 171-253-R202A K203A (B) showed no interaction with KPNB1
- Fig. 4.12 NFAT5_{cNLS} showed weaker interaction with KPNA1_{ARM} (B) than with His6-KPNB1 (A)
- Fig. 5.1 Analysis of the NFAT5 protein sequence for intrinsically disordered regions using the program VL3-BA
- Fig. 5.2 Design of NFAT5 constructs
- Fig. 5.3 Purification of NFAT5 constructs
- Fig. 5.4 SEC-MALS analysis of NFAT5 constructs for LLPS

- Fig. 5.5 Turbidity of NFAT5 constructs
- Fig. 5.6 LLPS formation of NFAT5 NLS and NFAT5 AED+NLS
- Fig. 5.7 Fusion of condensed NFAT5 full NLS (NFAT5₁₇₁₋₂₅₃) and condensed NFAT5 AED+NLS (NFAT5₁₃₂₋₂₅₃)
- Fig. 5.8 3D reconstruction of 0.6 mM NFAT5₁₃₂₋₂₅₃ LLPS droplets using fluorescence imaging
- Fig. 5.9 LLPS enrichment analyzed by sedimentation assay
- Fig. 5.10 Phase diagrams of NFAT5 constructs as a function of NaCl
- Fig. 5.11 Phase diagrams of NFAT5 constructs as a function of sorbitol with a fixed concentration of 100 mM NaCl
- Fig. 5.12 LLPS of NFAT5 constructs exhibited high mobility
- Fig. 5.13 STED monitored LLPS formation of endogenous NFAT5 under varying tonicity
- Fig. 5.14 LLPS formation of endogenous NFAT5 under changes of tonicity
- Fig. 5.15 NFAT5₁₋₅₄₃-AcGFP droplets fusion
- Fig. 5.16 NFAT5₁₋₅₄₃-AcGFP exhibits increased mobility under the hypotonic treatment
- Fig. 6.1 KPNB1 inhibits LLPS NFAT5₁₃₂₋₂₅₃ in a concentration-dependent manner
- Fig. 6.2 KPNB1 inhibits LLPS of NFAT5 in vivo
- Fig. 7.1 Characterization of KPNB1-NFAT5 full NLS complex by SDS-PAGE analysis

- Fig. 7.2 Characterization of cross-linked KPNB1-NFAT5 full NLS complex by SDS-PAGE analysis
- Fig. 7.3 Image analysis of KPNB1 and NFAT5 construct complex
- Fig. 7.4 Structure of KPNB1 and NFAT5 construct complex
- Fig. 7.5 Comparison study of the two KPNB1 structures in complex with NFAT5 and aIBB
- Fig. 7.6 Comparison study of the two KPNB1 structures in complex with NFAT5 and Ran-GTP
- Fig. 7.7 Structural analysis on KPNB1 binding to different ligands
- Fig. 8.1 Characterization of the interaction between RanQ69L and KPNB1
- Fig. 8.2 The competition for binding to KPNB1 by RanQ69L-GppNHp and NFAT5_{cNLS}
- Fig. 8.3 Characterization of the interaction between NFAT5_{cNLS} and KPNB1 mutants
- Fig. 8.4 Characterization of the interaction between NFAT5_{cNLS} and KPNB1 mutants
- Fig. 8.5 Characterization of the interaction between NFAT5_{eNLS} and KPNB1 mutants
- Fig. 8.6 K/R-rich bipartite cNLS is required for LLPS of NFAT5
- Fig. 8.7 Analysis of the subcellular localization of alanine-substituted FLAG-NFAT5₁₃₂₋₅₈₁ mutants
- Fig. 8.8 Alanine mutagenesis improves NFAT5 LLPS
- Fig. 8.9 Tonicity-driven phosphorylated sites are important for the LLPS of NFAT5

Abbreviations

NFAT5 nuclear factor of activated T-cells 5

TonEBP tonicity-responsive enhancer binding protein

OREBP osmotic-response element-binding protein

HCC hepatocellular carcinoma

AG arctigenin

NLS nuclear localization signal

NES nuclear export signal

RHD Rel-homology domain

AP-1 activator protein-1

DD dimerization domain

AD transactivation domain

SV40_{cNLS} SV40 T antigen-NLS

CRM1 export receptor exportin-1

CDK5 cyclin-dependent kinase 5

PLC-γ1 phospholipase C-γ1

ATM ataxia telangiectasia mutated

mTOR Mammalian target of rapamycin

TA Transactivating activity

NL Nuclear localization

PA Protein abundance

PKA Protein kinase A

PKC Protein kinase C

ERK Extracellular signal-regulated kinase

NPC nuclear pore complex

FG Nups phenylalanine-glycine (FG)-repeated nucleoporin

Karyopherin-β Kap

KPNA1 Karyopherin α1

KPNB1 Karyopherin β1

RCC1 regulator of chromosome condensation 1

RANGAP RanGTPase-activating protein

cNLS classical nuclear localization signal

PY-NLS proline-tyrosine nuclear localization signal

IK-NLS isoleucine-lysine nuclear localization signal

RS-NLS arginine-serine repeat nuclear localization signal

ARM armadillo repeats

TNPO1 transportin 1, Karyopherinβ2

ncNLS non-classical nuclear localization signal

PTHrP neuroendocrine peptide parathyroid hormone-related protein

IDRs intrinsically disordered regions

NTRs nucleocytoplasmic transport receptors

HEAT Huntingtin, elongation factor 3 (EF3), protein phosphatase 2A

(PP2A), and the yeast kinase TOR1

CRM1 chromosomal region maintenance 1 (exportin1)

GTP guanosine triphosphate

GDP guanosine diphosphate

IBB importin-β binding

LLPS Liquid-liquid phase separation

hnRNPA1 heterogeneous nuclear ribonucleoproteins A1

LCDs low-complexity domains

FUS Fused in Sarcoma

GFP Green Fluorescent Protein

Dextran a polysaccharide used as a molecular crowding agent

PEG Polyethylene glycol

FRAP Fluorescence recovery after photobleaching

RRMs RNA recognition motifs

Pab1 Poly(A)-binding protein 1

DYRK3 Dual specificity tyrosine-phosphorylation-regulated kinase 3

TORC1 Target of rapamycin complex 1

TCR T cell receptor

Grb2 Growth factor receptor-bound protein 2

pLAT Phosphorylated linker of activated T cell

Sos Son of Sevenless

N-WASP Neuronal Wiskott-Aldrich syndrome protein

F-actin Filamentous actin

Pol Polymerase

CTD C-terminal domain

LCD Low-complexity domain

DIC Differential interference contrast microscopy

hCTD Human C-terminal domain

yCTD Yeast C-terminal domain

ALS Amyotrophic lateral sclerosis

ATP Adenosine triphosphate

NPCs Nuclear pore complexes

FG-repeats Phenylalanine-glycine repeats

RGG-PY Arginine-glycine-glycine-proline-tyrosine

CRM1 Chromosome region maintenance 1

siRNA Small interfering RNA

ITC Isothermal titration calorimetry

AcGFP Aequorea coerulescens green fluorescent protein

PCR Polymerase Chain Reaction

cDNA Complementary DNA

EGFP Enhanced Green Fluorescent Protein

GST Glutathione S-transferase

TRX Thioredoxin

HRV 3C Human Rhinovirus 3C

LB Luria-Bertani

DH5α Escherichia coli strain DH5α

Tm Melting temperature

DB DNA binding buffer

BL21 (DE3) bacterial strain used for protein expression

CV column volume

IPTG isopropyl β-D-1-thiogalactopyranoside

NaCl sodium chloride

O.D.600 optical density at 600 nm

PMSF Phenylmethanesulfonyl fluoride

 β -ME β -Mercaptoethanol

Tris tris(hydroxymethyl)aminomethane

FPLC Fast Protein Liquid Chromatography

MS Mass Spectroscopy

SDS-PAGE Sodium Dodecyl Sulfate Polyacrylamide Gel Electrophoresis

PBS Phosphate-Buffered Saline

DTT Dithiothreitol

Cryo-EM Cryogenic-Electron Microscopy

DMSO Dimethyl sulfoxide

NaHCO₃ Sodium bicarbonate

EDTA Ethylenediaminetetraacetic acid

NHS N-Hydroxysuccinimide

HEPES 4-(2-hydroxyethyl)-1-piperazineethanesulfonic acid

Chapter 1 Introduction

1.1 NFAT5 is a tonicity-regulated transcription factor that regulates osmoprotective genes

1.1.1 NFAT5 promotes the transcription of osmo-protective genes in response to hypertonicity

When mammalian cells are exposed to solutions with different osmolarities, their volume changes as water flows across the cell membrane. Cells activate membrane electrolyte transporters to regulate intracellular solute concentration and prevent excessive changes in cell volume (Hoffmann et al., 2009). A hypertonic solution causes water to drain from the cell, leading to cell shrinkage. Within seconds, electrolyte transporters, such as Na⁺-K⁺-Cl⁻ cotransporters, Na⁺/H⁺ exchangers, and Cl⁻/HCO₃⁻ exchangers, transport ions including Na⁺, K⁺ and Cl⁻ into the cell to restore the intracellular and extracellular ionic concentration balance and cell volume (Lang et al., 1998). However, this process increases intracellular ionic strength and crowds intracellular molecules, potentially harming the cell. Furthermore, if the extracellular tonicity exceeds the cell's tolerance limit, it can cause detrimental effects, such as protein and DNA denaturation (Dmitrieva et al., 2004), mitochondrial dysfunction (Copp et al., 2005; Desai et al., 2002), protein translation suppression (Morley &

Naegele, 2002), cytoskeletal architecture remodeling (Di Ciano et al., 2002), cell cycle arrest and apoptosis (Dmitrieva et al., 2001).

In response to hypertonic stress, cells initiate a genetic program of osmo-adaptive responses to restore biochemical homeostasis (Yancey et al., 1982). The Nuclear Factor of Activated T-cell 5 (NFAT5), also known as Osmotic Response Element-Binding Protein (OREBP) or Tonicity Enhancer-Binding Protein (TonEBP), plays a crucial role by orchestrating the transcriptional program as the only known mammalian tonicitydriven transcription factor (Burg et al., 2007; Burg et al., 1997; Cheung & Ko, 2013). Specifically, NFAT5 translocates to the nucleus and promotes the expression of specific enzymes and transporters responsible for uncharged small organic osmolytes (Cheung & Ko, 2013). These organic osmolytes, such as sorbitol, betaine, myoinositol, taurine, and glycerophosphocholine, accumulate to a high level without disrupting macromolecular functions and progressively replace the excessive intracellular electrolytes (Garcia-Perez & Burg, 1991; Yancey et al., 1982). These enzymes and transporters' gene transcription is referred to as osmo-protective genes. Figure 1.1 depicts a timeline of the activation of the electrolyte transporters and NFAT5 regulated transcription of osmo-protective genes (Cheung & Ko, 2013).

NFAT5-mediated transcription programs are indispensable for various physiological processes and human diseases. For example, NFAT5 has a tumor-suppressive effect on hepatocellular carcinoma (HCC) (Qin et al., 2017) and a

reversible effect on arctigenin (AG), which regulates macrophage polarization (Ni et al., 2020). Additionally, epigenetic regulation of NFAT5 indicates its critical role in tissue-specific functions, such as cell proliferation, migration, chromatin remodeling, and angiogenesis. Therefore, comprehensive research on the regulation of NFAT5 activity is believed to offer novel insights into its functional role in clinical therapy.

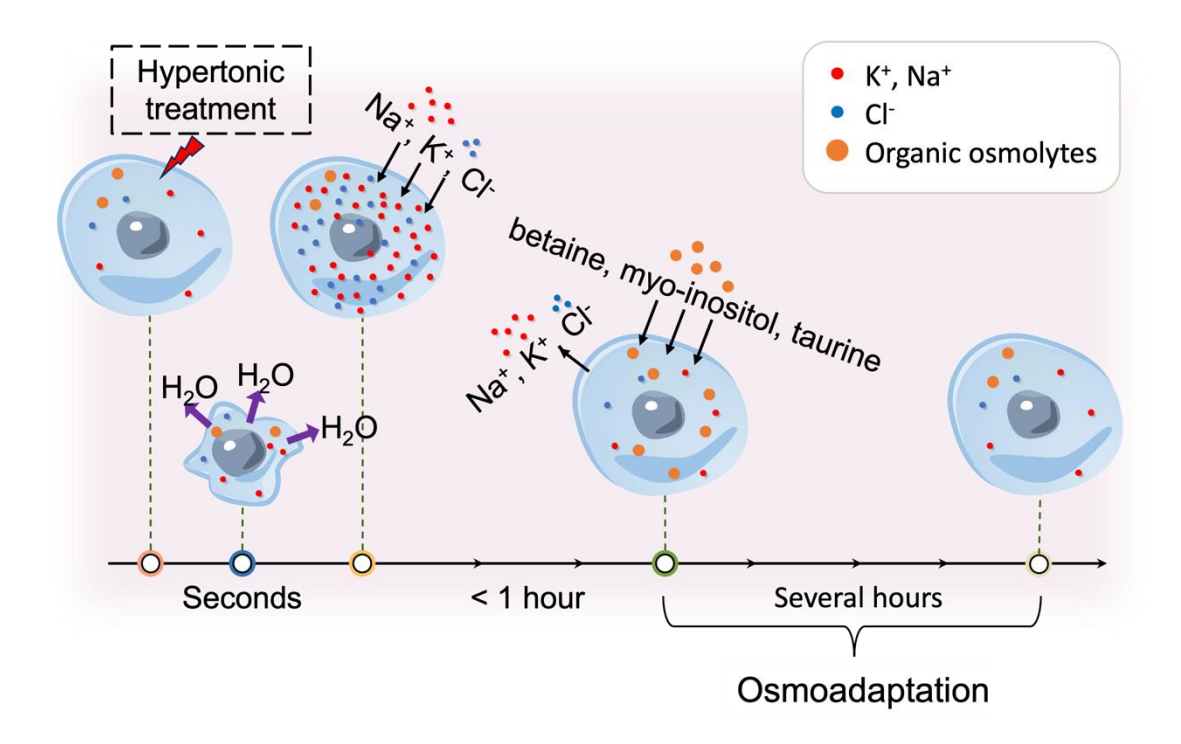
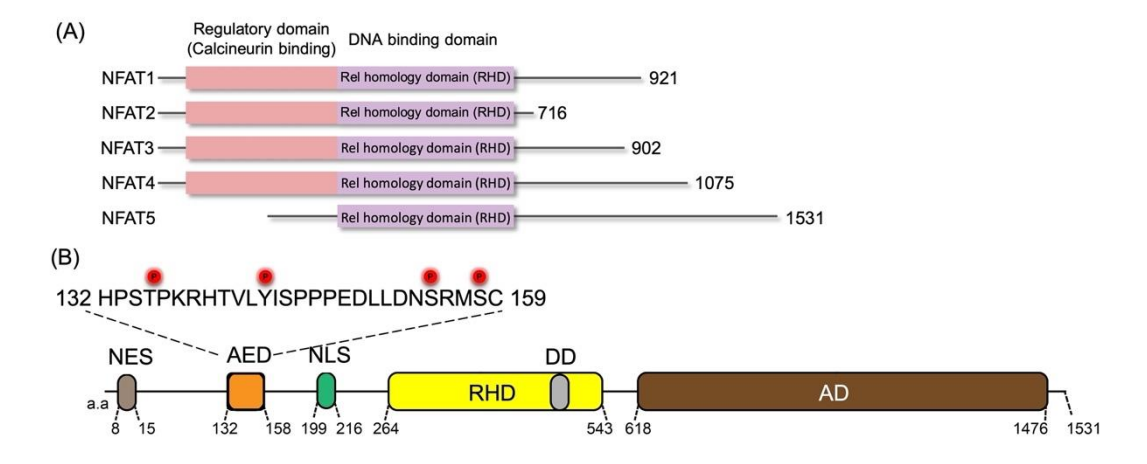


Fig. 1.1 Time frame of short-term and long-term adaptation to hypertonic stress. (Adapted from Cheung, C. Y. K. & Ko, B. C. B., 2013.)

1.1.2 The structure and functional domains of NFAT5

NFAT5 belongs to the Rel transcription factor family, which includes NFAT1-4 and NF-kappaB (NF-κB) (Zhou, 2016). As a large-sized protein, NFAT5 possesses several functional domains, including a leucine-rich canonical nuclear export sequence

(NES) at the N-terminal 19 amino acids, an auxiliary export domain (AED), and a consensus positively charged bipartite classical nuclear localization signal (cNLS) (Tong et al., 2006). These domains contribute to the efficient nucleocytoplasmic translocation of NFAT5. Additionally, the middle region contains a Rel-homology domain (RHD) that is a conserved DNA binding domain shared by all Rel family members (Fig. 1.2 A) (Cheung & Ko, 2013). The RHD domain of NFAT5 contains a dimerization domain (DD) that specifically recognizes the sequence of 5'-TGGAAA-3' within the promoter region of target genes, resulting in a classical "butterfly" binding model with high kinetic stability (Hogan et al., 2003; Li et al., 2022).NFAT5 also features a serine/threonine and proline-rich transactivation domain (AD) (residues 618-1476) that is intrinsically disordered (Fig. 1.2 B). Notably, unlike other NFAT family members, NFAT5 lacks a calcineurin binding domain that activates the nuclear import of NFAT1 to NFAT4 (Cheung & Ko, 2013; Zhao et al., 2021). Consequently, the calcium/calcineurin signaling cascade is dispensable in the activation and nuclear localization of NFAT5, and docking sites for phosphatase calcineurin are absent (Zhao et al., 2021). While NFAT1-4 contain many phosphorylation sites in their N-terminal regions, only four phosphorylation sites, namely T135, Y143, S155, and S158 have been reported in NFAT5. All of them are located in the AED domain (Fig. 1.2 B).



Adapted from Cheung, C. Y. K. & Ko, B. C. B., 2013.

Fig. 1.2 Members of NFAT family and NFAT5 functional domains schematic (Cheung & Ko, 2013). (A) Alignment of NFAT1-4 and NFAT5, showing absence of calcineurin-binding domain in NFAT5. (B) Structural features of NFAT5 include NES, AED, NLS, DD, RHD, and AD1-3. AED domain sequence is shown in parentheses, and phosphorylation sites are marked with red circles.

1.1.3 Regulations of NFAT5 activities

Regulation of NFAT5 nuclear abundance

NFAT5 undergoes active bidirectional transport. Under isotonicity, it is distributed in both the nucleus and cytoplasm, indicating that its nucleocytoplasmic shuttling is not activated by tonicity changes (Cheung & Ko, 2013). Extracellular tonicities play a significant part in regulating the translocation of NFAT5 to the cellular nucleus and its abundance in the cytoplasm. Our previous studies have shown that the nucleocytoplasmic transport of NFAT5 requires both NES and NLS domains.

Additionally, the AED domain is critical for export of NFAT5 under hypotonic conditions (Cheung & Ko, 2013). The alanine mutagenesis of RKR₂₀₂₋₂₀₄AAA in the NLS domain prevents NFAT5 being imported into nucleus under both isotonic and hypertonic conditions, suggesting an affiliation of NFAT5_{NLS} with classical monopartite NLS, similar to SV40 T antigen-NLS (SV40_{cNLS}) (Tong et al., 2006). The NES domain's leucine and isoleucine amino acid sequence is homologous to canonical NES, and the replacement of leucine to alanine, or inhibiting NES export receptor exportin-1 (CRM1), results in the nuclear abundance of NFAT5 under isotonicity (Cook et al., 2007; Tong et al., 2006). The AED domain, which contains four tonicity-driven phosphorylation sites, is suggested to be a regulatory domain for NFAT5 nuclear export.

Tonicity-triggered phosphorylation has been shown to drive nuclear import of NFAT5 under hypertonicity. Four phosphorylation sites, tyrosine 143 (Y143), threonine 135 (T135), serine 155 and 158 (S155 and S158), have been identified as crucial for NFAT5 activity regulation. Cyclin-dependent kinase 5 (CDK5) phosphorylates T135 of NFAT5 in HEK293 cells, leading to its nuclear import (Tong et al., 2006). Under hypertonic treatment, phospholipase C-γ1 (PLC-γ1) is predicted to bind to Y143 of NFAT5, activating transcription and transactivation, thereby leading to nuclear localization (Irarrazabal et al., 2010). Dual phosphorylation of S155 and S158 is essential residues of NFAT5 for its nuclear export (Xu et al., 2008). While phosphorylation sites of NFAT5 are expanding, the mechanism that phosphorylation regulates NFAT5's bidirectional nucleocytoplasmic translocation remains elusive.

The nuclear import activity of NFAT5 is regulated by a complex network of kinases. Notably, Brx, a guanine nucleotide exchange factor, serves as the osmo-sensor and actives specific small G proteins. Brx also recruits c-Jun N-terminal kinase (JNK)-interacting protein 4 (JIP4). Subsequently, JIP4 cooperates with MKK3 and MKK6, resulting in a stimulation of p38 α MAPK. This cascade involving p38 α MAPK and NFAT5 is then activated via phosphorylation, facilitating the nuclear import of NFAT5 (Zhao et al., 2021).

In addition to nuclear import, nuclear retention is also a factor contributing to the nuclear abundance of NFAT5. However, the regulation the nuclear retention remains unclear (Cheung & Ko, 2013).

Regulation of transactivation activity

C-terminal AD domain contributes to the transactivation activity, whereas only the region of amino acids 1039-1249 is regulated by tonicity changes. Although phosphorylation effectively regulates the nuclear localization of NFAT5, its effect on transactivation remains a subject of considerable debate. The lack of evidence on how phosphorylation sites located in AD domain influence the transactivation activity of NFAT5 adds to this uncertainty. In mammalian cells, overexpression of alanine mutants of NFAT5-S1997A, NFAT5-S1247A, and NFAT5-S1367A modestly reduces transactivation activity under isotonic and hypertonic conditions by inactivating ataxia

telangiectasia mutated (ATM) kinase (Irarrazabal et al., 2004; Zhou, 2016). Since multiple kinases are involved in tonicity-driven NFAT5 transactivation increase, the mechanism of regulating transactivation is complex (Zhou, 2016). Nevertheless, it remains to be explored how hypertonicity induces phosphorylation and regulation.

1.2 The molecular machinery of nucleocytoplasmic transport

1.2.1 The nucleocytoplasmic trafficking process transports a variety of cargo molecules across the nuclear pore complexes (NPCs)

The nuclear envelope in eukaryotic cells is double-membraned, which is able to isolate the genome from the surrounding microenvironment and selectively facilitates nucleocytoplasmic trafficking, a fundamental function of nuclear pore complexes (NPCs). The NPCs function as a threshold for macromolecules over 40 kDa. The intrinsically disordered phenylalanine-glycine (FG)-repeated nucleoporin (FG Nups) segments form a diffusion barrier. The asymmetric nucleoporins form a nuclear basket structure of NPC, with nucleoporins as the determining factor for directional transport. The cytoplasmic filaments of NPC provide docking sites for nuclear transport receptors, including the Karyopherin- β (Kap) family, which binds to FG repeats (Hoelz et al., 2011).

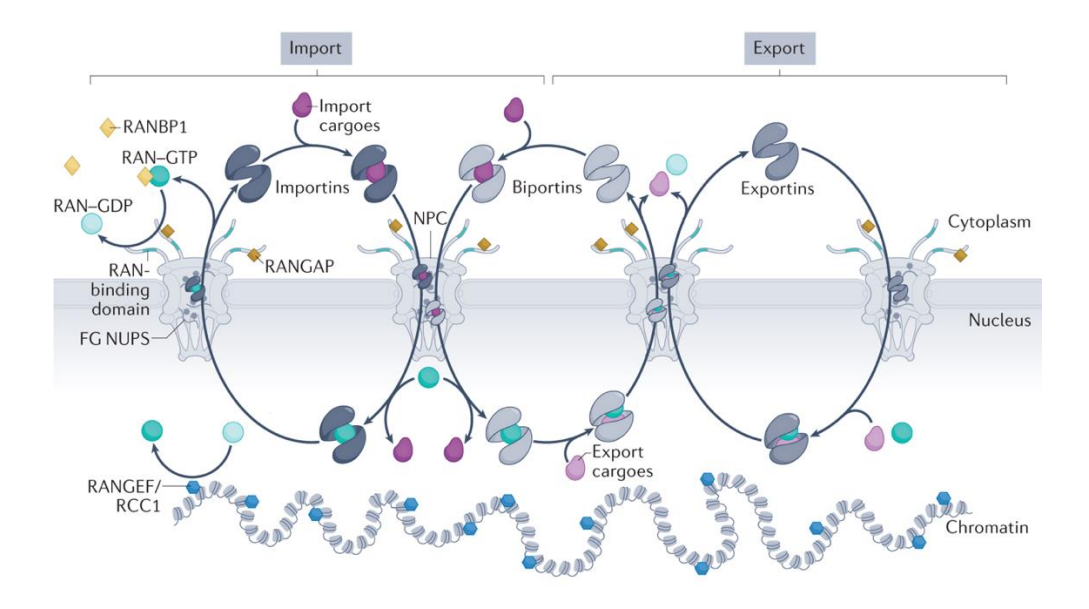
1.2.2 Karyopherin proteins as nucleocytoplasmic transport receptors (NTRs)

Karyopherin proteins, which mediate the transport of macromolecules, are large and range from 95-140 kDa. They consist of 19-24 HEAT repeats, each containing two antiparallel α -helices connected by a loop usually composed of 40-60 amino acids. Helix A is generally found on the outer surface, while helix B is on the inner surface.

The Kap family mediates the majority of macromolecule transport, which is classified into three types according to its direction across NPC, namely importins that bring the cargo from the cytoplasm into the nucleus, exportins that move proteins out of the nucleus, and biportins that function in bi-directional transport. Ten importins have been identified, including KPNB1, TNPO1, KPNB2B, and IPO4, to name a few, as well as five exportins, including CRM1, XPO2, XPO5, XPOT, and XPO6. Additionally, three biportins have been discovered (IPO13, XPO4, and XPO7), while two remain unknown (Wing et al., 2022).

The transport of the Kap family is initiated by recognizing cargoes possessing functional domains of nuclear localization signals (NLS) or export signals (NES). The transportation of Kap-cargo heterodimer across the nuclear pore complex involves the binding of the complex to FG Nups, followed by its separation to allow for the release of cargo in the target compartment (Matsuura, 2016).

The direction of Kap-regulated transport is determined by RanGTP/RanGDP gradient, which regulates cargo loading and unloading (Fig. 1.3). In detail, RCC1, a nucleotide exchange factor, binds to chromatin, primarily allowing nuclear RanGTP to localize in the nucleus. Conversely, RanGTPase-activating protein (RANGAP) and Ran-binding protein RANBP1 are present in the cytoplasm and to retain cytosolic Ran GDP-bound, stimulate GTP hydrolysis. Import cargo-binding Kaps exclude Ran-GDP and interact with export cargoes and Ran-GTP, leading to a directional determination. Importin-cargo and biportins-cargo complexes form in the cytoplasm and then pass across the NPCs to the nucleus, where they are eventually disassembled following Ran-GTP binding. Exportins and biportins, on the other hand, form ternary complexes in the nucleus with export payloads and Ran-GTP and subsequently translocate across NPCs to the cytosol, where the cargo is released after GTP hydrolysis (Wing et al., 2022).



Cited from Casey E. Wing et al., 2022.

Fig. 1.3 Kap-mediated nucleocytoplasmic transport (Wing et al., 2022).

1.2.3 The molecular machinery of nucleocytoplasmic transport involves specific cargo recognition by NTRs

Four classes of NLSs are distinct from sequence patterns, including classical NLS (cNLS), proline-tyrosine NLS (PY-NLS), isoleucine-lysine NLS (IK-NLS), and arginine-serine repeat NLS (RS-NLS), have been identified to target a specific kap (Soniat & Chook, 2015). Basic residue-riched NLSs are commonly intrinsically disordered, and binding to the acidic surface of Kap can cause extended or helical conformational changes.

The nuclear import of cargo with cNLS by the KPNA-KPNB system

Two types of classical NLSs (cNLSs), monopartite classical NLS (amino acid sequence: K-K/R-X-K/R) and bipartite cNLS (amino acid sequence: K/R-K/R-X₁₀₋₁₂-K/R_{3/5}, where X₁₀₋₁₂ is a linker of 10-12 any amino acids and K/R_{3/5} refers to three lysine or arginine within five consecutive amino acids), can be imported into the nucleus by the KPNA-KPNB1 system (Kalderon et al., 1984; Robbins et al., 1991). This system involves the cargo adaptors KPNAs and the adaptor-mediator KPNB1. The KPNAs contain three primary conserved structural features: an N-terminal IBB domain, armadillo (ARM) repeats, and a C-terminal region, including a highly conserved short acidic amino acid cluster. The ARM repeats typically contain ten repeats of a relatively 42-43 amino acid hydrophobic sequence, with the major and minor cNLS binding

domains being the ARM repeats 2-4 and 6-8, respectively. The cNLS binding surface is conserved across all KPNA subtypes. Additionally, the N-terminal IBB (KPNB1 binding) domain, which spans approximately the first 70 amino acids, serves an autoinhibitory function of binding to cNLS (Harreman et al., 2003; Soniat & Chook, 2015).

The nuclear import of cargo with PY-NLS by the TPNO1 system

The Karyopherin β2, also named transportin 1 (TNPO1), system recognizes the proline-tyrosine NLS (PY-NLS). In contrast to cNLSs, PY-NLSs are characterized by diverse and positively charged sequences. Some PY-NLSs share an N-terminal hydrophobic or basic motif and a C-terminal R/K/H-X₂₋₅-P-Y or R/K/H-X₂₋₅-P-φ motif (where φ is hydrophobic, H is histidine, P is proline, and Y is tyrosine) (Chook & Süel, 2011; Soniat & Chook, 2016; Wing et al., 2022). Despite their larger sizes and greater complexity than classical-NLSs, PY-NLSs consisting of 15-30 residues can bind to TNPO1 in extended conformations (Chook & Süel, 2011). As TNPO1 possesses a relatively wide and level binding site for nuclear localization signals (NLS), which combines with an acid/hydrophobic surface, it has the capability to bind diverse sequences. Notably, despite the different PY-NLSs that bind to TNPO1, the PY-NLS-binding region of TNPO1 remains unchanged (Chook & Süel, 2011).

The nuclear import of cargo with IK-NLS by IPO5

The yeast KAP121 recognizes IK-NLS with a consensus motif of K-V/I-X-K-X₁-2-K/H/R (where V is valine, I is isoleucine, K is lysine, and H/R can be histidine or arginine). Although the homologous human IPO5's (Importin 5) binding of IK-NLS is not well researched, residues of KAP121 that interact with IK-NLSs are conserved in IPO5 (Chook & Süel, 2011; Wing et al., 2022).

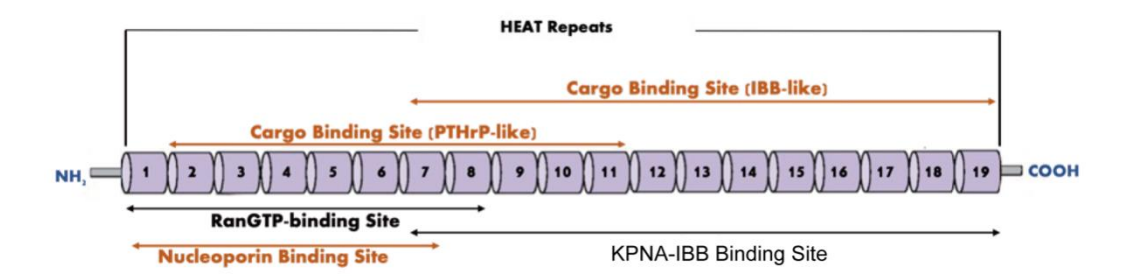
The nuclear import of cargos with RS-NLS by TNPO3 system

RS-NLSs recognized by TNPO3 (Transportin 3) are typically located at the c-terminal RNA-recognition motif (RRM) domain, and phosphorylation of serine amino acids is essential for interacting with many RS-NLS (Wing et al., 2022).

Diverse non-classical NLSs (ncNLSs) are imported directly by KPNB1

In the absence of KPNAs, at least 29 distinct cargo proteins are known to directly interact with KPNB1, with no clear common characteristics in the binding region (Wing et al., 2022). These cargoes are classified as "non-classical NLSs" (ncNLS) with notable examples including SREBP-2 (Nagoshi et al., 1999), the human T-cell leukemia virus type 1 (HTLV-1) protein Rex (Palmeri & Malim, 1999), TRF (Forwood & Jans, 2002), and the neuroendocrine peptide parathyroid hormone-related protein (PTHrP)

(Cingolani et al., 2002). The 28-residue intrinsically disordered region (IDR) of PTHrP binds to the 2-11 HEAT repeats (the PTHrP-like Cargo binding site) of KPNB1 as shown in **Fig. 1.4** (Cingolani et al., 2002).



Adapted from Cingolani et al., 2002; Harel & Forbes, 2004

Fig. 1.4 Scheme presentation of the structure and functional domains of KPNB1 (Cingolani et al., 2002; Harel & Forbes, 2004).

After comparing the structures of the KPNB1-KPNA1_{IBB} complex and the KPNB1-RanGTP complex, five key structural features are apparent (Macara, 2001). First, isolated KPNA1_{IBB} in its unstructured form leads to autoinhibition of cargo loading. However, in the KPNB1-KPNA1_{IBB} complex, IBB forms an α-helix. Secondly, IBB binds to the C-terminal of KPNB1 as demonstrated in **Fig. 1.4**. Thirdly, the acidic loop of KPNB1, which interacts with the basic patch of RanGTP confirmation, exhibits the same binding site as that of IBB. This observation suggests mutual exclusivity between IBB and RanGTP binding to KPNB1. Fourthly, the spoon-like conformation of KPNB1-RanGTP differs from the snail-like conformation of KPNB1-KPNA1_{IBB}. Finally, the binding models of KPNB1-RanGTP and KPNB1-KPNA1_{IBB} complexes share a remarkable similarity, with the acidic loop of the receptor restricting the basic

residues of the ligand, hence why they are referred to by the same name, "karyopherins", with " α s" and " β s" sharing this nomenclature.

1.3 Formation of membraneless organelles via phase separation

Phase separation is a physical-chemical process that involves the separation of materials into two or more phases that comprise polymer-rich and solvent-rich regions. In biology, phase separation refers to the separation of two phases: a dense and a dilute phase. Multivalency constitutes a critical driving force for phase separation in biological systems.

In eukaryotic cellular function, numerous molecular components work collectively to sustain it. In addition to membrane-encased organelles, membraneless organelles also participate in this cooperation. These globules, which are protein-based, can selectively manage cellular materials uptake and release. An example of how nuclear speckles function is by controlling gene expression, serving as storehouses for splice factors, and overseeing the processing and metabolism of pre-mRNA within the nucleus.

1.3.1 Membraneless stress granule as a well-studied example of LLPS

When cells experience stress, non-membrane-bound cytosolic structures known as stress granules are formed. These granules contain both mRNA and proteins as a response to cellular stress. Heterogeneous nuclear ribonucleoproteins A1 (hnRNPA1) constituent a significant component of stress granules. The temperature-sensitive and dynamic LLPS of hnRNPA1 has been identified as a notable characteristic (Molliex et al., 2015).

Electrostatic interactions and aromatic residues interactions lead to LLPS of stress granule

At its N-terminus, hnRNPA1 contains two RNA recognition motifs (RRMs), while its C-terminus is composed of a low complexity domain (LCD), housing the steric zipper motif (amino acids 259-264). The steric zipper motif is located at the center of the LCD. Electrostatic and aromatic residue interactions drive LLPS in hnRNPA1 stress granules. Cross-β fibrils constitute hnRNPA1 hydrogels and are believed to promote a thermodynamically trapped state. Interestingly, hnRNPA1 LLPS is not affected by steric zipper motif depletion but is affected by fibrilization. This suggests that LLPS and fibrilization are driven by distinct mechanisms (Molliex et al., 2015).

As a mechanism of LLPS, inter-molecular interactions have been identified. The LLPS of hnRNPA1 still occurs at low sodium concentrations, indicating that electrostatic interactions contribute to droplet formation (Molliex et al., 2015). Additionally, hexanediol disrupts LLPS, highlighting the importance of interactions between phenylalanines. Inter-molecular interactions of LCDs are involved in these LLPS-driving interactions, which include electrostatic interactions and those involving aromatic residues.

Protein concentration and microenvironment also influence stress granule assembly. Stress granules are riched in RNA, which facilitates LLPS (Molliex et al., 2015). Therefore, the multivalent interactions between RNA, RNA-binding proteins, LCDs, and other molecules and proteins drive stress granule LLPS in a concentration-dependent manner.

Stress granules formed via phase separation perform a sequestration function.

Molecular condensation through LLPS in living cells acts as a barrier to prevent undesired macromolecules' presence and avoid off-target effects. Cytoplasmic stress granules provide a clear illustration of sequestering via LLPS. (Wippich et al., 2013). In response to cellular heat stress, DYRK3, a kinase that regulates tyrosine phosphorylation, dissolves in stress granules, leading to the release of mTORC1 for signaling and boosting its activity. DYRK3 LCDs promote stress granule formation and

influence the phosphorylation status of mRNA-binding proteins. Eventually, sequestration of the target of rapamycin complex 1 (TORC1) into stress granules blunts TORC1 signaling.

1.3.2 Bilayer protein clustering is driven by a complex interplay between macromolecular interactions and environmental factors

The T cell receptor (TCR) signaling process alters T cell behavior through a hetero-protein trio that activates Ras, a main protein in the TCR signaling pathway. The trio consists of growth factor receptor-bound protein 2 (Grb2) and Son of Sevenless (Sos), which bind to the phosphorylated linker of activated T cell (pLAT) and the N-and C-termini of Grb2, respectively (Dustin & Muller, 2016; Su et al., 2016). The hetero protein trio forms pLAT clusters on a supported lipid bilayer that assemble into droplets, facilitating the shuttling of pLAT. The pLAT clusters interact with neuronal Wiskott-Aldrich syndrome protein (N-WASP) to contribute to forming an elongated filamentous actin (F-actin) that is solid-gel-like. Phosphorylation induces phase separation of downstream signaling proteins, which begins with TCR activation and ends with actin assembly.

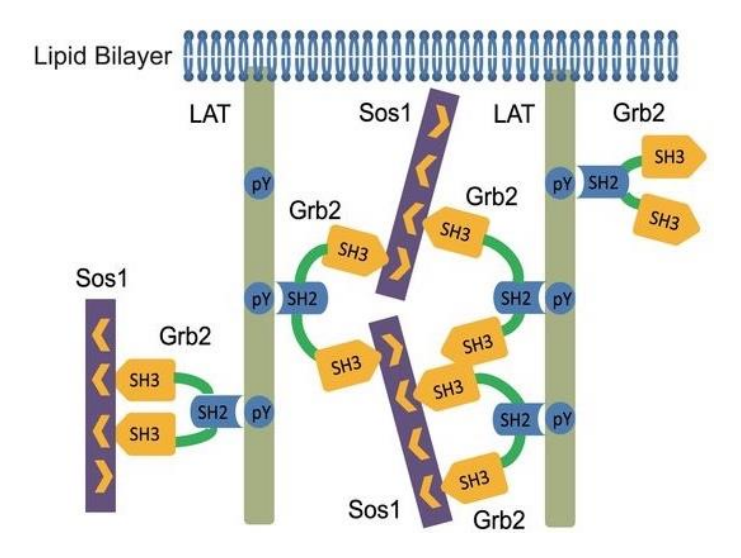
<u>Protein cluster assembly via a complex interplay between macromolecular</u> interactions and environmental factors

The formation of the two-dimensional phase-separated system of TCR depends entirely on multivalent protein-protein interactions that occur on top of a lipid-disordered bilayer, as shown in **Figure 1.5** (Su et al., 2016). The clustering of pLAT initially increases with the increase in pLAT density, but higher densities reduce clustering, indicating that the valency of phosphotyrosines on LAT influences clustering efficiency.

Furthermore, pLAT clusters form in the presence of Grb2 and Sos1, and dephosphorylation of pLAT causes clusters to disassemble. The SH3 domains of Grb2 act as crossing bridges and are determinants of cluster formation, while 75% of the C-terminal phosphotyrosines interact with the SH2 domain of Grb2. Therefore, the dynamically rearranging and multivalent protein-protein interactions drive the phase separation of LAT.

Furthermore, Su *et al.* demonstrated that the phosphorylation of LAT is facilitated by the cytosolic tyrosine kinase ZAP70 while hindered by the phosphatase SD45. The droplet shape alterations are reversible in the final step of TCR signal transduction. Depolymerization of F-actin, induced by latrunculin A, results in the reorganization of LAT clusters in a solid-gel-like state. ZAP70 creates a membrane environment that

promotes the phase separation of pLAT through multivalent protein-protein interactions, subsequently reorganized by F-actin polymerization.



Cited from Su, X. et al., Science, 2016.

Fig. 1.5 Schematic of the clustering assay, depicting the proteins and their interactions (Su et al., 2016). A His₈ tag is added to the N-terminal end of LAT, which can bind to the lipid bilayers containing Ni²⁺ to simulate the formation process. Initially, pLAT, which contains three phosphotyrosine residues on the C-terminal end, binds randomly to the lipid bilayer.

Phase separation, as "a signaling hub", promotes TCR signal transduction

As described earlier, phase separation of TCR is driven primarily by multivalent interactions. This physical and biochemical compartment, triggered by phase separation, facilitates TCR signaling transduction. Deleting LAT binding partners eliminates micro-clusters, impairing downstream signaling and transcriptional processes. TCR-

rich clusters, similar to protosynapses, exhibit near-identical size and shape, dynamic formation and selective transduction. These clusters function in signal amplification and switch-like behavior for downstream signaling. By forming a boundary for the selective exchange of ZAP70 and SLP-76, LAT clusters enhance and reorganize the actin cytoskeleton (Chong & Forman-Kay, 2016).

In summary, the signaling punctum driven by phase separation creates a microenvironment by actively sequestering specific proteins, enriching and prolonging the signal, and facilitating signaling transduction.

1.3.3 LLPS in transcription regulation: RNA polymerase (Pol) II

Low complexity domains (LCDs) of RNA polymerase (Pol) II activate pre-mRNA transcription and promote processing through protein clustering. The C-terminal domains (CTDs) of Pol II, containing multiple heptapeptide repeats (Y1S2P3T4S5P6S7), form micron-sized droplets when exposed to molecular crowders such as dextran and polysaccharide Ficoll at 5-10% concentrations. The droplets remain stable even after altering ionic concentrations or incubating at different temperatures (Boehning et al.).

The mechanism of Pol II CTD clustering resembles that of pLAT, relying on multivalent homo- and heterotypic interactions between LCDs. These interactions are

concentration-dependent, temperature-resistant, and remain resistant to changes in ionic strength. Additionally, when using maltose-binding protein (MBP)-tagged human C-terminal domain (hCTD) and yeast C-terminal domain (yCTD) to carry out phase separation assays (Boehning et al.), yCTD starts to phase separate at a 4-6-fold higher concentration of hCTD. hCTD contains more CTD repeat than yCTD, suggesting that higher numbers of CTD repeats lead to stronger CTD-CTD interactions. Furthermore, Pol II clustering was detected in three different human cell lines: cells expressing full-length CTD containing 52 repeats cells expressing truncated CTD, and cells expressing yeast-like CTD (25R). Based on an analysis of Ripley function $L(\gamma)$ curves, Pol II clustering is CTD-dependent and CTD length positively correlates with clustering. In contrast to pLAT clustering, phosphorylation has the opposite effect on Pol II phase separation. Phosphorylated S5 of CTD causes protein-concentrated droplets to dissolve.

Taken together, CTD-CTD multivalent interactions concentration- and CTD length-dependently induce phase separation of Pol II, which can be inhibited by phosphorylation.

1.3.4 NTRs mediate LLPS of NLSs

Phase separation of FG Nups functions as a barrier to macromolecular nuclearcytoplasmic transport (Celetti et al., 2019). However, when cargos need to be imported into the nucleus, KPNBs interrupt the phase separation of FG Nups, thereby inducing the "self-healing" of NPCs (Frey & Görlich, 2009; Yoshizawa & Guo, 2021).

Similarly, KPNBs serve as safeguards to reverse the aberrant phase transition of RNA-binding proteins. Lin *et al.* highlighted that NLSs behave as disaggregation signals in the cytoplasm, and TNPO1 dissolves phase-separated RNA-binding proteins' NLSs with its prion-like domains (Guo et al., 2018). TNPO1 inhibits spontaneous FUS, TAF15, EWSR1, hnRNPA1, hnRNPA2 fibrillization as well as seeded fibrils of FUS, TAF15, and EWSR1, and disease-associated PY-NLS mutants (Guo et al., 2018).

In addition to TNPO1, FUS forms stable complexes with members of KPNBs subfamilies, namely TNPO3, KPNB1, IPO7, and the KPNB1/7 heterodimer, respectively (Baade et al., 2021; Odeh et al., 2022). Deletion mapping further confirmed that the major binding region between these proteins is the RGG-PY motif, an LCD. The LCD of FUS is known to contribute to aid in LLPS, which is driven by π - π and cation- π interactions. These nuclear import receptors function as chaperones by binding to the multivalent RGG-PY region, hence interrupting the formation of cross- β structures and impeding LLPS.

1.4 Objectives

NFAT5 plays a vital role in maintaining intracellular osmotic balance. As an adaptive response, efficient and swift nuclear import of NFAT5 is necessary. However, the machinery underlying the nucleocytoplasmic transport of NFAT5 remains unclear. Previous studies suggest that, under hypertonic conditions, the predominant increase in nuclear abundance of NFAT5 is attributed to rapid nuclear import, not slow nuclear export. Thus, the focus of our research is the investigation of mechanisms involved in NFAT5 nuclear import.

1.4.1 Identifying the karyopherin members that carry out tonicity-driven nuclear import of NFAT5

As introduced in section 1.1.3, previous sequence analysis indicates that NLS of NFAT5 is a canonical monopartite type similar to SV40-cNLS. Hence, it is likely imported into the nucleus via the KPNA/KPNB1 pathway. If NFAT5-NLS belongs to the non-classical NLS (ncNLS) category, its nuclear import mechanism could involve the KPNB1-dependent pathway.

Our collaboration with Dr. Ko's lab aims to identify the specific karyopherin member responsible for the tonicity-driven nuclear import of NFAT5. Dr. Ko's lab will utilize siRNA to knock down each nuclear import receptor individually *in vivo*,

followed by immunofluorescence imaging to assess the nuclear abundance of NFAT5 in HeLa cells. Additionally, nuclear transport receptor (NTR) inhibitors will be employed to determine the exact receptor involved.

1.4.2 Mapping the NLS responsible for NFAT5 nuclear import

Once the nuclear import receptor of NFAT5 has been identified, the functional region of NFAT5 will be delineated by generating a series of truncated NFAT5 constructs. Deletion mapping will be conducted to analyze the nuclear localization of NFAT5 *in vivo*, and the functional domain displaying full nuclear import activity will be identified.

Subsequently, to identify the direct interaction between nuclear import receptor and NFAT5, corresponding NFAT5 fragments will be generated and purified. Pull-down assays and isothermal titration calorimetry (ITC) assays will be carried out to assess the binding between the functional domain of NFAT5 full NLS and the identified nuclear import receptor. Additionally, Dr. Ko's lab will conduct an *in vitro* reconstituted nuclear import assay using digitonin-permeabilized HeLa cells to further determine the *in vitro* nuclear abundance of the AcGFP-tagged NFAT5 fragments enabling the identification of its nuclear import machinery.

1.4.3 Characterizing possible tonicity-driven liquid-liquid phase separation within the NLS region of NFAT5

Structurally, except for the DNA binding domain (RHD domain), the N-terminal and C-terminal regions of NFAT5 are intrinsically disordered (IDRs). Given that IDRs have been found to promote LLPS in many proteins, it is likely that the IDR in NFAT5 may undergo a similar process.

To evaluate the phase separation properties of the N-terminal disordered region of NFAT5, we will screen a series of constructs *in vitro*. The formation of self-organized LLPS of NFAT5 will be characterized through biochemical reconstitution experiments. After confirming the LLPS behavior, we will detect the turbidity, morphology and material properties of condensed NFAT5 constructs using differential interference contrast (DIC) imaging, fluorescence imaging, and fluorescence recovery after photobleaching (FRAP) assay.

In collaboration, Dr. Ko's lab will conduct an *in vivo* assessment of NFAT5 LLPS. Immunofluorescence imaging will be utilized to demonstrate LLPS of endogenous NFAT5 in HeLa cells subjected to different tonicity extracellular environments. Afterward, epitopic expressed truncated NFAT5 with Aequorea coerulescens green fluorescent protein (AcGFP) tag will be assessed in terms of condensates properties. Similar to the *in vitro* assay, the FRAP assay will be performed to check their mobility.

1.4.4 Evaluating impact of KPNB1 on LLPS of NFAT5-NLS region through biochemical studies

As many NTRs have been reported to participate in the LLPS of NLSs, we will investigate the regulatory function of KPNB1 in NFAT5 LLPS after confirming the role of KPNB1 in nuclear import. The impact of KPNB1 will be evaluated through *in vitro* experiments, where purified KPNB1 mixed with different molar ratios of purified, fluorophore-labeled, condensed NFAT5 constructs will be analyzed using fluorescence imaging. In addition, our collaborator Dr. Ko's lab will use siRNA to knock down KPNB1 and assess the properties of condensed, endogenous NFAT5.

1.4.5 Structural study of the KPNB1-NFAT5_{NLS} complex to delineate the molecular mechanism of KPNB1-mediated nuclear import of NFAT5

Using Cryo-EM, we aim to demonstrate the identified interaction between KPNB1 and NFAT5 and reveal the binding interface of the KPNB1-NFAT5_{NLS} complex. Purified NFAT5 full NLS and KPNB1 will be mixed to prepare the sample. Due to the high flexibility of KPNB1, we will optimize the sample preparation conditions, including cross-linking preparation, non-crosslinking preparation, and protein concentration. We will also perform 2D class averaging and 3D classification to identify high-resolution particles. Additionally, we will use advanced image processing techniques such as local refinement to improve the quality of the structure.

Once the structure is determined, we will analyze the interaction interface between NFAT5-NLS and KPNB1 and the conformational changes of KPNB1 upon binding to NFAT5. The structure will also be compared with previously determined KPNB-NLS complexes to identify conserved and unique features of KPNB1-mediated nuclear import of NFAT5.

1.4.6 Structure-based mutational studies to delineate the molecular mechanism of tonicity-driven nuclear import of NFAT5 by KPNB1

KPNB1 mutations to confirm the binding site for NFAT5

Based on the Cryo-EM structure of the KPNB1-NFAT5_{NLS} complex and previous studies on KPNB1 structure and function, we will generate a series of KPNB1 mutations to confirm the binding site for NFAT5. Guided by the cargo-nuclear import receptor model and the bipartite NFAT5-NLS's sequence feature, we will focus on negatively charged residues in KPNB1 as potential mutant candidates.

Previous studies have identified specific regions in KPNB1 that are involved in binding to other cargoes. For example, HEAT repeats 1-7 of KPNB1 have been reported as the binding site for RanGTP. The acidic loop of KPNB1, a short sequence of amino acids that protrudes from the surface of KPNB1, is highly negatively charged due to multiple aspartic and glutamic acid residues. This acidic loop is involved in binding to

KPNA1-IBB, RanGTP, and PTHrP-ncNLS. HEAT repeats 1-8 are known to interact with KPNA1-IBB, and the N-terminal ten HEAT repeats have been found to bind to PTHrP-ncNLS and Histone.

Therefore, to aid us in making mutation selections, we will use our Cryo-EM structure and previous structural studies on KPNB1-cargo complexes as a guide.

NFAT5 mutations to confirm the role of LLPS in tonicity-drive nuclear import of NFAT5

Previous studies have indicated that NFAT5 N-terminal IDR senses osmolytes and hypertonicity, stabilizing its IDRs (Kumar et al., 2020). Because NFAT5 contains IDR that includes functional domains such as the AED domain regulating nuclear export of NFAT5 and the NLS domain in response to nuclear import of NFAT5, we propose that NFAT5 LLPS plays a role in its nucleocytoplasmic transport.

To assess the involvement of LLPS in tonicity-driven nuclear import of NFAT5, we will generate a series of mutants both *in vitro* and *in vivo*. Specifically, we will use alanine to replace positively charged residues in the cNLS of NFAT5 and residues that facilitate its nuclear import. Additionally, we will conduct alanine-mutagenesis in phosphorylation sites to explore the link between the activity of nucleocytoplasmic

transport and the LLPS of NFAT5. Through these mutations, we aim to clarify the relationship between the LLPS of NFAT5 and its nuclear import activity.

Chapter 2 Methodologies

2.1 Plasmid construction

Target genes were generated using Polymerase Chain Reaction (PCR) and ligation methods. Full-length NFAT5 and full-length KPNB1 were used as templates from Dr. Ben Ko's lab.

KPNB1_{H1-H10}, KPNB1_{H1-H11}, and KPNB1_{H1-H12} were inserted into BamHI and NotI restriction sites of a modified pGEX-4T.1 vector. KPNB1_{FL} was inserted into a modified pET-M vector. NFAT5 constructs were inserted into BamHI and EcoRI restriction sites of a modified pET-32m vector.

Prokaryotes expression vectors:

Vector	Tag	Fusion	Cleavage site	Selection
		protein		maker
pET-M	N terminal His×6	None	HRV 3C	Ampicillin
pET-32M	N terminal His×6	TRX	HRV 3C	Ampicillin
pGEX-4T.1	None	GST	HRV 3C	Ampicillin

For the cell assay, Bimax1 and Bimax2 are synthetic cDNAs inserted into the BamHI and EcoRI restriction sites of the pEGFP-N3 and the pCMV-C-Myc vectors,

respectively. NFAT5_{FL} and NFAT5 $_{1-543}$ were inserted into XhoI and BamHI restriction sites of pCMV-NFAT5-AcGFP-N1 vector for use in the cell assay.

Eukaryotes expression vectors:

Vector	Tag	Selection maker	
pEGFP-N3	C terminal EGFP	Kanamycin/Neomycin	
pCMV-C-Myc	C terminal Myc	Kanamycin/Neomycin	
pCMV-AcGFP-N1	terminal His×6	Ampicillin	

2.1.1 Polymerase Chain Reaction (PCR)

PCR amplified the target gene:

Reagents	Volume (µl)	
5×HF Buffer	4	
dNTP(10 mM)	0.4	
Template	0.3	
Forward primer (100 mM)	0.2	
Reverse primer (100 mM)	0.2	
Phusion TM High-Fidelity DNA Polymerases	0.2	
Nuclease-free water	Up to 20	

The mixture was centrifuged at 13,000 rpm for a few seconds and then placed in the Thermal Cycler. The PCR program was set as follows:

Step	Temperature (°C)	Duration (sec)	Cycles	
Initial Denaturation	98	180	1	
Denaturation	98	30		
Annealing	Tm	30	35-40	
Extension	72	45		
Final Extension	72	600	1	
Hold	4	∞	hold	

PCR products were identified and purified by agarose gel electrophoresis using a ladder as a standard. The target gene was extracted using a DNA extraction kit (BioTekeTM). Finally, using NanoDropTM 2000/2000c Spectrophotometers, the concentration and purity of the isolated gene were determined.

2.1.2 DNA digestion

The target gene, as an insert, and the target vectors were digested using specific Fast Digest® restriction enzymes (ThermoFisherTM), respectively:

Reagents	Volume (µl)	
10 × Fast Digest® buffer	2	
DNA (500-1000 ng)	-	
Restriction enzyme 1 (10 U/μl)	1	
Restriction enzyme 2 (10 U/μl)	1	
Nuclease-free water	Up to 20	

Gently mix the mixture and spin it down for several seconds. Incubate at 37 °C for 40 min.

2.1.3 Insert and linear vector purification

Linear vectors were determined and purified by agarose gel electrophoresis using a ladder as a standard and an undigested vector as a control. The extracted target gene with sticky ends was purified by adding 500 μl DB using a DNA extraction kit (BioTekeTM). The purification and concentration of DNA samples were measured using NanoDropTM 2000/2000c Spectrophotometers.

2.1.4 Ligation

Ligation was conducted by mixing linear vector and target insert at a molar ratio of 3:1, followed by $10 \times T4$ DNA ligase reaction buffer (2 μ l), T4 ligase (1 μ l)

(ThermoFisherTM), and nuclease-free water (up to $20~\mu$ l). The mixture was well blended, spun down for a brief period of time, then incubated for 20 minutes at 22 °C.

2.1.5 Transformation

20 μl of PCR products were directly added into a pre-cooled 1.5 ml tube containing 100 μl of freshly thawed DH5α competent cells on ice, followed by gentle mixing. After 30 minutes of incubation on the ice, the competent cells were subjected to a 90-second heat shock at 42°C. The tube was immediately put back on the ice and left to recover for 5 minutes. The competent cells were then cultured for 60 minutes at 37 °C and 250 rpm in a shaking incubator with 1 ml of pre-warmed, antibiotic-free LB buffer. Finally, a particular antibiotic was added to the cells before plating them onto a pre-warmed LB agar plate. The cells were then cultured overnight at 37°C in an incubator.

Colony verification was performed by picking a single colony and subsequent sequence identification.

2.1.6 Mutant generation

The Mut Express® MultiS Fast Mutagenesis Kit V2 (Vazyme) generated mutants. In the first round of the PCR procedure, two 25~30 base pair primers containing the target gene was expanded using mutant DNA sequence, meanwhile, using wild-type

constructs as templates. The first PCR product was purified, and amplification and methylated template digestion using enzyme DpnI followed. The resulting products were then purified, and after homologous recombination, the final products were transformed into Top10 competent cells.

2.2 Recombinant protein over-expression in Escherichia coli (E.coli)

To obtain satisfactory recombinant proteins with good solubility, parallel small-scale expression tests were performed by adjusting the expression temperature to 16 $^{\circ}$ C and 30 $^{\circ}$ C, respectively.

On **day 1**, plasmids with the identified sequence were purified and extracted using the Plasmid Mini-Prep Kit (BioTekeTM). Afterward, target plasmids were transformed into BL21 (DE3) Competent Cells (NovagenTM) (250 ng plasmid/100 µl cells).

On **day 2**, a single colony was inoculated into 500 µl of 37 °C pre-warmed LB buffer with the corresponding antibiotic. Subsequently, incubation was conducted at 37 °C in a 250 rpm shaking incubator for 2-3 hours. The activated bacterial strain was then 1:1000 (v/v) diluted into a certain antibiotic-containing 50 ml LB buffer, followed by an overnight 37 °C incubator.

On day 3, the overnight culture was 1:100 (v/v) diluted and then grown at 37 °C in a 250 rpm shaking incubator for 3.5 hours until O.D.600 reached 0.8. The cell culture was evenly separated into two aliquots and 0.5 mM IPTG was added as an inducer at 16 °C and 30 °C, respectively.

On day 4 and day 5, after a particular time for protein expression, centrifugation was used to separate the cells for 20 minutes at 4 °C at 5000 rpm. The cell pellet was then lysed for SDS-PAGE analysis. Before the lysis process, 1% (v/v) Phenylmethanesulfonyl fluoride (PMSF) and 0.7% (v/v) β-Mercaptoethanol (β-ME) were freshly added into different kinds of lysis buffer. His-binding buffer (20 mM sodium phosphate, pH 7.4, 500 mM NaCl, 20 mM imidazole, 10% glycerol), Tris-NaCl buffer (50 mM Tris-Hcl, 150 mM NaCl, pH 8.0, 10% glycerol), and PBS buffer (pH 7.4) with 10% glycerol are the three common choices. During the lysis, the samples were kept cool in an ice-water mixture. To separate the cell pellet and soluble protein, the lysate was centrifuged at 18000 rpm for 2 hours at 4 °C. SDS-PAGE analyzed the supernatant and pellet to confirm the solubility of the target protein. Protein bands were visualized by Coomassie brilliant staining, and the target protein could be verified by molecular weight using a protein ladder as a standard.

Once proper expression conditions were confirmed, the large-scale expression assay was performed in a similar way to the small-scale one (the timeline is shown in **Fig. 2.1**). The overnight culture was 1:100 (v/v) diluted into 800 ml of certain antibiotic-

containing LB buffer and 0.3 mM IPTG was added to induce the overexpression of target proteins, when the O.D.600 reached 0.8. An optimized lysis buffer was used during the sonication process. Meanwhile, the sonication program was set as follows: 50% amplitude, 10-sec pulse, 10-sec pause, 25 min. After sonication, the separated supernatant was filtered by a 0.22 µm membrane to get rid of small cell debris and bacteria.

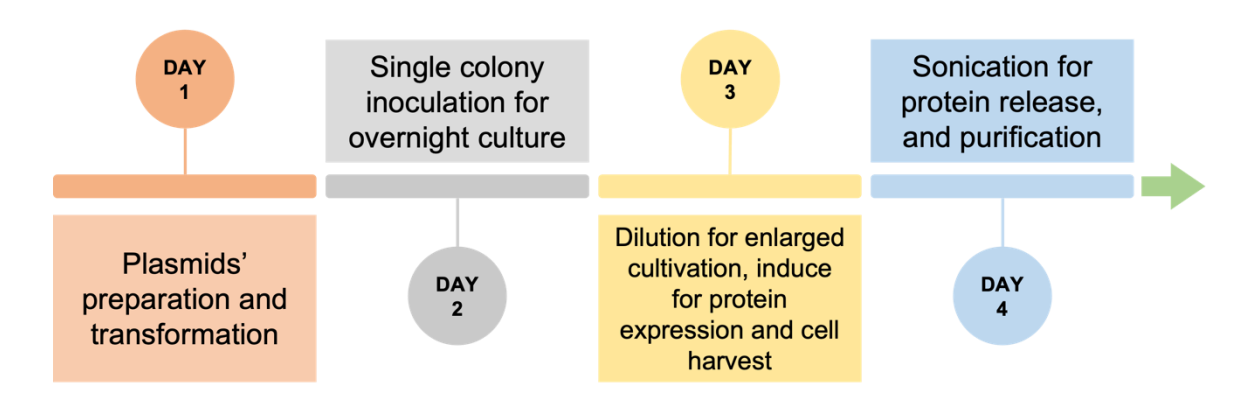


Fig. 2.1 Timeline for recombinant protein over-expression in *E.coli*

2.3 Purification

A series of protein purification methods were conducted to obtain a target protein with a satisfactory purity. The workflow was described as follows (Fig. 2.2).

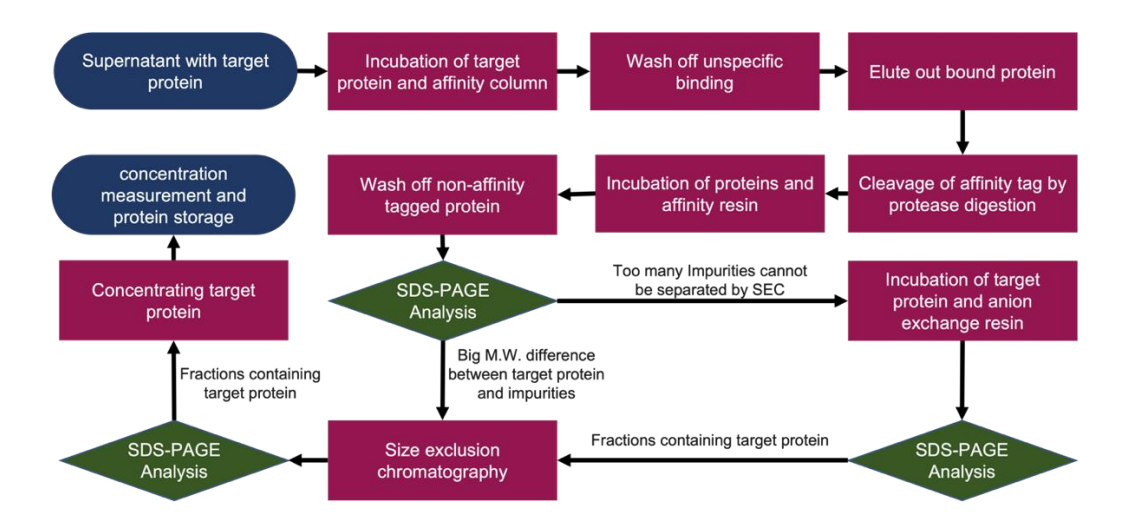


Fig. 2.2 The workflow for protein purification.

2.3.1 Affinity chromatography

Purification of His-tagged proteins

Fast protein liquid chromatography (FPLC, ÄKTAavantTM) was used to obtain purified His-tagged proteins. The purification process involved the use of three different buffers. The binding buffer consisted of 20 mM sodium phosphate, 0.5 M NaCl, 20 mM imidazole, pH 7.4, and 10% (v/v) glycerol. The elution buffer comprised 20 mM sodium phosphate, 0.5 M NaCl, 0.5 M imidazole, pH 7.4, while Tris buffer consisted of 50 mM Tris-HCl, 150 mM NaCl, pH 8.0.

Initially, the Ni²⁺ affinity column (HisTrapTM Fast Flow, CytivaTM) was washed using 5 column volumes (CV) of MilliQ water at a 5 ml/min flow rate, followed by 5 CV of elution buffer. After an equilibrium of washing with 6-8 CV binding buffer, the

protein sample was loaded at a 1 ml/min flow rate into the column using a 50 ml SuperloopTM assembly (CytivaTM). The flow-through sample was collected and kept cool on ice. An increase in UV280 was observed during the binding procedure, which eventually reached a plateau.

Next, the column was washed with the binding buffer at a 5 ml/min flow rate for 20 CV, and the last drop of the washing was collected. Non-specific binding impurities were commonly washed out at this step, resulting in a significant decrease in UV280, which gradually became a flat curve.

Bound proteins were eluted from the column using an elution buffer containing a high concentration of imidazole at a flow rate of 5 ml/min, and the eluted fraction was collected. The fraction was then concentrated, and the final volume was compressed using a corresponding molecular weight (M.W.) Amicon® Ultra 15 mL Centrifugal Filters (MerckTM). The buffer was changed to reduce the final concentration of imidazole to lower than 10mM by Tris buffer. At the elution step, UV280 increased dramatically, reached a peak value, and decreased to the baseline. Usually, a sharp peak was eventually formed.

Purification of Glutathione-S-transferase (GST) tagged proteins

Similar to the protocol for His tagged protein purification, the purification of GST-tagged proteins commonly uses two kinds of buffer:

- ◆ PBS buffer as the binding buffer
- ◆ Elution buffer: 50 mM Tris-HCl, 150 mM NaCl, pH 8.0, with 20 mM L-Glutathione (reduced, 98+%, Thermo Scientific™).

During the purification process, BeyoGoldTM GST-tag Purification Resin (BeyotimeTM) was used. The filtered protein sample was mixed with the GST resin and incubated on a roller at 4 °C for 1-2 hours. The mixture was then loaded into a Poly-Prep® Gravity flow column (Bio-RadTM), and the flow through was collected. The column was washed with 5 CV PBS with 0.1% (v/v) TritonTM X-100 (Sigma-Aldrich®) and 20 CV of PBS. The elution buffer was incubated with the resin for 20 minutes, and the last drop of the washing was collected. The eluted fraction containing the fusion protein was concentrated and buffer-exchanged to reduce the concentration of reduced L-Glutathione, using corresponding MW Amicon® Ultra 15 mL Centrifugal Filters (MerckTM). If the on-column digestion method was performed in the next step, the purification was stopped after the washing step.

2.3.2 Removal of the fusion tag using protease digestion

For off-column digestion, the eluted fusion protein was mixed with HRV-3C

protease (1 U/µl, 1 U for 0.5 mg protein) and incubated overnight at 4 °C. The digested

protein was then reloaded into the affinity column. The affinity tag, fusion partner, and

incompletely digested fusion proteins bound to the column, while the target protein

without the affinity tag and 3C protease flowed out with the wash buffer.

For on-column digestion, the protease was directly applied to the column and

incubated overnight at 4 °C. After the incubation, the target protein without the affinity

tag was separated by direct washing.

Finally, the fractions containing the target protein were concentrated.

2.3.3 Anion exchange chromatography

If the impurities had a similar molecular weight to the target protein or were a

series of impurities, anion exchange chromatography was performed to remove them.

Two types of buffer were used for anion exchange chromatography:

Buffer A: 10 mM Tris, 20 mM NaCl, pH 7.5

Buffer B: 10 mM Tris, 1 M NaCl, pH 7.5

42

Initially, the protein sample was changed into buffer A using Amicon®. The HiTrap Q HP anion exchange chromatography column (CytivaTM) was then eluted using buffer B for 8-column volumes, followed by equilibration with 8-column volumes of buffer A using FPLC. The sample was loaded into the column using a sample loop at a flow rate of 1 ml/min. Proteins were then eluted by gradient elution (increasing buffer B from 0% to 60% over 90 min). Different samples were eluted out as the concentration of NaCl increased. Fractions were collected for each peak.

After the SDS-PAGE analysis of the samples, the fractions containing pure target proteins were combined. Finally, the fractions were concentrated, and the buffer was exchanged into Tris buffer using Amicon[®].

2.3.4 Size exclusion chromatography (SEC)

Size exclusion chromatography was conducted for further purification. The protein's quality and folding can be assessed by analyzing the peak and retention time.

The Hi Load® Superdex 75 PG column (CytivaTM) was pre-equilibrated with cooled Tris buffer for 1 CV. The protein sample was then loaded into the column at a 1 ml/min flow rate. By separating different protein sizes, the target protein was washed out when the A_{280} increased dramatically and then decreased with the formation of a

single peak. SDS-PAGE tested fractions. Finally, the fractions containing pure target protein were combined and concentrated using Amicon[®].

2.3.5 Concentration measurement

The concentration of the purified protein was measured by NanoDropTM 2000/2000c Spectrophotometers. Nucleic acid contamination was assessed by checking the value of A260/280. A₂₈₀ shows the absorbance of tyrosine and tryptophan residues of the protein. Because of the linear relationship between A₂₈₀ and protein concentration, the concentration of purified protein can be calculated after dividing it by its extinction coefficient.

Another method was also used to double-confirm the protein concentration.

Bradford protein assay was used. PierceTM BCA Protein Assay Kit (Thermo FisherTM)

was used. The protein concentration can be calculated using bovine serum albumin with known concentration to generate the standard curve.

2.3.6 Storage of protein

The storage buffer is the Tris buffer. Considering the following requirements of experiments, no glycerol was added. The concentrated protein, with a concentration of

20 mg/ml or higher, was then divided into small aliquots, followed by fast frozen in liquid nitrogen, and subsequently stored at -80°C for long-term storage.

2.4 Biophysical and biochemical analysis

2.4.1 Light scattering

Light scattering was performed using a Wyatt Dawn 8+ system (Wyatt Technology) connected to an ÄKTA FPLC system (GE Healthcare) equipped with a size exclusion column (Superdex 200 10/30 GL, GE Healthcare). The purified protein (50-100 μg) was loaded into the column with a flow rate of 0.5 ml/min, following equilibration with the storage buffer. UV absorbance was detected at 280 nm, and a light scattering signal was detected at 662 nm. Data were analyzed using ASTRA 6.1 software (Wyatt Technology). The molecular weights of protein samples were calculated using their theoretical extinction coefficients at 280 nm, obtained from the ProtParam web server (ExPASy, http://web.expasy.org/protparam/).

2.4.2 Mass Spectroscopy (MS)

To confirm the molecular weight of Imp β and its constructs, 5 μ l of purified protein samples were loaded onto an ACQUITY UPLC BEH C18 Column, 130Å, 1.7 μ m, 3

mm X 100 mm. The Agilent 6460 Liquid Chromatography-Electrospray Ionisation
Triple Quadrupole Mass Spectrometer was used to collect and analyze MS spectra.

2.4.3 Pull-down assay

In order to identify protein-protein interactions *in vitro*, a pull-down assay was conducted. His₆-KPNB1_{FL} and its mutations were used as the "bait" proteins, and GST-tagged or untagged NFAT5 constructs were used as the "prey" proteins. The "bait-prey" heterogeneous complexes were eluted out of HisPurTM Ni-NTA Resin (Thermo ScientificTM), and the results were analyzed by SDS-PAGE stained with brilliant commissure blue.

2.4.4 Isothermal titration calorimetry (ITC)

Isothermal titration calorimetry (ITC) was performed using the MicroCalTM PEAQ-ITC (Malvern Panalytical Ltd). NFAT5 constructs and KPNB1 (full length and its constructs) were dialyzed into a buffer of 50 mM Tris-HCl, pH 8.0, and 150 mM NaCl or 10 mM Na₂HPO₄·7H₂O, 1.8 mM KH₂PO₄, 2.7 mM KCl, pH 7.4, and 150 mM NaCl. 150 μl of NFAT5 constructs at 1.5-1.75 mM was titrated into a sample cell loaded with 400 μl of KPNB1_{FL} at 50 μM. Typically, titrations consisted of 19 injections of 2 μl, with 150 s equilibration between injections. The data were analyzed using MicroCalTM PEAQ-ITC Analysis Software.

KPNB1 and RanQ69L-GppNHp were dialyzed into a buffer of PBS with 10% glycerol, 5 mM MgCl₂, and freshly added 2 mM DTT. His₆-KPNB1 (wild type and its mutants) and KPNA1 were dialyzed into a buffer of 50 mM Tris-HCl, pH 8.0, and 150 mM NaCl. ITC assays were performed for NFAT5_{cNLS} and KPNB1 (wild type and its mutants), NFAT5_{cNLS} and KPNA1_{ARM}, and RanQ69L-GppNHp and KPNB1, using a MicroCal VP-ITC calorimeter (Malvern) at 25°C. Each injection was a 10 μl aliquot of one protein in the syringe into its binding protein in the cell, with a time interval of 120 s to ensure that the titration peak returned to the baseline. The titration data were fitted to the one-site binding model using Origin 7.0 software.

2.5 Structure analysis: Single-particle cryo-electron microscopy (Cryo-EM)

2.5.1 Biochemical sample preparation

Crosslinked KPNB1_{FL}-NFAT5₁₇₁₋₂₅₃ complex preparation

To ensure the KPNB1_{FL}-NFAT5₁₇₁₋₂₅₃ complex remains intact at a concentration of 0.05- 5 μM for Cryo-EM, freshly purified KPNB1_{FL} and NFAT5₁₇₁₋₂₅₃ were mixed with a molar ratio 1: 3 and incubated on ice for 30 min. The complex was isolated by Hi Load® Superdex 75 PG column (CytivaTM) in 50 mM Tris-HCl, 150 mM NaCl, pH 8.0 buffer. Single peak fractions were analyzed on SDS-PAGE and collected. After concentration, the complex (0.2 mg/ml) was cross-linked by adding glutaraldehyde to

the final concentration of 0.1 % and incubating the mixture for 2 min at 37 °C. The reaction was stopped by adding 1 M Tris-HCl, pH 8.0 (final concentration is 150 mM). SDS-PAGE checked the cross-linked sample. Peak fractions were analyzed on the SDS-PAGE and collected using size-exclusion Hi Load® Superdex 75 PG column (CytivaTM) to remove higher order cross-links and aggregates further. Combined target samples were concentrated by 10K MW Amicon®.

No-crosslinked KPNB1_{FL}-NFAT5₁₇₁₋₂₅₃ complex preparation

Freshly purified KPNB1_{FL} and NFAT5₁₇₁₋₂₅₃ was mixed with different molar ratio (1: 10, 1: 20, 1: 30, and 1: 50), respectively, to check whether KPNB1_{FL} fully inhibited the phase separation behavior of NFAT5₁₇₁₋₂₅₃. Each mixture was incubated on ice for 30 minutes and centrifuged at 4 °C, 12,700 rpm for 30 minutes. Carefully took supernatant for Cryo-EM sample preparation. The buffer conditions of all samples were 50 mM Tris-HCl, 150 mM NaCl, and pH 8.0.

2.5.2 Single-particle cryo-electron microscopy (Cryo-EM)

Negative staining

Biochemical prepared samples (80 μ M, 107 KDa) were diluted into 30 folds for negative staining using Tris buffer. Negative staining revealed the solvent-excluded

surface, the shape of molecules, monodisperse, and homogeneity. 2 % (w/v) uranyl acetate (2% UA) in deionized H₂O solution was used as a staining reagent. 3ul diluted sample was applied onto a copper grid (continuous carbon, copper-made, 300 mesh) that was glow-discharged using PELCO easiGlowTM Glow Discharge Cleaning System. The sample was incubated on the grid for 30 seconds to 1 minute. Afterward, gently dry blot the grid from the side using filter paper. Then wash the grid twice with 3ul Tris buffer. Using 3 ul 2% UA solution staining for 20 seconds, blot away the staining leftover with filter paper and let it try completely before microscope imaging.

Vitrification and data collection

80 μM, 3 μl protein sample was applied onto the carbon side of the glow-discharged QuantifoilTM R 2/2 gold grid with 300 mesh and plunge-frozen into liquid ethane using Thermo Scientific Vitrobot IV. Blotting time was 4.5 s with blotting force 0. Thermo Scientific Krios G3i cryo-TEM microscope and Gatan K3 camera were used for data collection. Around 4620 movies were collected with a calibrated pixel size of 1.06 angstrom per pixel. Each one has 40 frames with a total exposure of 50 electrons per angstrom square.

2.6 In vitro Liquid-Liquid Phase Separation (LLPS) assays

For the LLPS assay, multiple buffers were prepared:

HS buffer: 50 mM Tris-HCl, pH 8.0, 500 mM NaCl or 25 mM HEPES, pH 7.4, 500

mM NaCl

LS buffer: 50 mM Tris-HCl, pH 8.0 or 25 mM HEPES, pH 7.4.

2.6.1 Protein labeling using fluorophore and labeling efficiency analysis

Alpha Fluor 488 NHS Ester (AAT Bioquest) was dissolved into DMSO as a final

concentration of 10 mM and used as a fluorophore to label NFAT5 constructs. Purified

NFAT5 constructs were exchanged into freshly made labeling buffer (100 mM NaHCO₃,

500 mM NaCl, 1 mM EDTA, and 1 mM DTT, pH 8.3) using a Hi-Trap desalting column

(CytivaTM). Alpha Fluor 488 NHS Ester was then added to the protein solution with a

1:1 molar ratio, and the mixture was incubated at room temperature for 1 h. After

quenched by 200 mM Tris-HCl, pH 8.2, the labeled protein was exchanged into High

Salt buffer (HS buffer) containing 50 mM Tris-HCl, pH 8.0, 500 mM NaCl, or 25 mM

HEPES, pH 7.4, 500 mM NaCl, using Hi-Trap desalting column. Fluorescence labeling

efficiency was detected using Nanodrop 2000 Spectrophotometer (ThermoFisherTM).

The final labeled proteins were adjusted to 1% by mixing with corresponding unlabeled

proteins at a ratio of 1:99.

2.6.2 *In vitro* droplet formation assay (DIC imaging and Fluorescence imaging)

50

Target proteins were diluted by the corresponding buffer to reach the targeted condition. For fluorescence imaging, 1% of the labeled protein was added. The Nikon Eclipse Ti2-E live-cell imaging system and Leica TCS SP8 MP Confocal Microscope with an HC PL Apo 63×/1.40 CS2 Oil objective lens were used for imaging droplet formation, respectively. A compartment of double-sided tape, a slide, and a cover slip was used for sample loading and sealed by vacuum grease after sample injection.

2.6.3 Phase diagram as a function of different influence factors

A series of sodium chloride and sorbitol concentrations were tested for the phase diagram as a function of different influence factors. Using Nikon Eclipse Ti2-E livecell imaging system, DIC imaging was used to measure different phase separation behaviors.

Target protein stocks were diluted into corresponding buffer conditions and protein concentrations. The samples were imaged, as long as an injection of the sample. A five-minute video was taken and followed by imaging of 3 randomly selected fields. If the number of droplets changed obviously within five minutes, and droplets were observed at all 3 different fields, the phase separation behavior can be identified under the condition.

2.6.4 In vitro fluorescence recovery after photobleaching (FRAP) assay and analysis

The FRAP assay *in vitro* was performed on Leica TCS SP8 MP Confocal Microscope at room temperature. Alexa 488 labeled proteins were used to label corresponding liquid droplets. FRAP experiments recorded three or four images before photobleaching at 10-s intervals. Defined regions were photobleached at 488 nm, and their proportional fluorescence intensities were collected every 30 s. Meanwhile, a neighboring region with a similar size was selected as a control for fluorescence intensity correction for each experiment. A third nearby region in the background was also selected as background signal subtraction during intensities' collection. All experiments were completed within 1 hour.

For data analysis, the intensity at the pre-bleach point was normalized to 100%, and the intensity right after the bleaching was set to 0%. All data are shown as mean \pm s.e.m., and graphs were generated by GraphPad Prism 8.

2.6.5 Sedimentation assay

Sedimentation assay was performed in a 50-µl volume system. Target protein stocks were diluted with LS buffer to proportional final protein concentration and buffer conditions. After a 5-minute incubation on ice or at room temperature, the samples were

centrifuged at 18,213 rcf and 4 °C for 10 minutes. The supernatant and pellet were immediately separated. The pellet was then resuspended and dissolved in 50 µl buffer, followed by vertexing for 10 seconds. SDS-PAGE analyzed the supernatant and pellet fractions, and protein bands were visualized by Coomassie brilliant staining. Each assay was repeated three times.

2.6.6 Turbidity assay

Target proteins were mixed with or without KPNB1 (at a 1:1 molar ratio) for the turbidity assay and diluted into a final protein concentration using LS buffer in a 100-μl volume system prior to the assay. The turbidity at O.D 395 or 500 nm was measured using a Nanodrop 2000 (ThermoFisherTM).

2.6.7 Quantification and Statistical Analysis

Parameters of statistics, such as the meanings and precise values of n (n refers to technical replicates, number of droplets, randomly selected fields, *etc.*), distributions, and variances are reported in the figures and corresponding figure legends. Statistical analysis was conducted using GraphPad Prism 8 software. All data were presented as mean \pm SD or \pm SEM. n.s., not significant, p > 0.05; ****, p < 0.0001 using one-way ANOVA with Tukey's or Dunnett's multiple comparisons test accordingly. No

statistical methods were used to determine the sample size whether the data met the statistical approaches' assumptions.

2.7 Cell-based experiments

2.7.1 Immunocytochemistry (ICC) assay

HeLa cells were cultured in Dulbecco's Modified Eagle's Medium (DMEM) (Sigma-Aldrich, D7777) supplemented with 10% FBS (GibcoTM, 26140079) and 1% penicillin-streptomycin (P.S.) (GibcoTM, 15140122) in a 5% CO₂, 37 °C incubator. Regular testing were performed to confirm that they were mycoplasma-free.For the ICC assay, HeLa cells were transfected with the corresponding cDNA using LipofectamineTM 2000 (Thermo Fisher Scientific, 11668027). Before transferring to a hypertonic or hypotonic media, transfected HeLa cells were maintained for 24 hours in an isotonic growth medium.

Transfected cells were treated with a hypertonic or hypotonic medium for multiple intervals. Afterward, the cells were washed thrice with pre-cooled PBS buffer at 4 °C. Then, the cells were fixed with 4% (w/v) paraformaldehyde (PFA) (Thermo ScientificTM) for 15 minutes, 4 °C. After three washes, the fixed cells were permeabilized with 1% (v/v) TritonTM X-100 (Sigma-Aldrich) in PBS buffer. Then, a solution of 0.5% TritonTM X-100 with 3% bovine serum albumin (BSA) (Sigma-

Aldrich) in PBS was used for blocking at room temperature for 30 minutes. The indicated proteins were then labeled with primary antibodies and corresponding secondary antibodies. Specifically, Anti-NFAT5 antibody (Abcam, ab33446), Myc-Tag antibody (Cell signaling technology, 9B11), Alexa 488 (Thermo ScientificTM, A11001, A11008) and Alexa 594 (Thermo ScientificTM, A21027) were used, respectively. The cells' nuclei were visualized by staining with 4,6-diamidino-2-phenylindole (DAPI; Sigma) or Hoechst 33342 (Thermo Fisher Scientific).

To record images and assess the nuclear-cytoplasmic shuttling and phase separation behavior of endogenous NFAT5 or transfected NFAT5 fragments, a Leica TCS SP8 MP confocal microscope system (with a 63× objective) was used.

2.7.2 Live cell imaging of phase separation behavior on NFAT5

HeLa cells transfected with AcGFP-NFAT5₁₋₅₄₃ were seeded on a 35mm confocal dish one day prior to imaging. Live-cell imaging was conducted using a Leica TCS SP8 MP Multiphoton/Confocal Microscope with a live-cell incubation chamber. The cell culture medium was replaced with a hypotonic medium just before imaging.

2.7.3 *In vivo* FRAP assay

HeLa cells transfected with AcGFP-NFAT5₁₋₅₄₃ or together with siControl or siKPNB1 were seeded on a 35mm confocal dish one day prior to imaging. Two hours before FRAP analysis, the transfected cells were incubated with the isotonic, hypotonic, or hypertonic medium. FRAP was performed using Leica TCS SP8 MP Multiphoton/Confocal Microscope with a 63x oil immersion objective. The region of interest (ROI) was bleached with 40% laser power, and the fluorescence recovery was monitored for the 60s (1 frame/2 s). The fluorescence intensity was quantified using Lecia LAS X software.

Chapter 3 Tonicity-driven nuclear import of NFAT5 depends only on KPNB1

3.1 NFAT5 undergoes tonicity-driven nucleocytoplasmic shuttling

Immunofluorescence imaging was carried out by our collaborator Dr. Ben Ko's lab to identify the bi-directional trafficking of endogenous NFAT5 (**Fig. 3.1**). The imaging results revealed that, under the isotonic condition, endogenous NFAT5 exhibited both nuclear and cytoplasmic localization under the isotonic condition at 120 minutes. Under the hypertonic condition, NFAT5 exhibited a predominant nuclear localization. However, under the hypotonic condition, NFAT5 became located predominantly in the cytosol with almost no presence in the nucleus.

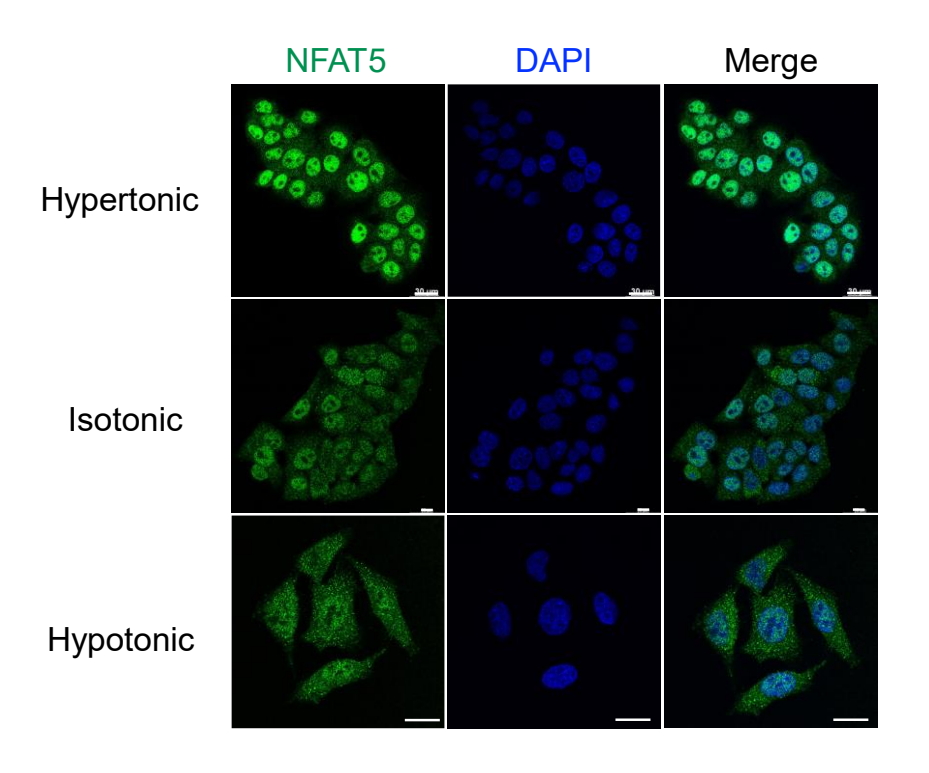


Fig. 3.1 Endogenous NFAT5 undergoes nuclear-cytoplasmic shuttling regulated by extracellular tonicity. HeLa cells were subjected to hypertonicity, isotonicity, and hypotonicity for 120 min. After treatments, cells were fixed and stained with an anti-NFAT5 antibody and Alexa 488 secondary antibody. Fluorescence images were captured using a confocal microscope. Scale bar: 30 μm.

3.2 Nuclear import of NFAT5 depends exclusively on KPNB1

3.2.1 Nuclear import of NFAT5 depends only on KPNB1 but not other KPNB members

A series of KPNBs have been identified to interact with different classes of NLS and mediate their nuclear import. To identify which member of KPNB family is involved in the nuclear import of NFAT5, Dr. Ko's lab performed siRNA knockdown assays depleting specific KPNBs, including KPNB1, TNPO1 (Kapβ2), IPO4 (Importin 4), IPO5 (Importin 5), IPO7 (Importin 7), IPO8 (Importin 8), IPO9 (Importin 9), IPO11 (Importin 11), IPO13 (Importin 13), and TNPO3 (Trn-SR). The knockdown efficiency of individual siRNAs has been examined (**Fig. 3.2 A**).

As a reporter, cytoplasmic phosphoenolpyruvate carboxykinase (PEPCK-C, also known as PCK1), is employed to characterize NLS activity (Theodore et al., 2008). Subcellular localization of Flag-NFAT5₁₃₂₋₂₆₄-PEPCK was studied in isotonic and

hypertonic conditions. The depletion of KPNB1 significantly suppressed the nuclear localization of Flag-NFAT5₁₃₂₋₂₆₄-PEPCK, whereas depletion of other KPNBs has little effect (**Fig. 3.2 B and C**). Western blotting supported these results, revealing a significant reduction in nuclear localization of the NFAT5 reporter when KPNB1 was knocked down with siRNA under both isotonic and hypertonic treatments (**Fig. 3.2 D**). In comparison, knockdown of other KPNB members such as TNPO1 or IPO4 had no effect (**Fig. 3.2 B**). Overall, these findings suggest that, among the many members of the KPNB family, only KPNB1 is essential for nuclear import of NFAT5.

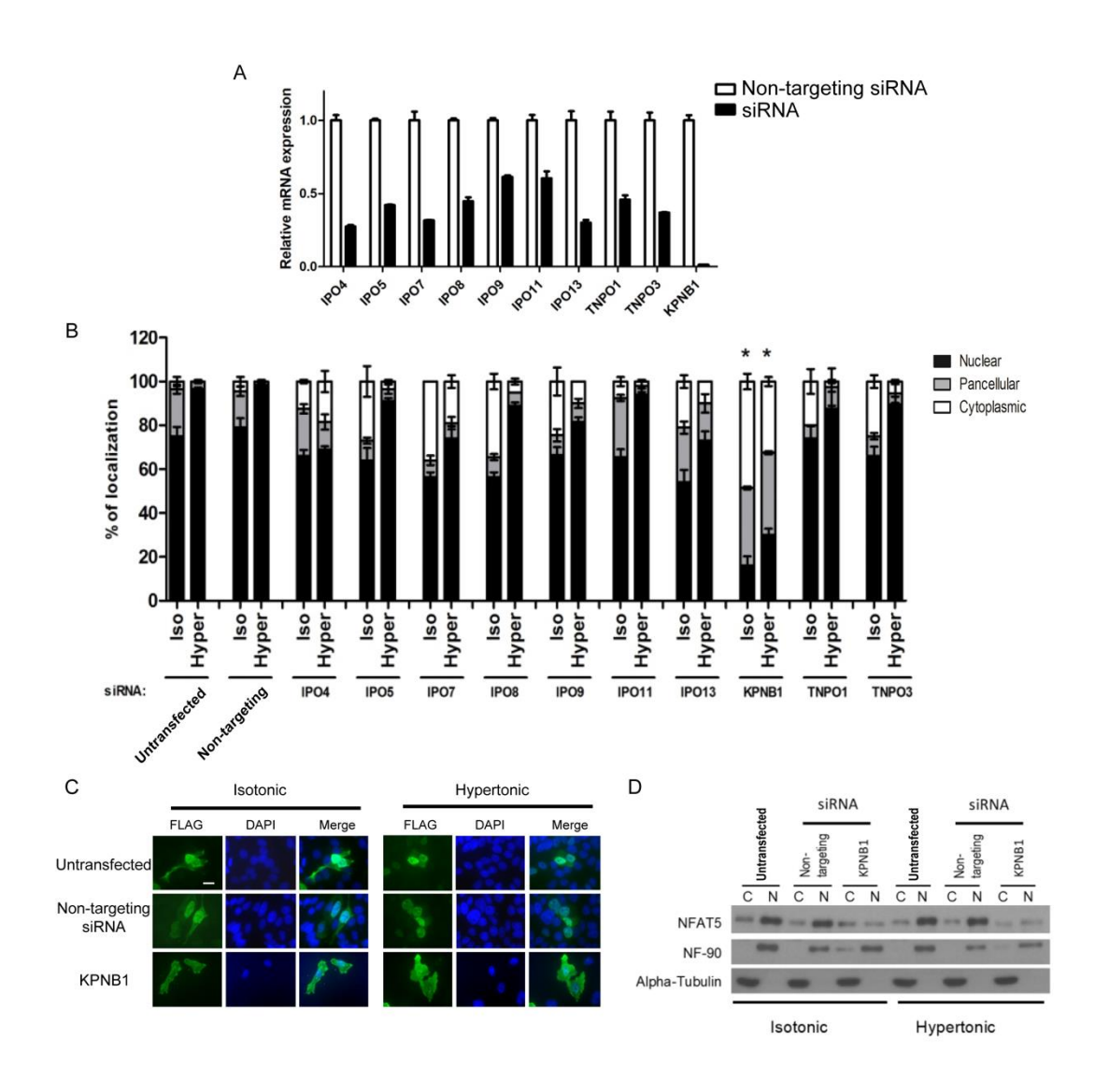


Fig. 3.2 KPNB1 is required for nuclear import of NFAT5. (A) Real-time quantitative PCR analysis of the expression of the indicated genes in non-targeting siRNA- and gene-specific siRNA-transfected cells. (B) Quantitative analysis of the subcellular localization of the fluorescent signal of flag-tagged proteins in HeLa cells transfected with Flag-NFAT5₁₃₂₋₂₆₄-PEPCK and siRNA targeting members of KPNB family, followed by 90-minute treatments with isotonic (Iso) or hypertonic (Hyper) medium. Anti-flag antibody and FITC-labeled secondary antibody were used to stain the cells, which were then counterstained with DAPI. In each condition, at least 100 cells were scored. The results were presented as the mean \pm s.e.m. of three independent experiments. (C) Immunofluorescence images of FLAG-NFAT5₁₃₂₋₅₈₁ in cells when KPNB1 was knocked down. FLAG antibodies were used, followed by FITC-labeled secondary antibodies and DAPI counterstaining. Scale bar is 30 µm. (D) Western blotting analysis of endogenous NFAT5 distribution in HeLa cells transfected with siRNA targeting KPNB1 at various extracellular tonicities. For the purpose of identifying nuclear and cytoplasmic markers, NF-90 and α-tubulin antibodies were utilized. Three independent experiments are represented.

3.2.2 Nuclear import of NFAT5 does not require KPNA family

To investigate the potential involvement of KPNA family in NFAT5 nuclear import, siRNA was designed to target various KPNA family members, including KPNA1 (IPOA5), KPNA2 (IPOA1), KPNA3 (IPOA4), KPNA4 (IPOA3), KPNA5 (IPOA6),

KPNA6 (IPOA7), and SNUPN (snurportin 1). Unlike KPNB1 knockdown, however, KPNA family depletion did not affect the nuclear import of Flag-NFAT5₁₃₂₋₂₆₄-PEPCK under isotonic and hypertonic treatments (**Fig. 3.3**). These findings imply that KPNAs are not necessary for the nuclear import of NFAT5.

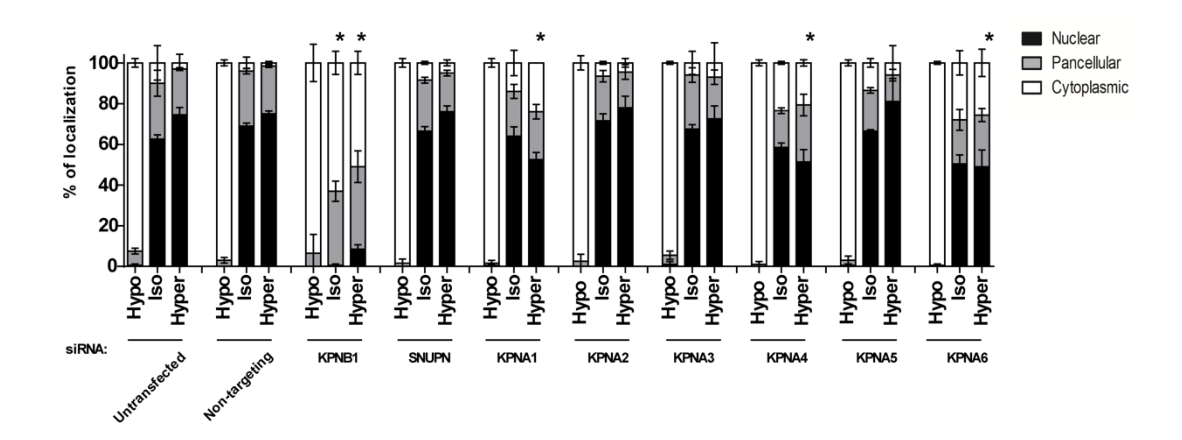


Fig. 3.3 KPNA family is not required for the nuclear import of NFAT5. Quantitative investigation of the immunofluorescence signal's subcellular localization in HeLa cells expressing Flag-NFAT5₁₃₂₋₅₈₁ and siRNAs that specifically target KPNB1 and the KPNA family members mentioned. Prior to fixation, cells were exposed to hypotonic (Hypo), isotonic, or hypertonic media for 90 min. Anti-flag antibody, FITC-labeled secondary antibody, and DAPI counterstaining were then used to identify the cells. More than 100 cells were scored in each condition. Data are presented as mean \pm s.e.m. of three independent experiments.

We examined the impact of peptide inhibitors for the KPNA/KPNB1 pathway, Bimax1 and Bimax2, to confirm that KPNAs were not engaged in NFAT5 nuclear import.(Kosugi et al., 2008). The cDNAs for Bimax1 and Bimax2 were inserted into

the BamHI and EcoRI sites of the pEGFP-N5 vector to generate the respective plasmids.

The target peptides were fused to the EGFP tag at the C-terminal end.

As demonstrated by immunofluorescence imaging, inhibition of KPNAs by ectopic expressed peptide inhibitors Bimax1 and Bimax2 had no effect on nuclear import of NFAT5 (**Fig. 3.4 A and B**). Under hypotonic conditions, nevertheless, the expression of Bimax1-EGFP and Bimax2-EGFP had no effect on the nuclear export of endogenous NFAT5 (**Fig. 3.4 A and B**). In contrast, the absence of KPNAs resulted in a loss of nuclear localization of Flag-SV40 large T antigen NLS fused to PEPCK (Flag-SV40_{NLS}-PEPCK) (**Fig.3.4 D**). These findings confirmed that the KPNA family is not involved in NFAT5 nuclear import.

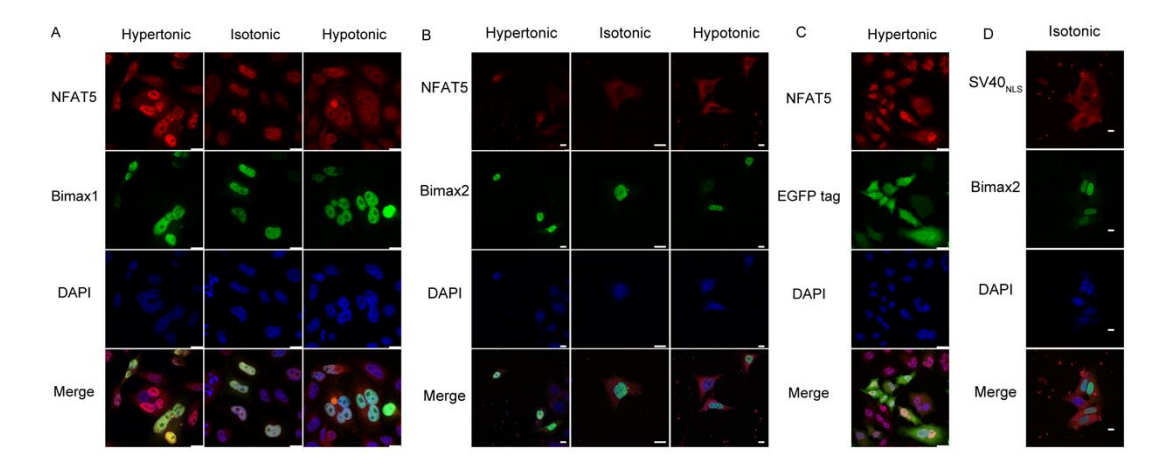


Fig. 3.4 Nuclear import of NFAT5 was not abolished by Bimax1 and Bimax2. (A and B) Cellular immunofluorescence images of endogenous NFAT5 nuclear localization. Bimax1-EGFP (A) and Bimax2-EGFP (B) were transfected into HeLa cells. (C) Endogenous NFAT5 nuclear localization under the expression of transfected EGFP as a control. (D) Flag-SV40_{NLS}-PEPCK was co-transfected with Bimax2-EGFP

as a control. After a 40-minute treatment, HeLa cells were fixed and incubated with corresponding antibodies. NFAT5 was detected using anti-NFAT5 antibody. Flag-SV40_{NLS}-PEPCK was detected using anti-flag antibody. NFAT5 and Flag-SV40_{NLS}-PEPCK were stained with Alexa 594 secondary antibody (red). The nucleus was stained with DAPI (blue). The scale bar is $10~\mu m$.

3.2.3 Reconstituted nuclear import assay confirms that the nuclear import of NFAT5 only depends on KPNB1

Since there was an underlying disparity between the required amino acid residues of NFAT5 for binding to KPNB1 *in vitro* and the process of nuclear import *in vivo*, Dr. Ko's lab developed and carried out *in vitro* nuclear transport experiments to better understand the underlying process.

Digitonin-permeabilized HeLa cells were used in the *in vitro* nuclear transport assay, along with recombinant proteins containing N-terminal His₆-tag, C-terminal monomeric green fluorescent protein (AcGFP), and NFAT5₁₇₁₋₂₅₃. Purified recombinant proteins His₆-SV40_{NLS} fused to AcGFP (His₆-SV40_{NLS}-AcGFP) and His₆-AcGFP were also used as controls.

First, both His6-NFAT5₁₇₁₋₂₅₀-AcGFP and His6-SV40_{NLS}-AcGFP were able to relocate to the nucleus when cytosolic extracts, an ATP-regeneration mixture, and

RanGTP were added. However, the nuclear pore inhibitor wheat germ agglutinin (WGA), high concentrations of GTP, or nonhydrolyzable GTP analog (GTPγS) inhibited their nuclear import activities (**Fig. 3.5 A**). His₆-AcGFP was not imported into the nucleus as a control because it lacked a NLS domain. These results showed that His₆-SV40_{NLS}-AcGFP and His₆-NFAT5₁₇₁₋₂₅₀-AcGFP both undergo ATP/GTP-dependent nuclear import via nuclear transport receptors (NTRs), which are universal cytosolic factors.

To investigate the mechanism of His6-NFAT5₁₇₁₋₂₅₀-AcGFP nuclear import, NTRs, including KPNA1 and KPNB1, and defined factors such as RanGTP, nuclear transport factor 2 (NTF2), an ATP-regenerating mixture, and WGA were tested *in vitro*. Both His6-NFAT5₁₇₁₋₂₅₀-AcGFP and His6-SV40_{NLS}-AcGFP failed to translocate into the nucleus in the absence of any of the aforementioned factors (**Fig. 3.5 B, lane 1**). In the absence of KPNB1, the nuclear import of His6-NFAT5₁₇₁₋₂₅₀-AcGFP was completely lost, whereas KPNA1 was not required for its nuclear import (**Fig. 3.5 B, lane 3, lane 4, and lane 5**). WGA effectively blocked the import of both His6-NFAT5₁₇₁₋₂₅₀-AcGFP and His6-SV40_{NLS}-AcGFP in the presence of exogenous factors (**Fig. 3.5 B, lane 2 and 3**), indicating that SV40_{NLS} nuclear import was mediated via the KPNA/KPNB1 pathway (**Fig. 3.5 B, lane 3 and lane 4**). These findings confirmed that NFAT5 nuclear import was entirely dependent on KPNB1.

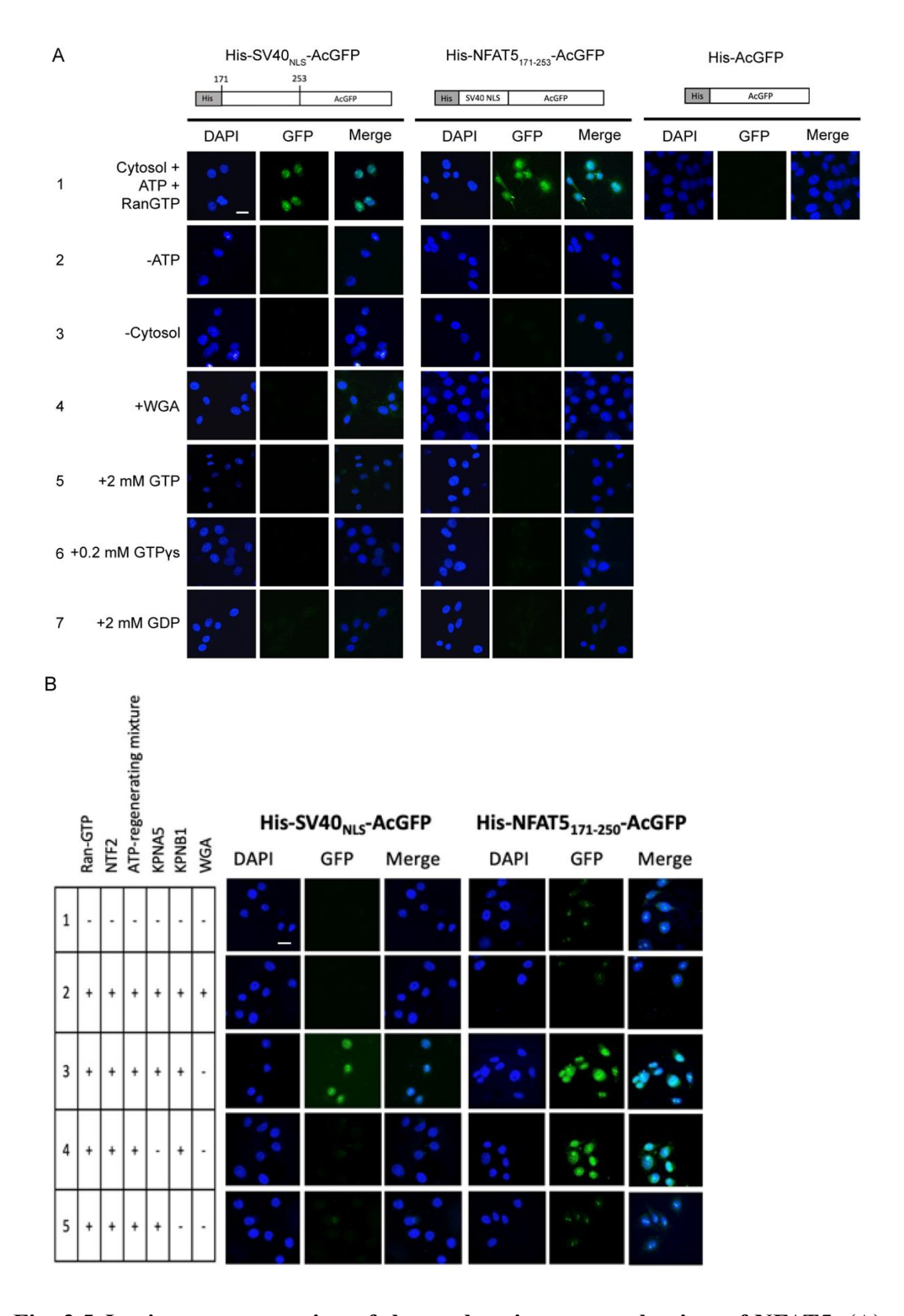


Fig. 3.5 In vitro reconstruction of the nuclear import mechanism of NFAT5. (A)

Digitonin-permeabilized HeLa cells were used to assess nuclear import of His6-SV40 $_{NLS}$ -AcGFP, His6-NFAT5 $_{171-250}$ -AcGFP, and His6-AcGFP. (B) The nuclear

localization of His₆-SV40_{NLS}-AcGFP and His₆-NFAT5₁₇₁₋₂₅₀-AcGFP was determined using digitonin-permeabilized HeLa cells supplemented with the indicated nuclear transport factors. The transport assay lasted 30 minutes at 37 °C. Fluorescence images were captured using a confocal microscope after cells were fixed and stained with DAPI. The scale bar represents 30 μ m. Three independent technical repeats are represented by the images.

Chapter 4 Biochemical and functional mapping of the full NLS segment in NFAT5 responsible for tonicity-driven nuclear import

4.1 Functional mapping confirms NFAT5₁₇₁₋₂₅₃ as the full NLS for tonicity-driven nuclear import

Previous research from our collaborator Dr. Ko's lab has shown that Flag-NFAT5₁₃₂₋₅₈₁, which lacks the N-terminal NES and C-terminal transactivation domains, retains the same bidirectional transport activity as endogenous NFAT5 in response to changes in tonicity (Tong et al., 2006; Xu et al., 2008). This truncated recombinant NFAT5 contains an AED domain, which is essential for nuclear export activity under hypotonicity. It also has a putative cNLS domain (NFAT5₁₉₉₋₂₁₆) and a Rel-homology DNA-binding (RHD) domain (residues 264-581). However, this construct does not contain the NES domain that facilities nucleocytoplasmic trafficking of NFAT5 under isotonic circumstances. To further identify the minimal region of NFAT5 responsible for its nucleocytoplasmic shuttling, Dr. Ko's lab generated a series of deletion mutants, including Flag-NFAT5₁₃₂₋₂₆₄-PEPCK that consists of AED and cNLS domain and Flag-NFAT5₁₉₈₋₂₁₇-PEPCK that contains cNLS domain (**Fig. 4.1 A**).

Under hypotonic and isotonic conditions, Flag-NFAT5₁₃₂₋₅₈₁ was localized to the cytoplasm. It was imported into the nucleus under hypertonicity (**Fig. 4.1 B**). To assess whether the RHD domain is required for tonicity-driven nuclear import, we swapped it

with the cytoplasmic phosphoenolpyruvate carboxykinase (PEPCK-C) to generate a Flag-NFAT5₁₃₂₋₂₆₄-PEPCK construct. This protein is large (M.W. ~83 KDa) and can preclude a passive nuclear transport mechanism. As shown in Fig. 4.1B, Flag-NFAT5₁₃₂₋₂₆₄-PEPCK was located in the nucleus under hypertonic conditions and in the cytosol under hypertonic conditions. This pattern is similar to that seen in Flag-NFAT5₁₃₂₋₅₈₁. However, replacing RHD with PEPCK lead to a moderate decrease of the nuclear import, indicating that RHD plays a minor role in NFAT5 nuclear import. Dr. Ko's lab also generated another construct Flag-NFAT5₁₉₈₋₂₁₇-PEPCK, which only contains the cNLS domain and PEPCK. This construct did not localize to the nucleus under hypertonicity or in the cytoplasm under hypotonicity (Fig. 4.1B). Flag-PEPCK, as a control, was distributed uniformly throughout the cell and did not respond to changes in extracellular tonicity (Fig. 4.1 B). These findings suggest that NFAT5's nucleocytoplasmic transport activity is mediated by residues 132-264, which consist of AED (residues 132-156), cNLS (residues 199-216), and the flanking sequences around cNLS. Notably, the cNLS domain alone is essential of but insufficient for nuclear import.

For the next step, Dr. Ko's lab further delineated the minimal region that is necessary for nuclear import. Firstly, a series of Flag-NFAT5- PEPCK constructs that scanned through the 132-264 region of NFAT5 were generated (**Fig. 4.1 C**). When the AED domain was removed, Flag-NFAT5₁₅₉₋₂₆₄-PEPCK maintained its nuclear import activity but lost its nuclear export ability when cells were subjected to tonicity stress

(Fig. 4.1 C). This is consistent with Dr. Ko's previous findings that AED regulate the nuclear export of NFAT5. In the deletion mapping analysis, Flag-NFAT5₁₇₄₋₂₆₄-PEPCK had a comparable percentage of nuclear localization to Flag-NFAT5₁₅₉₋₂₆₄-PEPCK (Fig. **4.1** C). It means the removal of residues 159-173 of NFAT5 did no effect on the nuclearimport activity. In comparison, the percentage of nuclear localization of Flag-NFAT5₁₈₉-₂₆₄-PEPCK was decreased. It indicates that the amino acid residues 174-189 play a significant role in nuclear import. Similarly, when amino acid residues 189-198 were removed, the nuclear import of Flag-NFAT5₁₉₈₋₂₆₄-PEPCK was completely abolished and was always located in cytosol regardless of extracellular tonicity. The result indicates the importance of residues 189-198 for nuclear import. Flag-NFAT5₁₇₄₋₂₅₀-PEPCK and Flag-NFAT5₁₇₄₋₂₆₄-PEPCK showed a comparable nuclear localization percentage. This reveals that residues 250-264 are not required for nuclear import. However, removing residues 240-250 (Flag-NFAT5₁₇₄₋₂₄₀-PEPCK) and 230-240 (Flag-NFAT5₁₇₄₋₂₃₀-PEPCK) resulted in a significant loss of nuclear import ability. This suggests the importance of residues 230-250 for nuclear import.

In summary, the above studies confirm that while the cNLS of NFAT5 plays a crucial role in its nuclear import, it is not sufficient on its own. To achieve full tonicity-driven nuclear import activity, residues 174-250, termed as the full NLS, is required.

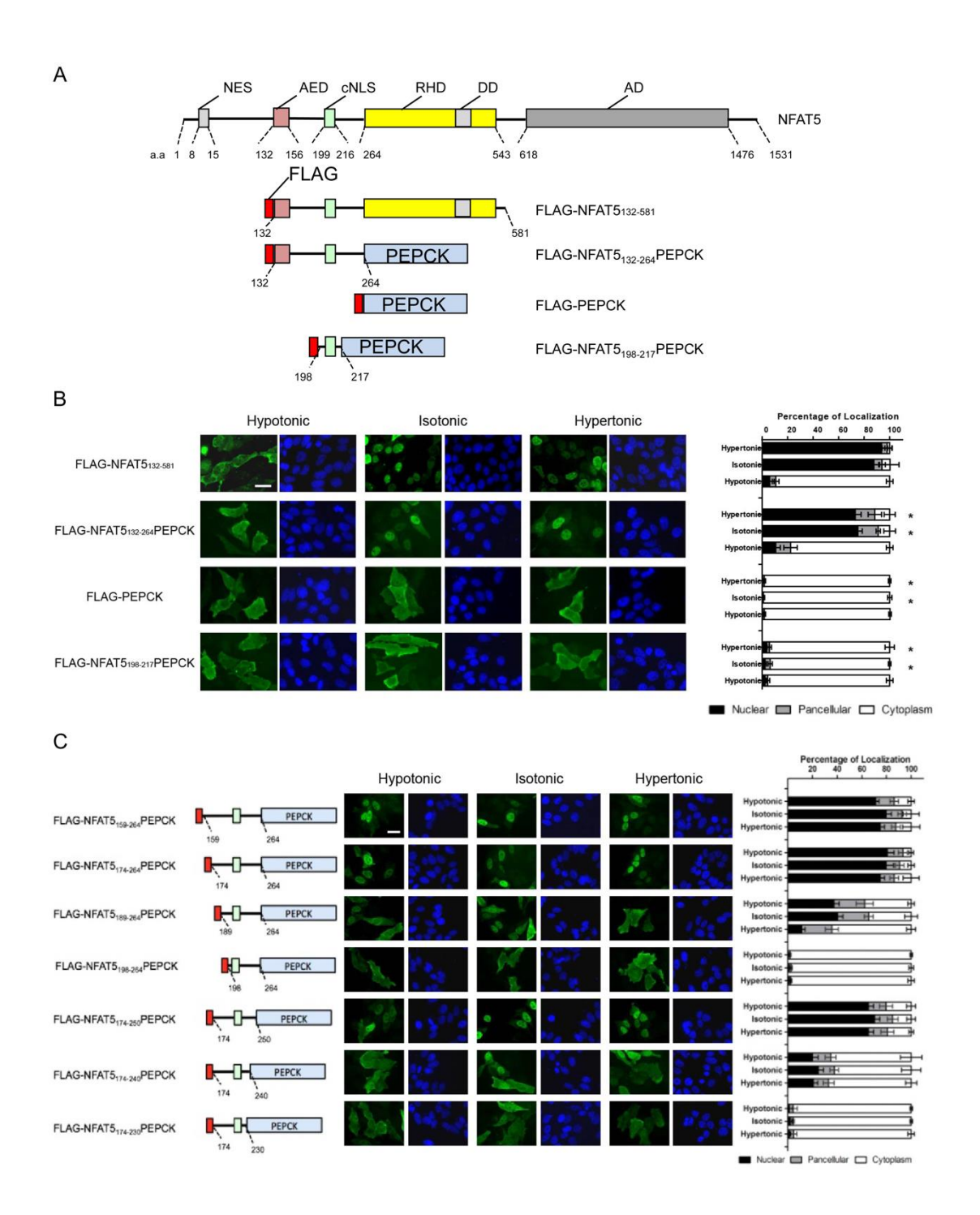


Fig. 4.1 Functional mapping of the minimal required domain for NFAT5 nuclear-import function. (A) Schematic diagram showing the functional domains of NFAT5, including the dimerization domain (DD), transactivation domains (AD), and amino acid residue numbers (a.a.). (B) Left: immunofluorescence images of corresponding fusion proteins. For 90 minutes, HeLa cells were exposed to hypotonic, isotonic, or hypertonic

media. Cells were counterstained with DAPI (blue) after being stained with a FLAG antibody and FITC-labeled secondary antibody (green). Right: Quantitative data demonstrating the subcellular localization of the FLAG-NFAT5 and FLAG-NFAT5-PEPCK constructs' fluorescence signals under each condition. (C) Deletion mapping analysis of the minimal functional domain of NFAT5 for its nuclear import. Left: Immunofluorescence images of corresponding fusion proteins. Structural features were shown, and amino acids were labeled. Middle: Immunofluorescence images of cells expressing the recombinant FLAG fusion constructs. Cells were treated with hypotonic, isotonic, or hypertonic medium for 90 minutes. Right: Quantification data showing the percentages of subcellular localization of the FLAG fusion NFAT5 fragments' fluorescence signal in HeLa cells expressing corresponding fusion constructs in each condition. In (B) and (C), more than 100 cells were scored in each treatment. The data are presented as mean ± s.e.m. of three independent experiments. *P<0.0001 (one-way ANOVA with Bonferroni's multiple comparison test). Scale bar: 30 μm.

4.2 Reconstituted nuclear import assay confirms NFAT5₁₇₁₋₂₅₃ is sufficient for tonicity-driven nuclear import

Dr. Ko's lab has identified the minimal region needed for nuclear import of NFAT5. However, since there was a discrepancy between the required amino acid residues of NFAT5 for binding to KPNB1 *in vitro* and nuclear import *in vivo*, the lab conducted *in vitro* nuclear transport assays with NTRs and defined factors. They purified a series of

His₆-NFAT5_{NLS} fragments fused to a monomeric green fluorescent protein (AcGFP) (**Fig. 4.2**).

Using HeLa cells that have been digitonin-permeabilized and added with RanGTP, NTF2, and ATP-regenerating mixture, with or without the addition of KPNB1, nuclear import of these purified proteins was evaluated. The results showed that the nuclear import of cNLS requires the heterodimer formation of KPNA1-KPNB1 since nuclear localization of His₆-SV40_{NLS}-AcGFP was eliminated in the absence of KPNA1 (**Fig. 4.2, lane 1**).

Compared with His6-NFAT5₁₇₁₋₂₅₀-AcGFP, both His6-NFAT5₁₇₁₋₂₂₀-AcGFP and His6-NFAT5₁₉₀₋₂₅₀-AcGFP were localized to the nucleus, indicating that neither the deletion of amino acid residues 220-230 nor the deletion of amino acid residues 171-189 affected the KPNB1-mediated nuclear import (**Fig. 4.2, lane 2, lane 3, and lane 5**). However, nuclear localization of His6-NFAT5₂₂₀₋₂₅₀-AcGFP was severely inhibited when amino acid residues 171-220 were removed, revealing the critical role of amino acid residues 171-220 (**Fig. 4.2, lane 6**). Additionally, although the fusion protein contained the cNLS domain, no localization of His6-NFAT5₁₉₀₋₂₃₀-AcGFP was detected (**Fig. 4.2, lane 4**).

Notably, the nuclear localization of all NFAT5 fusion proteins was abolished without the precipitation of KPNB1 (Fig. 4.2). In light of these findings, it is evident

that NFAT5_{NLS} amino acids 189-250 represent the minimal region required for nuclear import activity.

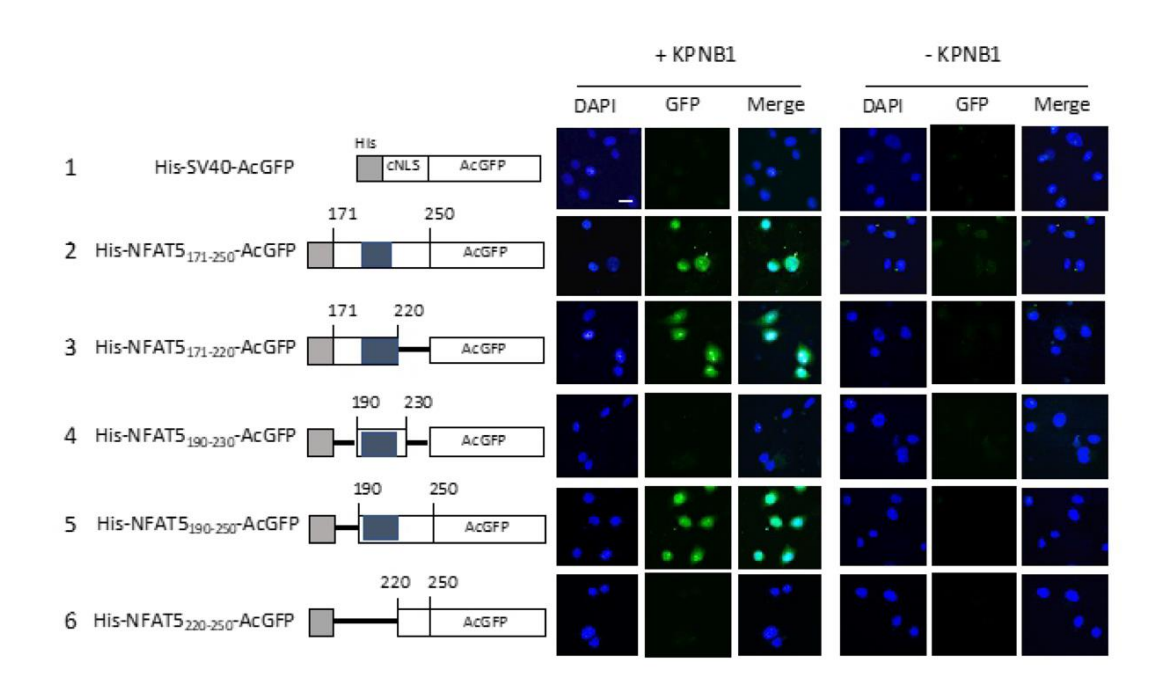


Fig. 4.2 The determination of nuclear import of His₆-tagged NFAT5 fragments with C-terminal AcGFP. The left panel shows the schematic representation of the corresponding constructs. Shaded regions indicate NFAT5-cNLS. In the right panel, *in vitro* nuclear import assay of His₆-SV40_{NLS}-AcGFP and the indicated NFAT5 fusion proteins was performed using digitonin-permeabilized HeLa cells supplemented with RanGTP, NTF2, and ATP-regenerating mixture, with or without the addition of KPNB1. The transport assay was carried out for 30 minutes at 37 °C. Cells were then fixed, followed by staining with DAPI. Confocal microscopy was used to capture fluorescence images. The scale bar represents 30 μm. Images represent three independent experiments.

In addition, Dr. Ko's lab previously found that the triple-mutant R202A_K203A_R204A of NFAT5_{cNLS} eliminated the nuclear import of NFAT5, supporting the important role of cNLS in the nuclear import of NFAT5 (**Fig. 4.3**) (Tong et al., 2006).

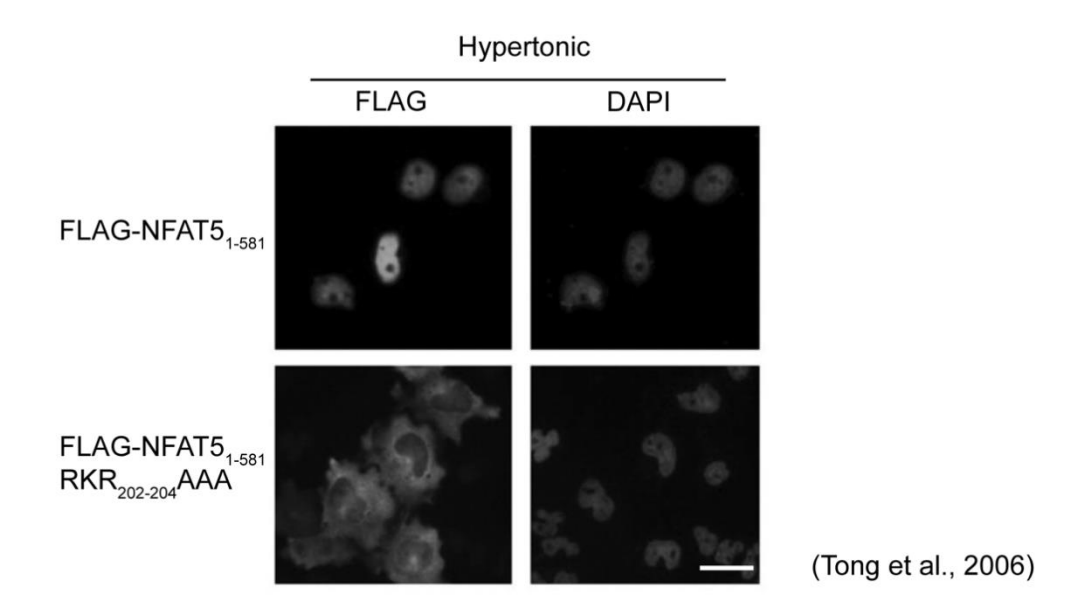


Fig. 4.3 Mutational analysis of the NFAT5_{cNLS} (published data). Representative fluorescence images of fixed HeLa cells expressing FLAG-NFAT5₁₋₅₈₁, FLAG-NFAT5₁₋₅₈₁RKR₂₀₂₋₂₀₄AAA. The NFAT5-expression plasmids were transfected into the appropriate cell types. The cells were then exposed to the hypertonic media for 90 minutes. Using a FLAG antibody and a secondary antibody that was FITC-labeled, FLAG signal was seen following fixation. The cells were examined using fluorescence microscopy after being counterstained with DAPI. Scale bar, 100 μm.

4.3 Biochemical mapping confirms the interaction between the full NLS of NFAT5 and KPNB1

4.3.1 Design, expression, and purification of various NFAT5 constructs to scan through the full NLS region

To investigate the direct interaction between NFAT5 full NLS proteins and KPNB1, we generated a series of NFAT5 constructs that scanned the full NLS region (amino acid 171-253).

To obtained target proteins, Trx-His6-NFAT5₁₇₁₋₂₅₃, for example, was purified. It was overexpressed for 6 hours at 30 °C after being induced with 0.3 mM IPTG. After 15 minutes of centrifugation at 6000 rpm, the bacteria were collected. In the Hisbinding lysis buffer, the bacterial pellet was sonicated for 30 minutes at a 55 percent amplitude to lyse it. After 60 minutes of centrifugation at 20,000 rpm, the supernatant was loaded onto a nickel-charged immobilized metal affinity chromatography (IMAC) column. The fusion protein was then eluted using a gradient of 45–500 mM imidazole. The protein was then reloaded onto a nickel-charged IMAC column after being digested by HRV 3C protease. NFAT5₁₇₁₋₂₅₃ was then washed out by Tris buffer (**Fig. 4.4 A**). Following gel filtration, high-purity NFAT5₁₇₁₋₂₅₃ was obtained (**Fig. 4.4 B**). The same purification procedure was used for NFAT5₁₅₁₋₂₁₆, and the purified proteins were determined by SDS-PAGE (**Fig. 4.4 C**).

Mass spectrometry was performed to confirm the molecular weights of purified proteins. The mass spectrum showed that the measured molecular weight of NFAT5₁₅₁₋₂₁₆ and NFAT5₁₇₁₋₂₅₃ was 7.8 kDa and 9.5 kDa, respectively, consistent with their theoretical values of 7.6 kDa and 9.3 kDa (**Fig. 4.4 D and E**). These results indicate that target proteins were obtained with the purity of over 80%.

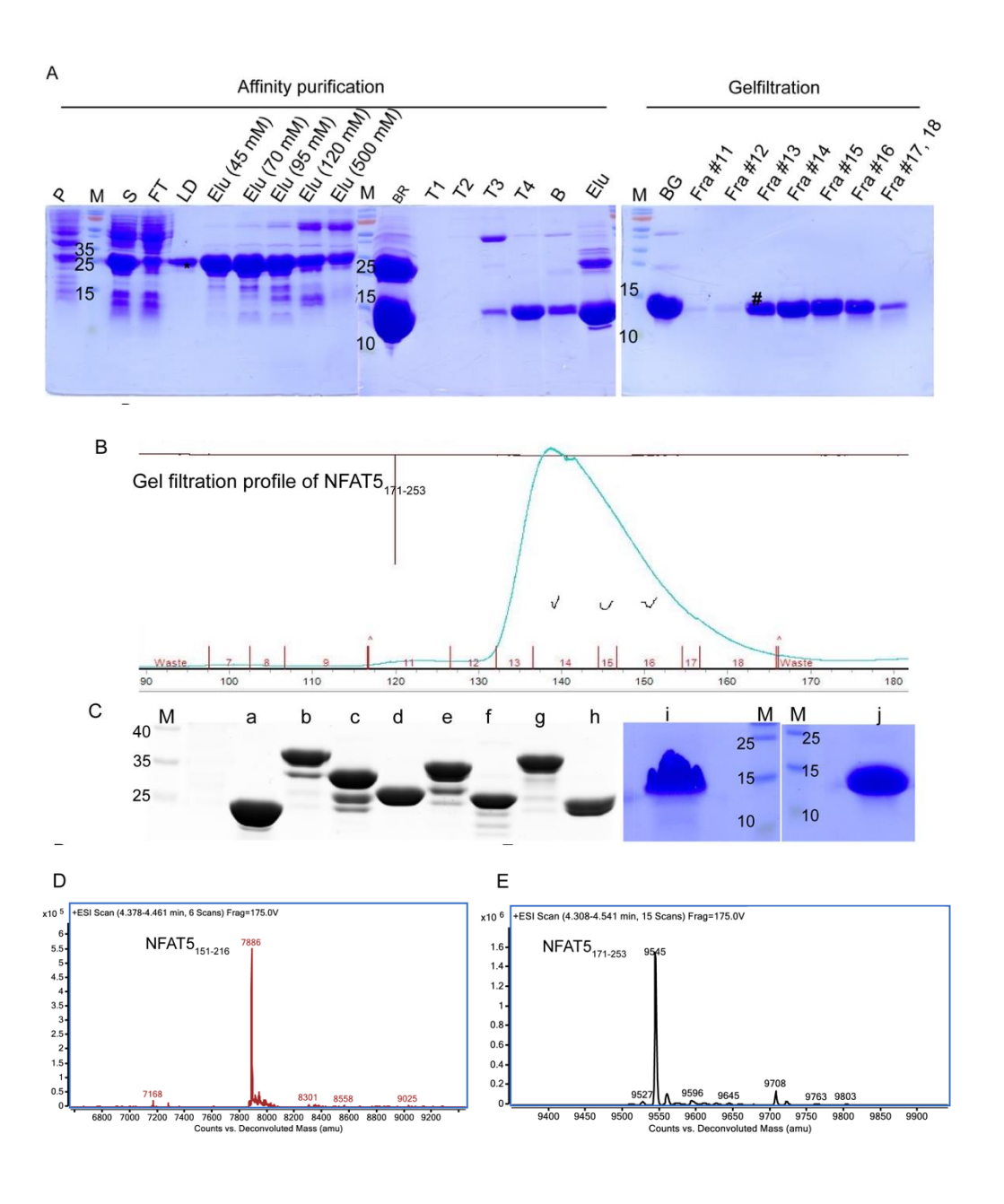
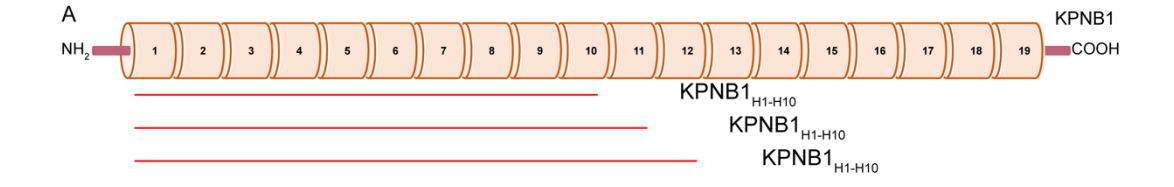


Fig. 4.4 Purification of NFAT5 constructs. (A) SDS-PAGE analysis of NFAT5₁₇₁₋₂₅₃: the target fusion protein is indicated by an asterisk on the left; purification of NFAT5₁₇₁-253 after removing the fusion tag in the middle; fractions after gel filtration were collected, and NFAT5₁₇₁₋₂₅₃ was indicated by a pound sign on the right. SDS-PAGE was used to characterize the protein solubility and purification of NFAT5 constructs after IMAC. "P" and "S": the pellet (P) and supernatant (S) of the cell lysate after centrifugation. "FT" (flow-through): the protein not captured by the affinity column during sample loading. "LD" (last drop of wash): the last drop of the wash procedure using a binding buffer containing 20 mM imidazole. "Elu": the target proteins that were eluted out by the elution buffer containing the corresponding concentration of imidazole. "BR" and "BG": the samples before loading to the affinity column (BR) or size exclusion column (BG). "T1", "T2", "T3", "T4" and "B": samples that were washed out by Tris buffer (T) for four fractions, or by binding buffer with 40 mM imidazole (B). "Elu": the tag and nonspecific bound impurities that were eluted out by the elution buffer with 500 mM imidazole. "Fra #11,12 - #18": collected fractions. (B) The profile of gel filtration of NFAT5₁₇₁₋₂₅₃. (C) Final purity of concentrated proteins. M: marker, a: GST tag, 26 kDa; b: GST-NFAT5₁₇₁₋₂₅₃, 35.5 kDa; c: GST-NFAT5₁₇₁₋₂₂₀, 32.13 kDa; d: GST-NFAT5₂₂₀₋₂₅₃, 29.7 kDa; e: GST-NFAT5₁₉₀₋₂₅₃, 33.3 kDa; f: GST-NFAT5₁₉₈₋₂₁₇, 27.9 kDa; g: GST-NFAT5_{171-253-R202AK203A}, 35.4 kDa; h: GST-SV40_{NLS}, 26.36 kDa; i: NFAT5₁₅₁₋₂₁₆, 7.6 kDa; j: NFAT5₁₇₁₋₂₅₃, 9.3 kDa. (D) Mass spectrum of NFAT5₁₅₁₋₂₁₆ and NFAT5₁₇₁₋₂₅₃.

4.3.2 Expression and purification of KPNA1_{ARM}, KPNB1 and its constructs

Our results suggest that KPNB1 acts as both the adaptor and receptor for the nuclear import of NFAT5. KPNB1 composes of 19 HEAT repeats, with the N-terminal 12 HEAT repeats (KPNB1_{H1-H12}) reported as the binding surface for cargoes (**Fig. 4.5 A**). To map the binding region within KPNB1 for NFAT5 binding, we generated three KPNB1 constructs within the N-terminal 12 HEAT repeats, including KPNB1_{H1-H10}, KPNB1_{H1-H11} and KPNB1_{H1-H12}. KPNB1 was inserted into BamHI and NotI restriction sites of the pETM vector containing a His₆ tag and HRV 3C protease digestion site. KPNB1_{H1-H10}, KPNB1_{H1-H11} and KPNB1_{H1-H12} were inserted into the BamHI and NotI sites of the pGEX-4T.1 vector containing a GST tag and HRV 3C protease digestion site. KPNB1_{H1-H10} was purified using IMAC, followed by anion exchange chromatography and size exclusion chromatography. The target protein was then concentrated after SDS-PAGE analysis. As shown in **Fig. 4.5 B-D**, KPNB1_{H1-H10} was purified and obtained with high purity of over 80%.



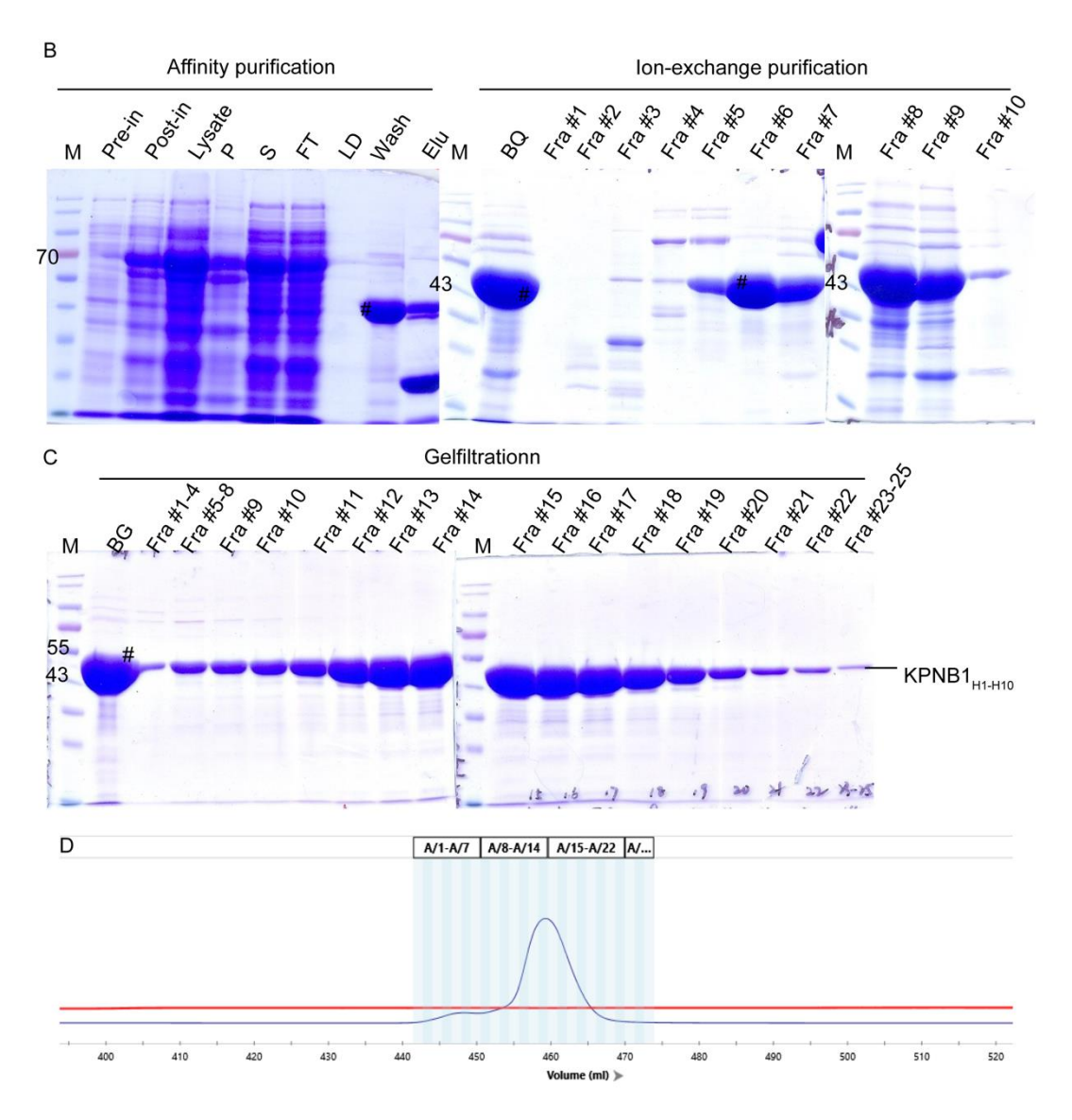


Fig. 4.5 KPNB1 Constructs Design and Purification. (A) Schematic diagram of KPNB1 and its constructs. (B and C) SDS-PAGE analysis of the purification of KPNB1_{H1-H10}. (D) Gel filtration profile of KPNB1_{H1-H10}. M: marker; pre-in and post-in: whole cell lysate before (pre) or after (post) IPTG induction; Lysate: sonicated cell pellet before centrifugation; P an S: pellet (P) or supernatant (S) of cell lysate after centrifugation; FT (flow-through): protein that wasn't captured by the affinity column during sample loading; LD: the last drop of wash procedure using binding buffer containing 40 mM imidazole; Elu: fractions of elution buffer were collected; BR, BQ and BG: before loaded samples to the affinity column (BR), ion-exchange column (BQ)

or size exclusion column (BG); "T1, T2"; "B1, B2": sample was washed out by Tris buffer (T) or binding buffer with 40 mM imidazole (B), and two fractions were collected; Elu: Tag and nonspecific bound impurities were eluted out by elution buffer with 500 mM imidazole; Fra #1, 2, 3, etc.: samples were washed out by corresponding buffer, and fractions were collected.

In addition, our previous findings in Chapter 3 confirmed that KPNB1 was essential for the nuclear localization of NFAT5, while KPNA1 was not required. We therefore investigated the differences in the binding affinity of NFAT5_{cNLS} to KPNB1 and NFAT5_{cNLS} to KPNA1 through ITC experiments.

According to previous research, in KPNA/KPNB1 pathway, cNLS was imported into the nucleus by binding to the C-terminal ARM domain of KPNA1 (Pumroy et al., 2012). Following this, we purified KPNA1_{ARM} (residue 66-538) using a purification protocol similar to that used for KPNB1_{H1-H10}.

Final purity of the target proteins was assessed by SDS-PAGE (**Fig. 4.6 A**). Mass spectrometry was conducted to confirm the molecular weights of purified KPNA1_{ARM}, KPNB1, and its constructs. The results showed that KPNB1_{H1-H10} was 49.6 kDa, KPNB1_{H1-H11} was 54.1 kDa, KPNB1_{H1-H12} was 60.2 kDa, KPNB1 was 97.2 kDa, and KPNA1_{ARM} was 52.7 kDa, all of which are equal to their theoretical values 49.63 kDa, 54.15 kDa, 60.2 kDa, 97 kDa, and 52.8 kDa, respectively (**Fig. 4.6 B-F**).

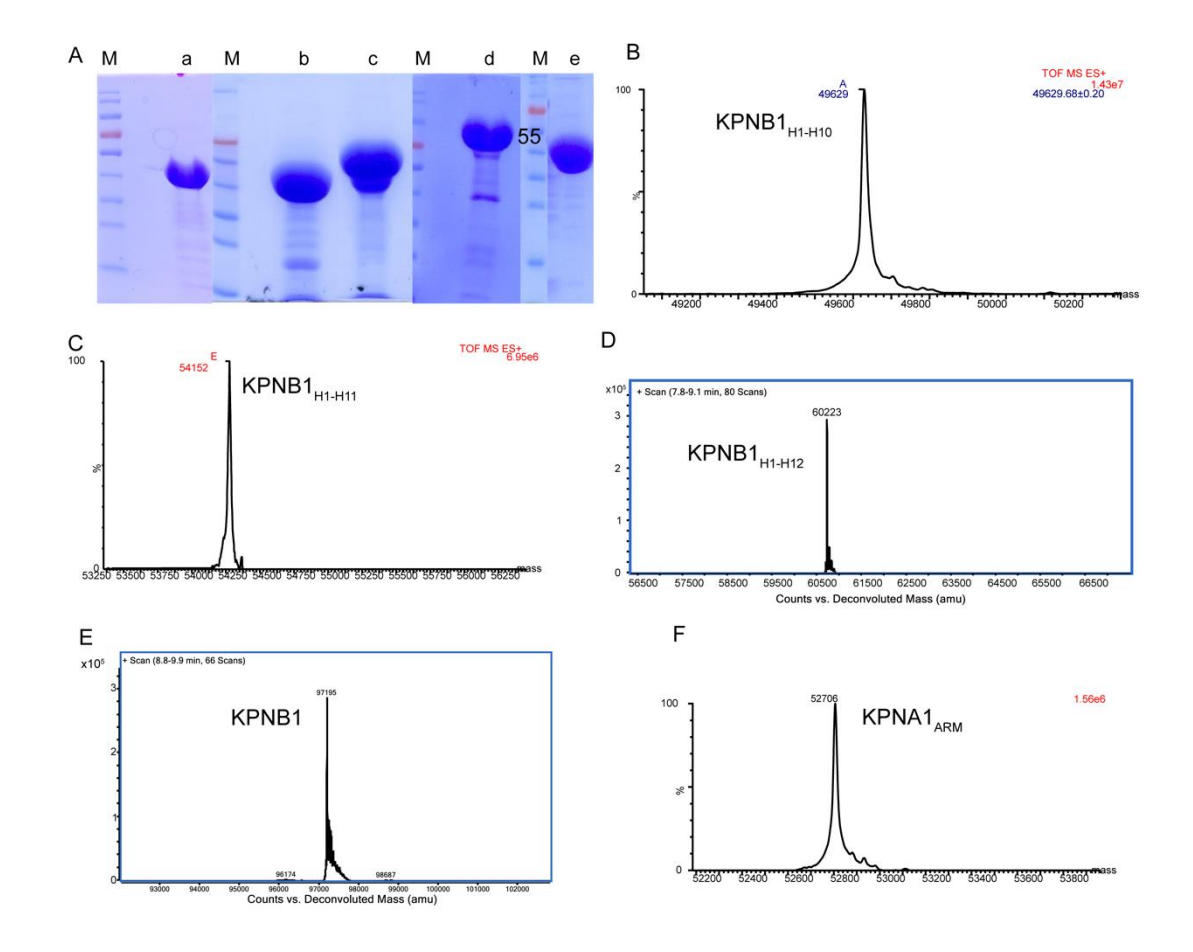


Fig. 4.6 Characterization of KPNA1_{ARM}, **KPNB1**, and its constructs by **SDS-PAGE** analysis and Mass spectrometry. (A) SDS-PAGE was used to detect the final purity of concentrated target proteins. M: marker; a: KPNB1_{H1-H10}, 49.63 kDa; b: KPNB1_{H1-H10}, 54.15 kDa; c: KPNB1_{H1-H12}, 60.2 kDa; d: KPNB1, 97 kDa; e: KPNA1_{ARM}, 52.8 kDa. (B-F) Mass spectrum of KPNB1 and its constructs, as well as KPNA1_{ARM}.

4.3.3 Pull-down assay shows a direct interaction between full NLS of NFAT5 and KPNB1

We carried out *in vitro* pull-down experiments to investigate the interaction between NFAT5 putative NLS region fusion proteins and KPNB1. His₆-tagged KPNB1 was used as the "bait" (**Fig. 4.7 A**). Our results showed that GST-NFAT5₁₇₁₋₂₅₃ was effectively pulled down by His₆-KPNB1 bound to Ni²⁺ agarose beads, while the negative control, GST, was not (**Fig. 4.7 B, right, compare lane 3 and lane 2**). Removing either terminal from GST-NFAT5₁₇₁₋₂₅₃ moderately weakened their binding affinity to KPNB1 (**Fig. 4.7 B, right, compare lanes 4 and 6 with lane 3**). Notably, despite the fact that NFAT5_{eNLS}-PEPCK has no nuclear import activity, GST-NFAT5₁₉₈₋₂₁₇, which only contains the cNLS domain of NFAT5, was significantly pulled down by His₆-KPNB1 at a level comparable to that of GST-NFAT5₁₇₁₋₂₅₃ (**Fig. 4.7 B, right, compare lane 7 and lane 3**). However, when the cNLS domain (NFAT5₁₉₉₋₂₁₆) was removed entirely, no interaction was detected between NFAT5₂₂₀₋₂₅₃ and KPNB1 (**Fig. 4.7 B, right, lane 5**).

Previous research has shown that substituting the three core residues of cNLS in Flag-NFAT5₁₋₅₈₁ with R202_K203_R204 completely abolished nuclear import, indicating that cNLS alone is necessary to support nucleocytoplasmic transport (Tong et al., 2006). Consistently, we observed that the interaction was completely abolished when the core basic amino acids (R202 K203) were replaced by alanine (GST-

NFAT5_{171-253-R202A_K203A), indicating the importance of these residues for nuclear import activity (**Fig. 4.7 B, right, lane 8**). Additionally, no interaction was detected between KPNB1 and the negative control GST-SV40_{NLS}. In summary, these findings support a direct interaction between NFAT5_{cNLS} and KPNB1, with the full NLS of NFAT5 playing the most crucial role, whereas the N- and C-terminal regions facilitate the activity.}

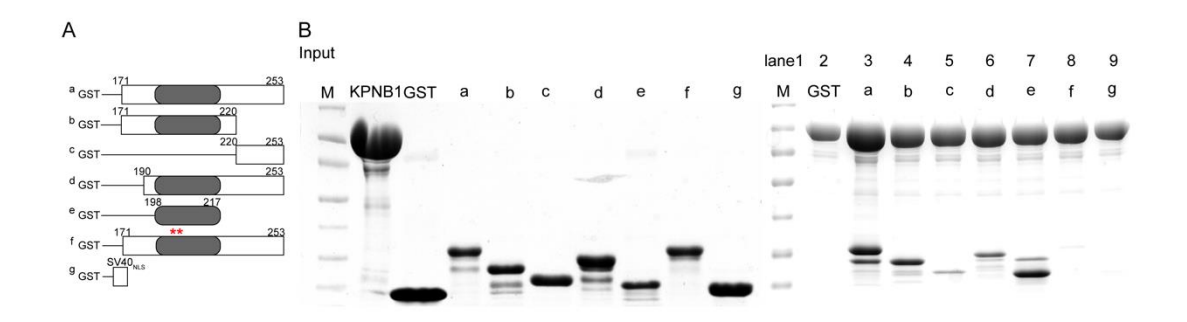


Fig. 4.7 *In vitro* **pull-down assay to characterize the interaction between full NLS of NFAT5 constructs and KPNB1.** (A) Schematic representation of different GST-NFAT5 and GST-SV40_{NLS} fusion proteins. The gray boxes represent the NFAT5_{eNLS}, and the numbers indicate the NFAT5 amino acid positions. Asterisks mark the position of the mutated residues in GST-NFAT5₁₇₁₋₂₅₃-R202A_K203A. (B) *In vitro* pull-down assay. Left: input samples of GST-NFAT5 fusion proteins after purification using glutathione Sepharose column. Target proteins with expected molecular weights were analyzed by SDS-PAGE analysis. Right: *in vitro* pull-down analysis using His₆-KPNB1. For lanes 2-8, His₆-KPNB1 was immobilized on Ni-NTA agarose, and the indicated GST-NFAT5 fusion proteins (as labeled in the schematic) or GST alone were added. After washing, proteins were eluted with excess imidazole. The proteins were analyzed

using SDS-PAGE followed by Coomassie Blue staining. The gel shown is representative of three independent experiments.

4.3.4 Isothermal titration calorimetry (ITC) shows that full NLS of NFAT5 interacts with KPNB1 and its N-terminal constructs

After confirming the direct interaction between NFAT5 NLS and KPNB1, we utilized isothermal titration calorimetry (ITC) to measure the binding affinities of different NFAT5 constructs to KPNB1. We titrated three synthetic peptides (NFAT5_{cNLS}, NFAT5₁₈₉₋₂₁₆, and NFAT5₁₉₉₋₂₂₆) and purified NFAT5₁₇₁₋₂₅₃ and NFAT5₁₅₁₋₂₁₆ into a sample cell loaded with 400 μ l of KPNB1 at 40 μ M. Our results showed that all NFAT5 constructs exhibited similar binding affinities to KPNB1 (**Fig. 4.8**). Specifically, NFAT5₁₅₁₋₂₁₆ and NFAT5₁₇₁₋₂₅₃ exhibited slightly stronger binding affinities (Kd of ~1.27 μ M and ~1.9 μ M, respectively; as shown in **Fig. 4.8 D and E**).

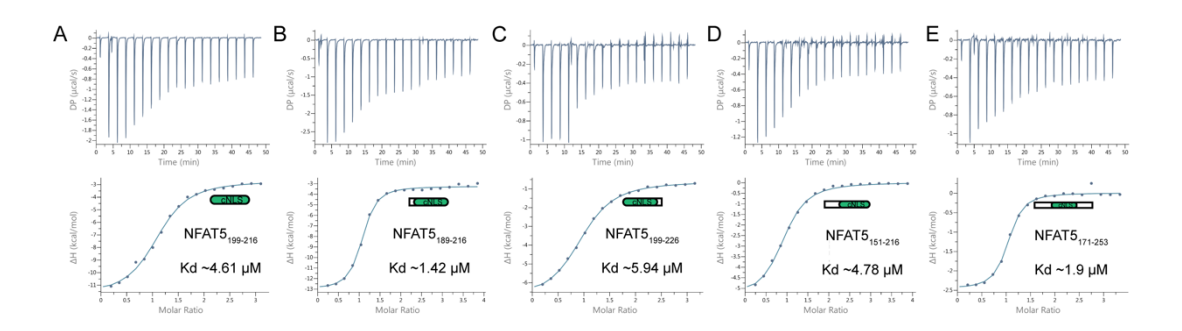


Fig. 4.8 ITC profiles measuring the binding affinity of NFAT5 fragments including residues 199-216 (cNLS, A), 189-216 (B), 199-226 (C), 151-216 (D) and 171-253 (E) to KPNB1. DP, differential power; ΔH , enthalpy.

We assessed the binding affinity between the extensive NFAT5_{cNLS} and N-terminal KPNB1 constructs in the next step. Synthetic peptides NFAT5_{cNLS} (amino acids 199-216) and NFAT5₁₈₉₋₂₁₆ were titrated into a sample cell containing 400 μ l of KPNB1 N-terminal constructs at 40 μ M. Our results showed that synthetic peptide NFAT5_{cNLS} binds to KPNB1_{H1-H10}, KPNB1_{H1-H11}, and KPNB1_{H1-H12} with similar binding affinities (Kd of ~1.61 μ M, ~0.11 μ M, and 0.62 μ M; Fig. 4.9 A-C). Additionally, we found that the N-terminal 10-residue extension of NFAT5_{cNLS} (NFAT5₁₈₉₋₂₁₆) interacts with N-terminal KPNB1 constructs at comparable binding affinities (Kd of ~2.45 μ M and ~3.15 μ M, and 1.07 μ M respectively; Fig. 4.10 A-C).

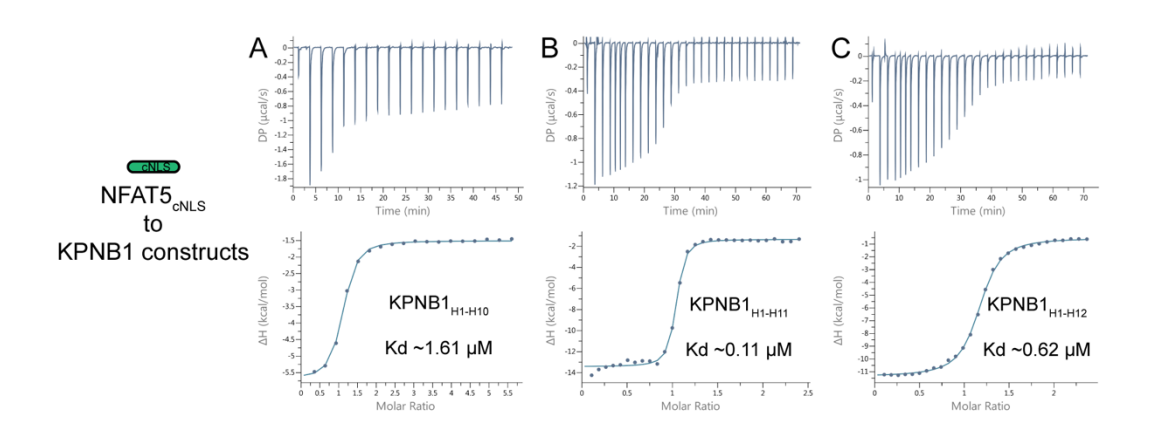


Fig. 4.9 ITC profiles measuring the binding affinity of synthetic peptide NFAT5_{cNLS} to N-terminal KPNB1 constructs KPNB1_{H1-H10}, KPNB1_{H1-H11}, and KPNB1_{H1-H12}. DP, differential power; ΔH, enthalpy.

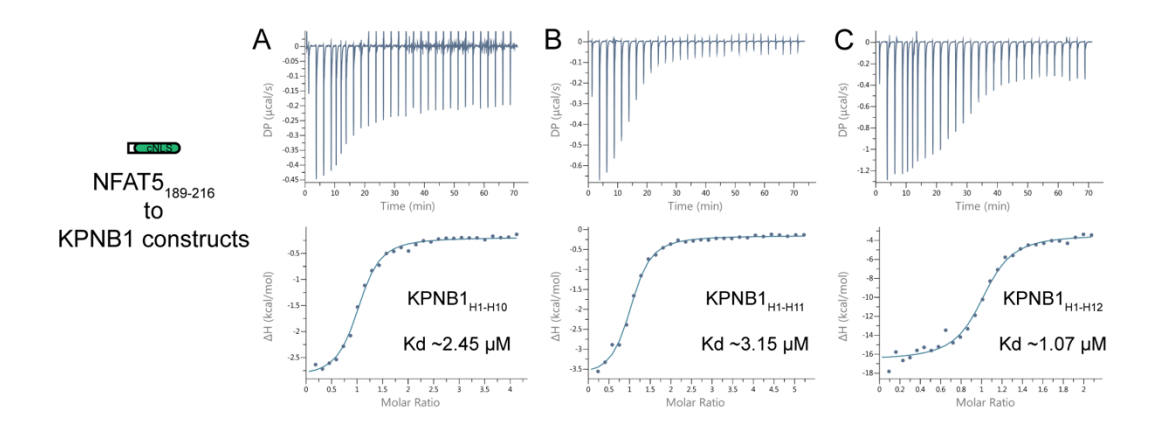


Fig. 4.10 ITC profiles measuring the binding affinity (Kd) of synthetic peptide NFAT5₁₈₉₋₂₁₆ to N-terminal KPNB1 constructs KPNB1_{H1-H10}, KPNB1_{H1-H11}, and KPNB1_{H1-H12}. DP, differential power; ΔH, enthalpy.

Our pull-down assay showed that removing cNLS and substituting core basic amino acids R202_K203 with alanine abolished the interaction with KPNB1. Consistently, ITC measurements showed that the deletion of cNLS (NFAT5₂₂₀₋₂₅₃) completely eliminated the interaction between NFAT5₂₂₀₋₂₅₃ and KPNB1 (**Fig. 4.11 A**). When R202 and K203, two essential basic amino acids, were changed to alanine (NFAT5₁₇₁₋₂₅₃-R202A_K203A), the binding of NFAT5₁₇₁₋₂₅₃-R202A_K203A and KPNB1 was abolished (**Fig. 4.11 B**). These results support our earlier findings that cNLS and amino acids R202 K203 of NFAT5 are crucial for its nuclear import.

ITC measurements corroborated the results of our pull-down assays and confirmed the direct interaction between NFAT5 full NLS and KPNB1.

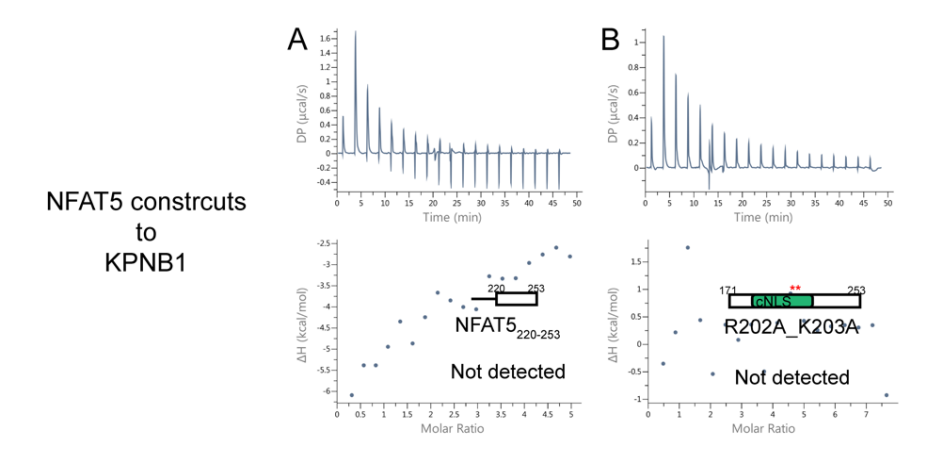


Fig. 4.11 NFAT5 putative NLS region 220-253 (A) and the mutation of 171-253-R202A_K203A (B) showed no interaction with KPNB1. DP, differential power; ΔH , enthalpy.

We compared the binding affinities of NFAT5_{cNLS} to KPNA1 and KPNB1, given their differing functional effects on the nuclear import of NFAT5. Synthetic NFAT5_{cNLS} peptide was titrated into a sample cell containing either KPNB1 or KPNA1_{ARM} at 20 μ M. Our results showed that NFAT5_{cNLS} binds to KPNA1_{ARM} with a weaker binding affinity (Kd ~6 μ M) than His₆-KPNB1 (Kd ~0.58 μ M; **Fig.4.12**). These findings support the results of *in vivo* assays and highlight the crucial role of NFAT5_{cNLS} in its interaction with KPNB1.

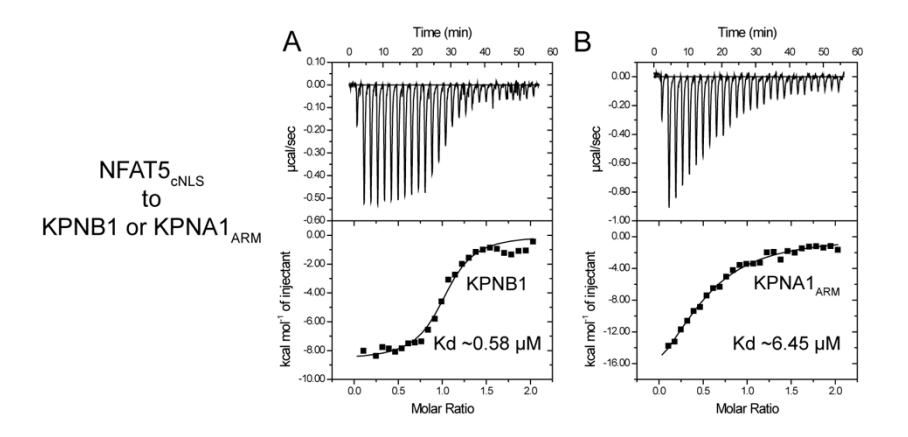


Fig. 4.12 NFAT5_{cNLS} showed weaker interaction with KPNA1_{ARM} (B) than with His₆-KPNB1 (A).

Chapter 5 The intrinsically disordered AED+NLS region of NFAT5 undergoes liquid-liquid phase separation (LLPS)

5.1 The N-terminal intrinsically disordered domain of NFAT5 undergoes phase separation *in vitro*

The VL3-BA program prediction suggests that both the N-terminal AED+NLS region (residues 132-253) and the C-terminal AD domain (residues 618-1476) of NFAT5 are intrinsically disordered (**Fig. 5.1**). As intrinsically disordered regions (IDRs) have been found to promote liquid liquid phase separation (LLPS) in many proteins, we reason the IDRs in NFAT5 may undergo LLPS as well.

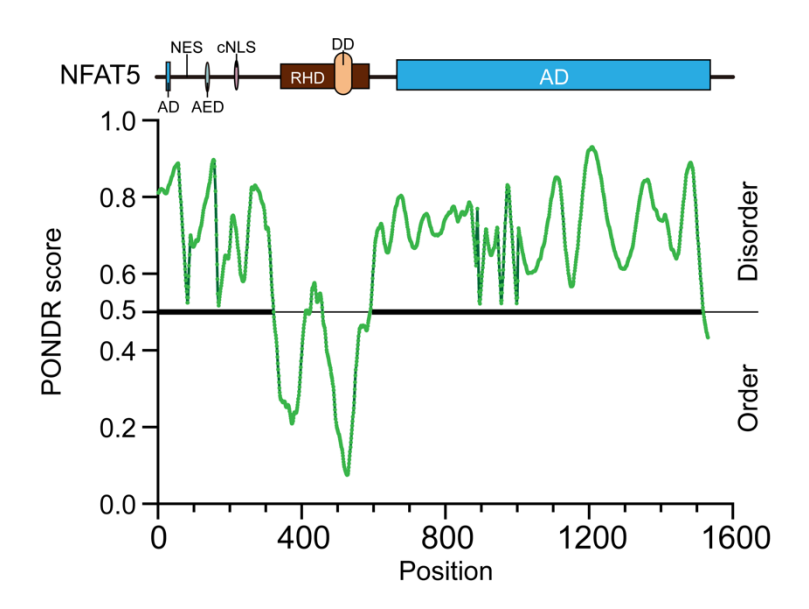


Fig. 5.1 Analysis of the NFAT5 protein sequence for intrinsically disordered regions using the program VL3-BA. The linear amino acid location was represented

by the x-axis, and the disordering propensity was represented by the y-axis. The N- and C-terminal parts of NFAT5 showed a significant propensity for abnormality.

5.1.1 Design, expression, and purification of NFAT5 constructs covering the N-terminal AED+NLS region

To investigate the potential for LLPS in the N-terminal AED+NLS region, we designed several NFAT5 constructs to scan through this segment. Based on the prediction and its nuclear import functional domain, NFAT5₂₁₋₁₄₅, NFAT5₅₁₋₁₄₅, NFAT5₁₃₂₋₂₅₃, NFAT5₁₅₁₋₂₁₆, NFAT5₁₇₁₋₂₅₃, and NFAT5₂₂₀₋₂₅₃ were generated (**Fig. 5.2**). Specifically, NFAT5₂₁₋₁₄₅ and NFAT5₅₁₋₁₄₅ were mapped to the duplicate NES domain and partially reserved AED domain of NFAT5, while the others were assigned to either the N-terminal or C-terminal regions of the putative NLS domain.

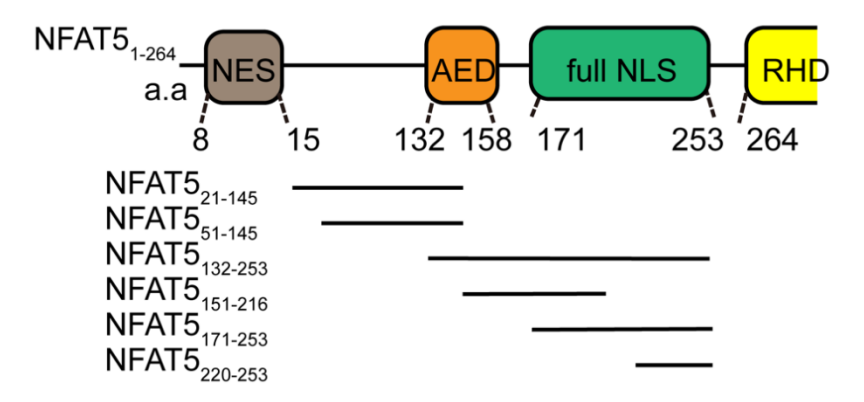
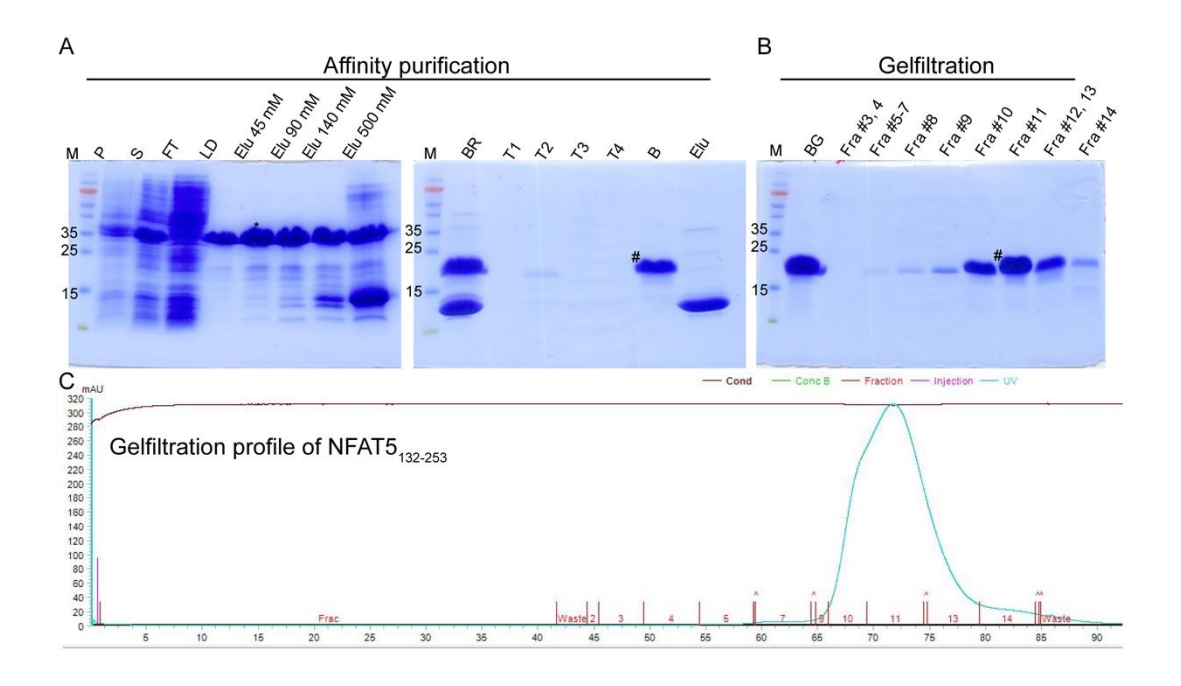


Fig. 5.2 Design of NFAT5 constructs.

All NFAT5 constructs were inserted into a pET-32M vector containing an N-terminal Trx-His₆ fusion tag. NFAT5₁₃₂₋₂₅₃ was purified using the protocol identical to that used for KPNB1 (**Fig. 5.3 A-C**). Specifically, NFAT5₂₂₀₋₂₅₃ was purified without the digestion of the fusion tag due to its small molecular weight.

Target proteins were successfully purified to over 80% purity (**Fig. 5.3 D**). Mass spectrometry was performed to confirm the masses of NFAT5₁₃₂₋₂₅₃, NFAT5₁₅₁₋₂₁₆, and NFAT5₁₇₁₋₂₅₃, which were 13.7 kDa, 7.8 kDa, and 9.5 kDa, respectively (**Fig. 5.3 E-G**). These values were close to their theoretical values (13.4 kDa, 7.6 kDa, and 9.3 kDa, as computed by the ExPASy ProtParam, http://web.expasy.org/protparam/).



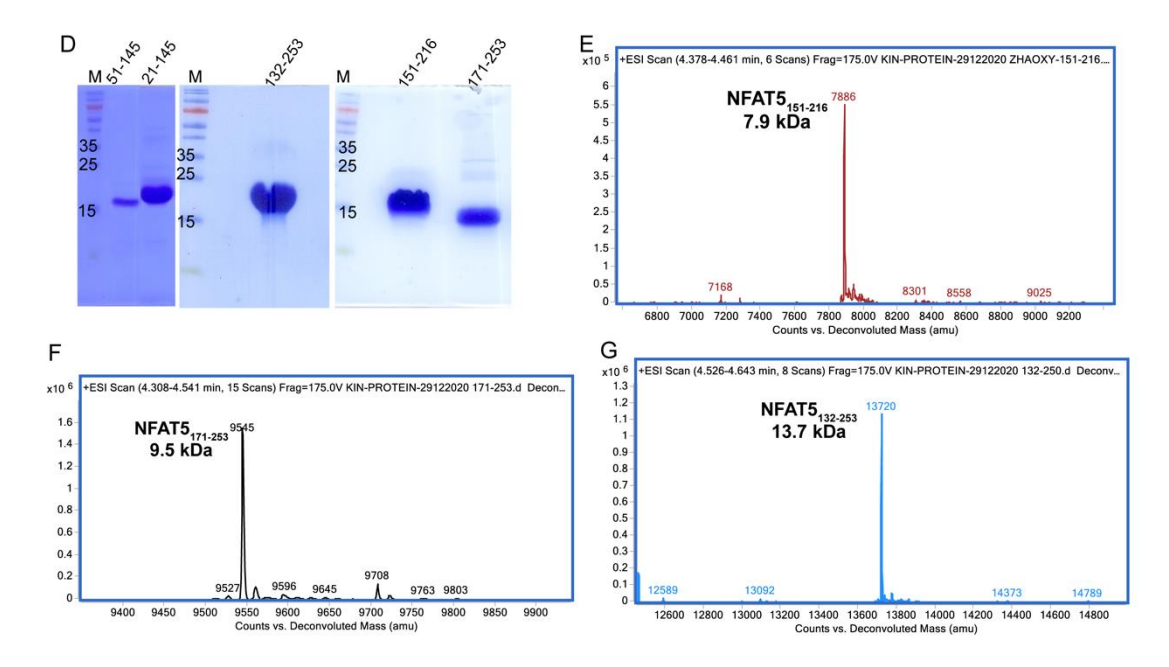


Fig. 5.3 Purification of NFAT5 constructs. SDS-PAGE was used to characterize the purification of Trx-His6-NFAT5₁₃₂₋₂₅₃ by affinity chromatography followed by protease digestion to remove the Trx tag (A), gel filtration (B) & (C). "P" and "S": the pellet (P) and supernatant (S) of the cell lysate after centrifugation. "FT" (flow-through): the protein not captured by the affinity column during sample loading. "LD" (last drop of wash): the last drop of the wash procedure using a binding buffer containing 20 mM imidazole. "Elu": the target proteins that were eluted out by the elution buffer containing the corresponding concentration of imidazole. "BR" and "BG": the samples before loading to the affinity column (BR) or size exclusion column (BG). "T1", "T2", "T3", "T4" and "B": samples that were washed out by Tris buffer (T) for four fractions, or by binding buffer with 40 mM imidazole (B). "Elu": the tag and nonspecific bound impurities that were eluted out by the elution buffer with 500 mM imidazole. "Fra #3 -#14": collected fractions after gel filtration. (C) The profile of gel filtration of NFAT5171-253. (D) SDS-PAGE analysis of purified samples. "51-145": NFAT5₅₁₋₁₄₅, 9.7 kDa; "21-145": NFAT5₂₁₋₁₄₅, 13.2 kDa; "132-253": NFAT5₁₃₂₋₂₅₃, 13.4 kDa; "151-

216": NFAT5₁₅₁₋₂₁₆, 7.6 kDa; "171-253": NFAT5₁₇₁₋₂₅₃, 9.3 kDa. (E-G) The mass spectrum of NFAT5₁₅₁₋₂₁₆, NFAT5₁₇₁₋₂₅₃, and NFAT5₁₃₂₋₂₅₃, show their molecular weights match with the theoretical values of \sim 7.9 kDa, \sim 9.55 kDa, and \sim 13.7 kDa, respectively.

At 280 nm, theoretical extinction coefficient of modified NFAT5 constructs were 0.75 and 0.934, respectively. Light scattering analysis showed their molecular weights were approximately 16 kDa and 10.1 kDa respectively, consistent with their theoretical values (**Fig. 5.4 A and B**). SEC-MALS analysis indicated that NFAT5₁₃₂₋₂₅₃ and NFAT5₁₇₁₋₂₅₃ were present in the solution containing 500 mM NaCl as monomers.

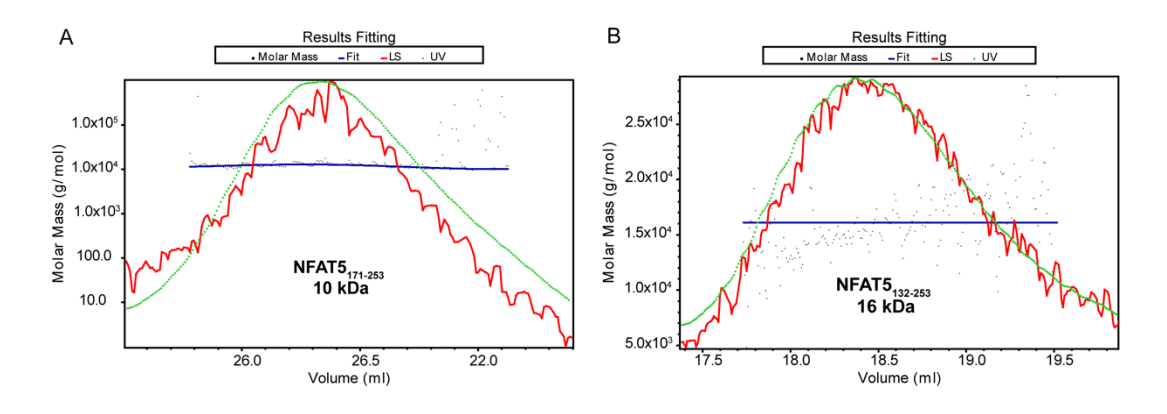


Fig. 5.4 SEC-MALS analysis of NFAT5 constructs for LLPS. Light scattering profiles of NFAT5₁₇₁₋₂₅₃ and NFAT5₁₃₂₋₂₅₃ with calculated molecular weights of ~10 kDa and ~16 kDa, respectively. The elution profiles were shown as "UV" detected at 280 nm and in pale green. The LS signals collected after a gel filtration column were represented as "LS" and colored in red. The calculated molecular weight of each LS signal was represented by a black square labeled "Molar Mass". The fitted results

showed the measured molecular weights, represented by "Fit" and shown by navy blue.

The experimentally measured molecular weights of the target proteins were labeled.

The bottom axis showed the eluted volumes of the target proteins.

5.1.2 Turbidity of purified NFAT5 constructs

When we concentrated purified proteins, we observed that reducing the NaCl concentration caused sample solutions to become opalescent immediately. As shown in **Fig. 5.5**, compared with the control transparent buffer solutions, the freshly purified proteins NFAT5₁₅₁₋₂₁₆, NFAT5₁₇₁₋₂₅₃, and NFAT5₁₃₂₋₂₅₃ at 5 mM became opalescent when the concentration of NaCl was lowered to 50 mM. Notably, after incubating for 3 hours at 4°C, NFAT5₁₅₁₋₂₁₆ displayed visible stratification (**Fig. 5.5 A**).

We found that NFAT5 constructs containing the cNLS domain exhibited turbidity, while NFAT5₂₂₀₋₂₅₃, without the AED and cNLS domain, NFAT5₂₁₋₁₄₅, and NFAT5₅₁₋₁₄₅ containing the AED domain, remained transparent under the same conditions. These findings suggest that N-terminal NFAT5 constructs covering full NLS are susceptible to LLPS.

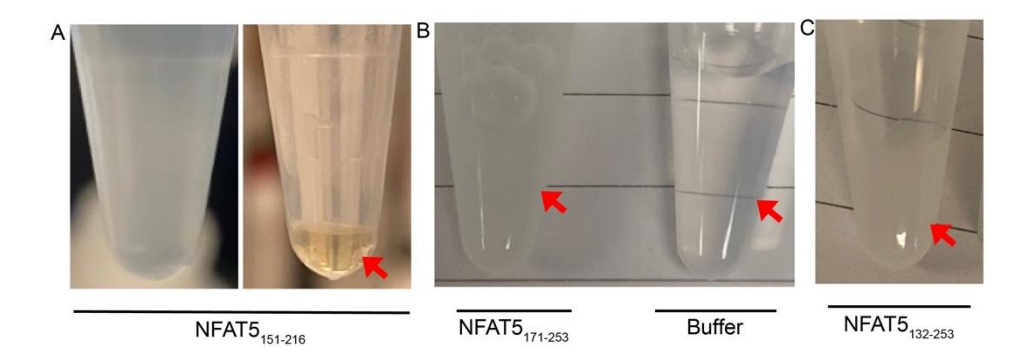


Fig. 5.5 Turbidity of NFAT5 constructs. (A-C) Turbidity was observed in freshly purified proteins NFAT5₁₅₁₋₂₁₆ (A-left), NFAT5₁₇₁₋₂₅₃ (B), NFAT5₁₃₂₋₂₅₃ (C), at a concentration of 5 mM in 50 mM Tris, 150 mM NaCl, pH 8.0, compared to the control Tris buffer (A-right). (A-left) Stratification of NFAT5₁₅₁₋₂₁₆ after incubating over time at 4°C.

5.1.3 Both NFAT5 full NLS and NFAT5 AED+NLS form condensed liquid-like droplets

We then examined the opalescent solutions containing NFAT5 full NLS (amino acid 171-253) or NFAT5 AED+NLS (amino acid 132-253) and the transparent solution containing NFAT5₂₂₀₋₂₅₃ using differential interference contrast (DIC) microscope. We observed numerous small spherical droplets with varying diameters in the solutions of NFAT5₁₃₂₋₂₅₃ and NFAT5₁₇₁₋₂₅₃ (**Fig. 5.6 A and B**). Specifically, NFAT5₁₃₂₋₂₅₃ droplets were tiny and rigid, whereas NFAT5 full NLS (NFAT5₁₇₁₋₂₅₃) droplets exhibited a wetting phenotype when attached to the coverslip surface, resulting in irregular droplets (**Fig. 5.6 B and G**). Due to their different material properties, NFAT5₁₇₁₋₂₅₃ formed fewer droplets than NFAT5₁₃₂₋₂₅₃ under the same condition (**Fig. 5.6 H**). In contrast,

NFAT5₂₂₀₋₂₅₃, either with or without a fusion tag, remained clear in aqueous solutions under the same conditions (**Fig. 5.6 C and D**).

To analyze the component of the droplets, we observed Alexa 488-labeled NFAT5₁₃₂₋₂₅₃ and NFAT5₁₇₁₋₂₅₃ using fluorescence microscopy. As shown in **Fig. 5.6 E** and **F**, NFAT5₁₃₂₋₂₅₃ and NFAT5₁₇₁₋₂₅₃ formed fluorescent droplets, revealing the characteristics of LLPS.

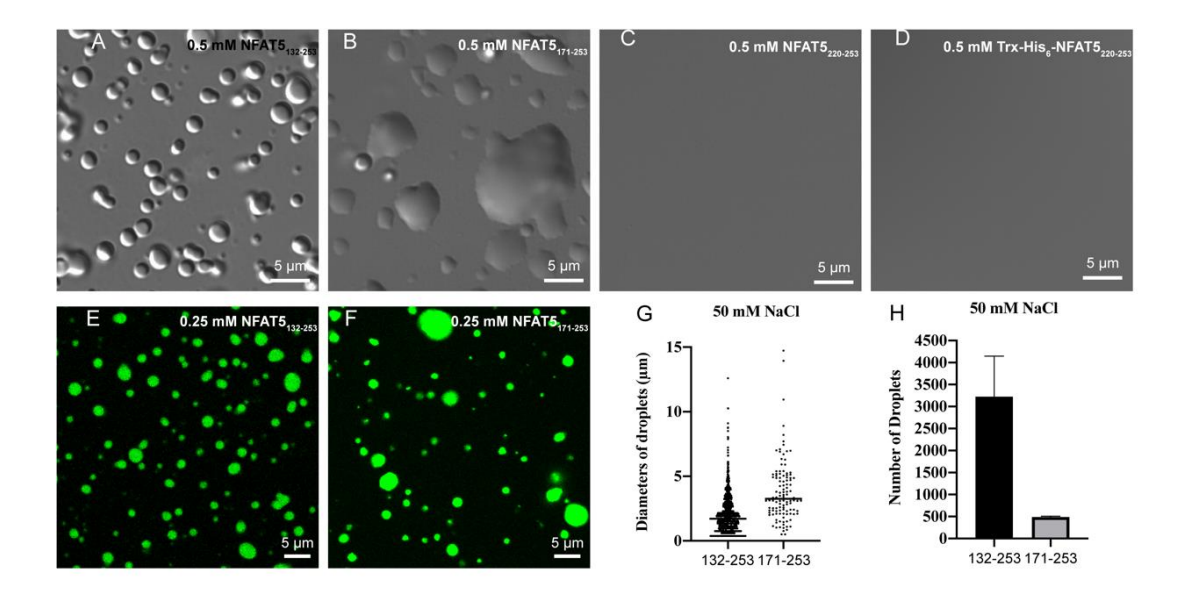


Fig. 5.6 LLPS formation of NFAT5 NLS and NFAT5 AED+NLS. (A-D) At 5 minstewing, differential interference contrast (DIC) microscopy images of droplets formed by purified NFAT5₁₃₂₋₂₅₃ (A), NFAT5₁₇₁₋₂₅₃ (B), NFAT5₂₂₀₋₂₅₃ (C), and Trx-His6-NFAT5₂₂₀₋₂₅₃ (D), at a concentration of 0.5 mM of each protein under 100 mM NaCl, pH 7.5. (E-F) At a concentration of 0.25 mM, NFAT5₁₃₂₋₂₅₃ (E) and NFAT5₁₇₁₋₂₅₃ (F) formed droplets in the presence of 70 mM NaCl. Fluorescence images were shown, where each protein was labeled with fluorophore Alexa 488. (G) Column scatter charts

showed the droplet size of 0.5 mM NFAT5₁₃₂₋₂₅₃ (132-253) and NFAT5₁₇₁₋₂₅₃ (171-253) at 50 mM NaCl. Data were shown as mean \pm S.E.M of droplets combined from three fields (171 \times 171 μ m) for each reaction. (H) The number of 0.5 mM NFAT5₁₃₂₋₂₅₃ (represented as 132-253) and NFAT5₁₇₁₋₂₅₃ (represented as 171-253) at 50 mM NaCl per field (171 \times 171 μ m) in reactions. Three fields were quantified for each. Data were shown as mean \pm S.E.M. Scale bars: 5 μ m.

5.1.4 Fusion of phase separated NFAT5 constructs possess liquid property

To further confirm the phase separation behavior of the NFAT5 full NLS (residues 171-253) and NFAT5 AED+NLS (residues 132-253), we monitored the formation process of droplets. Both NFAT5 full NLS and NFAT5 AED+NLS underwent phase separation in low-salt circumstances, forming protein droplets that fused and coalesced over time. Specifically, condensed droplets of NFAT5₁₃₂₋₂₅₃ fused over 5 minutes, while phase-separated NFAT5₁₇₁₋₂₅₃ coalesced within 1 minute (**Fig. 5.7**).

Taken together, NFAT5 full NLS and NFAT5 AED+NLS exhibited fusion, wetting, and growth phenotypes, suggesting the occurrence of LLPS.

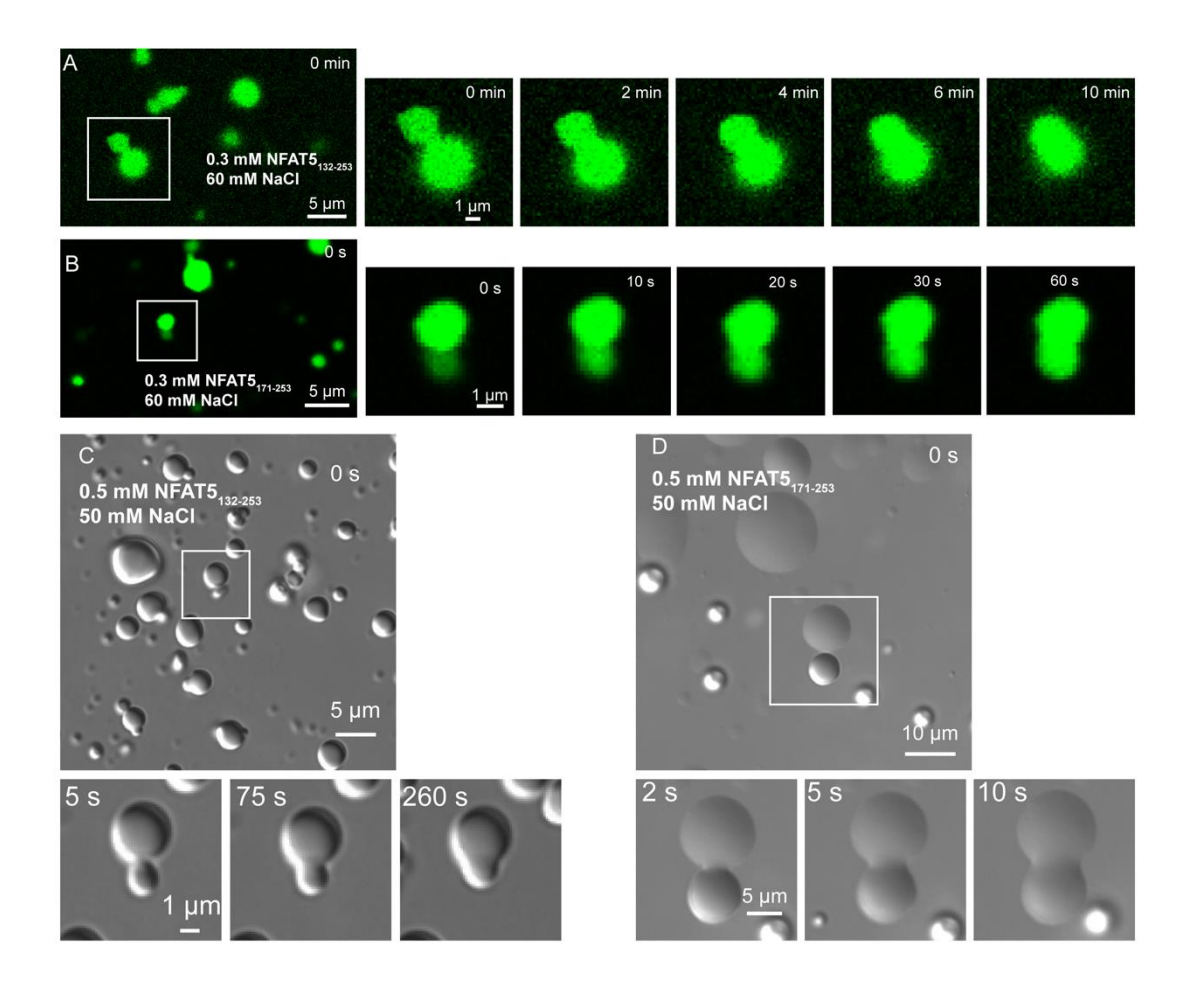
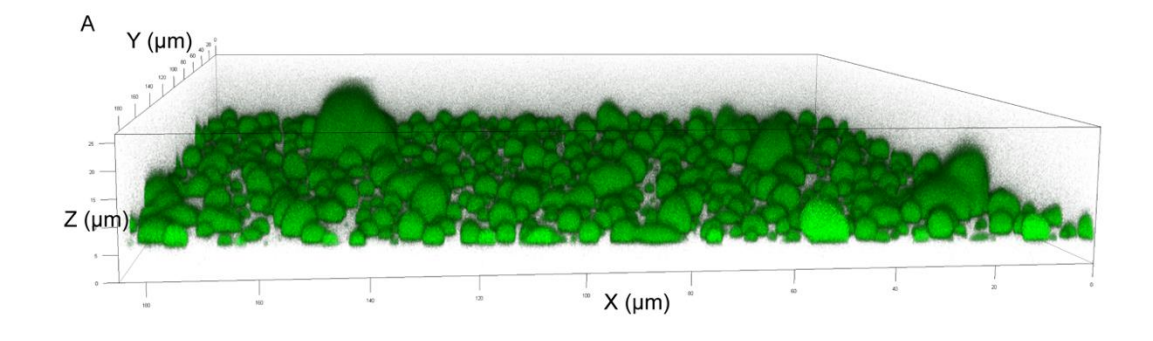


Fig. 5.7 Fusion of condensed NFAT5 full NLS (NFAT5₁₇₁₋₂₅₃) and condensed NFAT5 AED+NLS (NFAT5₁₃₂₋₂₅₃). (A-B) Fluorescence imaging showing the fusion of 0.3 mM NFAT5₁₃₂₋₂₅₃ droplets (A) and NFAT5₁₇₁₋₂₅₃ droplets (B) in 60 mM NaCl, captured over 10 minutes. (C-D) DIC imaging capturing the fusion of 0.5 mM NFAT5₁₃₂₋₂₅₃ droplets (C) and NFAT5₁₇₁₋₂₅₃ droplets (D) in 50 mM NaCl over 5 minutes. The timeline was shown in the upper-right corner of each photo. For fluorescence imaging, 1% of corresponding proteins were labeled using the fluorophore Alexa 488. Each experiment was independently repeated three times. Scale bars: as shown, 1 μm, 5 μm, and 10 μm, respectively.

5.1.5 LLPS of NFAT5 AED+NLS exhibits rigid interfacial boundaries

To demonstrate the rigid material properties of condensed NFAT5 AED+NLS (NFAT5₁₃₂₋₂₅₃), three-dimensional (3D) reconstruction was performed (**Fig. 5.8 A**). We collected 89 z-stacks of images covering 26.27 µm and projected them. NFAT5₁₃₂₋₂₅₃ droplets had firm interfacial boundaries and no notable morphological alterations (**Fig. 5.8 C**). Side views showed that the droplets formed an acute angle with the attached surface from the y- and x-axes (**Fig. 5.8 B and D**). The angle of 79° for the selected droplet was measured manually (**Fig. 5.8 D**).

NFAT5 AED+NLS displayed rigid interfacial boundaries, whereas deleting the AED domain led to NFAT5 full NLS condensates being unable to maintain their shapes, resulting in a failure of 3D reconstruction.



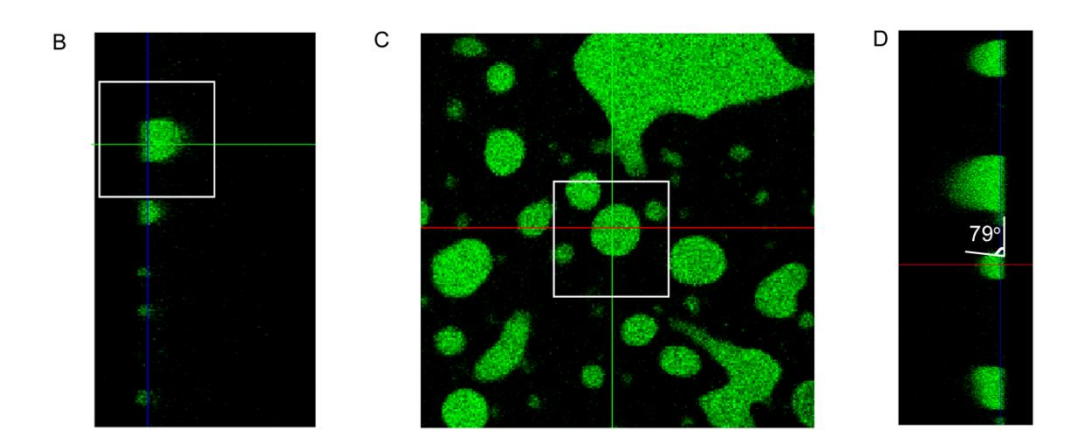


Fig. 5.8 3D reconstruction of 0.6 mM NFAT5₁₃₂₋₂₅₃ LLPS droplets using fluorescence imaging. (A) Eighty-nine z stacks were scanned, resulting in a physical length of 184.52 μm × 184.52 μm ×26.27 μm; 1% NFAT5₁₃₂₋₂₅₃ was labeled with fluorophore Alexa 488. (B-D) Slipped side views from Y, Z, and X axes, respectively, with physical length indicated by colored lines. The experiment was repeated three times independently.

5.1.6 Sedimentation assay shows molecular compositions of condensed NFAT5 full NLS and NFAT5 AED+NLS

We used a centrifugal sedimentation technique to separate the condensed phase from the bulk water solutions in order to examine the molecular compositions of the condensed liquid phase. Next, we assessed the protein components in each fraction using SDS-PAGE and Coomassie blue staining. (**Fig. 5.9 A**). The enrichment of the two NFAT5 constructs in the condensed phase was evaluated (**Fig. 5.9 B**). Both NFAT5 full NLS and NFAT5 AED+NLS were detected in the condensed phase at 100 mM and 70 mM NaCl. Specifically, NFAT5₁₃₂₋₂₅₃ (NFAT5 AED+NLS) was enriched in the

condensed phase, with over 50% of the protein in the pellet fraction at various ionic strengths. In contrast, NFAT5₁₇₁₋₂₅₃ (NFAT5 full NLS) exhibited lower enrichment in the condensed phase, with no more than 30% of the protein in the pellet fraction (**Fig. 5.9 B**).

The enrichment difference was more obvious when the NaCl concentration was decreased to 70 mM. Over 65% of NFAT5₁₃₂₋₂₅₃ was detected in the condensed phase, whereas only 15% of NFAT5₁₇₁₋₂₅₃ was in the condensed phase. These results revealed that NFAT5 AED+NLS displayed a higher enrichment in the condensed phase than NFAT5 full NLS, indicating distinct LLPS behaviors between the two constructs.

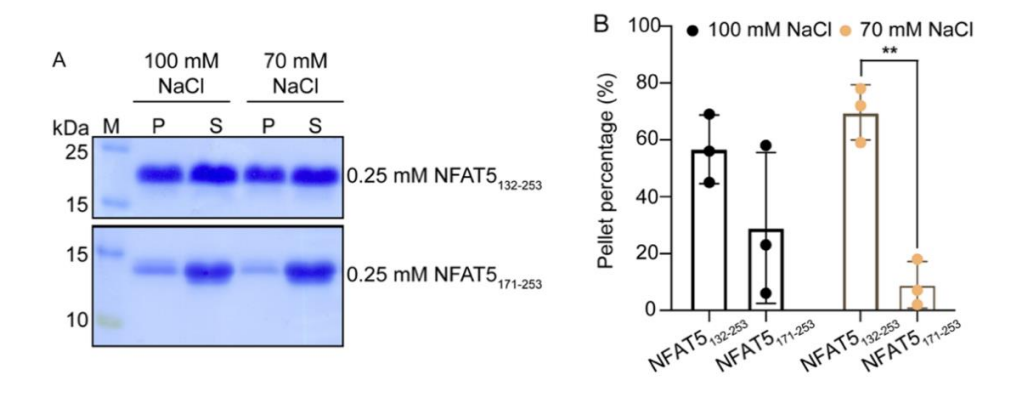


Fig. 5.9 LLPS enrichment analyzed by sedimentation assay. 0.25 mM NFAT5 constructs were induced to LLPS by reducing the concentration of NaCl to 100 mM and 70 mM, respectively. The mixture was incubated at room temperature for 5 min and centrifuged at 18,213 rcf for 10 minutes. (A) SDS-PAGE analysis of the component in pellet fraction and supernatant fraction. M: marker; NFAT5₁₃₂₋₂₅₃: 13.4 kD; NFAT5₁₇₁₋₂₅₃: 9.3 kD. P: pellet, the fractions of proteins recovered in the condensed

phase; S: supernatant, the fractions of proteins diffused in the dilute phase. (B) Quantification of LLPS enrichment. The fractions of "P" were quantified from three independent repeats of the experiment. The fraction of "S" was normalized to 1. Statistic data were presented as mean ± s.e.m with results from 3 independent batches of sedimentation trails. n.s., not significant; *, p<0.05; **, p<0.01; ***, p<0.001; ****, p<0.001 using one-way ANOVA with Dunnett's multiple comparisons tests.

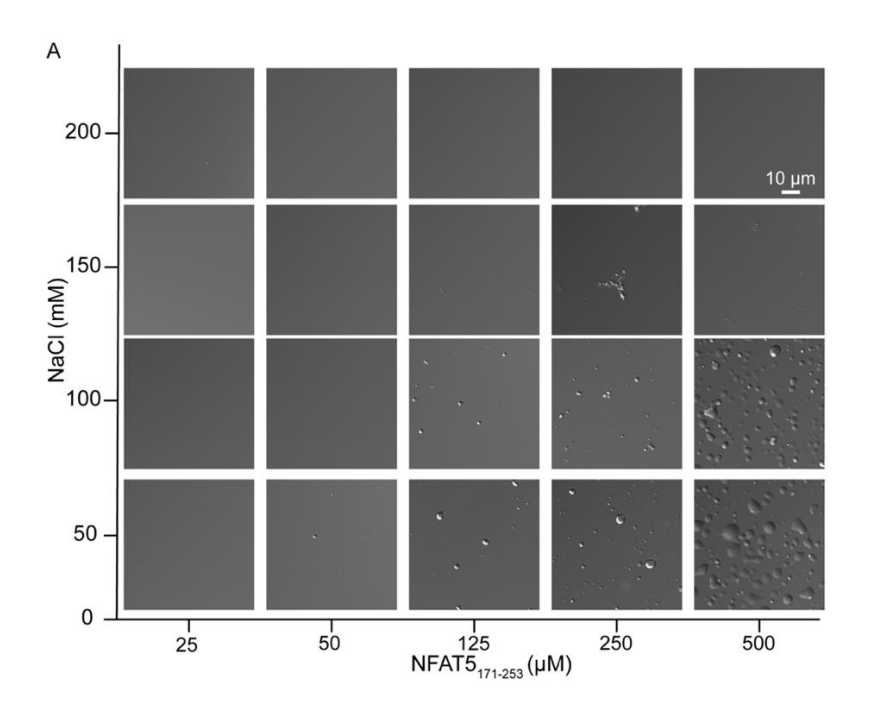
5.1.7 Phase diagram of NFAT5 condensates as a function of NaCl indicates electrostatic interaction-driven self-assembly

The LLPS of NFAT5 full NLS (amino acids 171-253) and NFAT5 AED+NLS (amino acids 132-253) were induced by lowering the concentration of NaCl. To assess their NaCl-sensitivity, we generated phase diagrams for NFAT5₁₃₂₋₂₅₃ and NFAT5₁₇₁₋₂₅₃ as a function of NaCl.

The phase diagram of NFAT5₁₇₁₋₂₅₃ showed that at the same concentration of NFAT₁₇₁₋₂₅₃, condensed droplets were dispersed as NaCl concentration was increased. This suggests that LLPS of NFAT5 full NLS is sensitive to salt concentration (**Fig. 5.10 A and C**). At the same NaCl concentration, increasing protein concentration resulted in a growth in the size of condensed droplets, revealing that LLPS of NFAT5 full NLS is also concentration-dependent. Similarly, LLPS of NFAT5₁₃₂₋₂₅₃ was NaCl-sensitive and concentration-dependent, as shown in **Fig. 5.10 B and D**.

Specifically, 500 μ M NFAT5₁₇₁₋₂₅₃ failed to undergo phase separation at NaCl concentration higher than 200 mM (**Fig. 5.10 C**). In comparison, 125 μ M and 250 μ M NFAT5₁₃₂₋₂₅₃ were resistant to 200 mM NaCl (**Fig. 5.10 D**). These results suggest that the LLPS threshold boundary of NFAT5₁₃₂₋₂₅₃ is broader than that of NFAT5₁₇₁₋₂₅₃.

Our results demonstrate that the LLPS threshold of NFAT5₁₃₂₋₂₅₃ is higher than that of NFAT5₁₇₁₋₂₅₃ in response to different NaCl and protein concentrations. Furthermore, our findings suggest that electrostatic interactions trigger the LLPS of NFAT5, as evidenced by its sensitivity to changes in ionic strength.



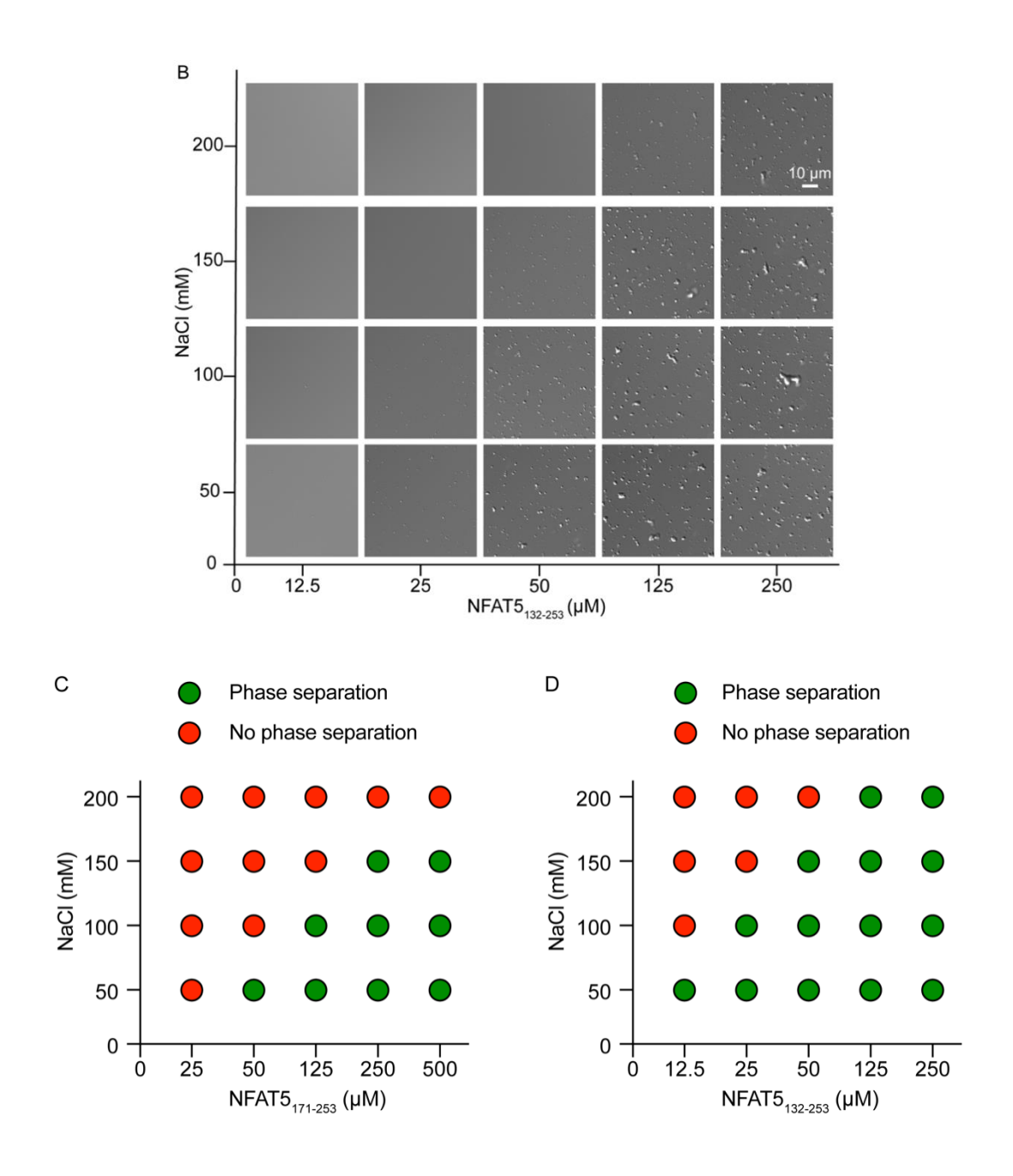


Fig. 5.10 Phase diagrams of NFAT5 constructs as a function of NaCl. (A) Formation of NFAT5₁₇₁₋₂₅₃ droplets. (B) Formation of NFAT5₁₃₂₋₂₅₃ droplets. (C) Phase diagram of NFAT5₁₇₁₋₂₅₃. (D) Phase diagram of NFAT5₁₃₂₋₂₅₃. "Phase separation" and "No phase separation" was denoted by green and red circles. Protein samples were freshly prepared, and their LLPS was induced by diluting samples to corresponding NaCl concentrations. DIC images were captured after standing for 5 minutes. Three fields

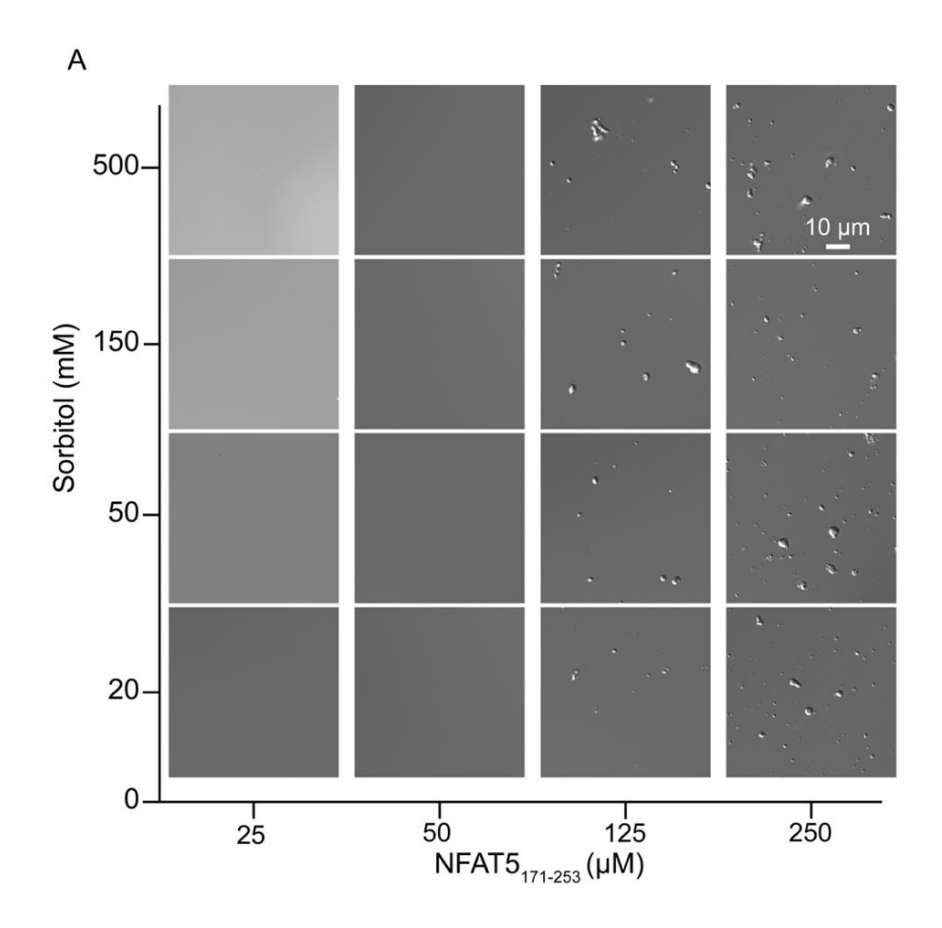
were randomly selected. The condition was assessed as "phase separation" if protein droplets were observed in all selected fields and vice versa. Scale bars: $10 \, \mu m$.

5.1.8 The crowder sorbitol has no effect on LLPS of NFAT5 constructs at a fixed concentration of 100 mM NaCl

Previous research showed that the N-terminal IDR of NFAT5 underwent a disorder-to-order shift, resulting in a higher average secondary and tertiary structure in the presence of sufficient NaCl or sorbitol (Kumar et al., 2020). Sorbitol and NaCl function synergistically to stabilize the structure of NFAT5. Our study aims to determine the role of environmental crowder (sorbitol) in stabilizing the LLPS of NFAT5 by examining the behavior of NFAT5 full NLS (amin acids 171-253) and NFAT5 AED+NLS (amino acids 132-253) in the presence of sorbitol. We first used the phase diagrams of NFAT5₁₇₁₋₂₅₃ and NFAT5₁₃₂₋₂₅₃ in **Fig. 5.11** as a reference and identified 100 mM NaCl as the most LLPS-stable ionic strength for NFAT5 constructs. We then investigated the LLPS behavior of both NFAT5₁₇₁₋₂₅₃ and NFAT5₁₃₂₋₂₅₃ in terms of protein and sorbitol concentration while maintaining a constant ionic strength of 100 mM NaCl.

At a constant protein concentration, similar LLPS behaviors of NFAT5₁₇₁₋₂₅₃ were observed regardless of the different concentrations of sorbitol (20 mM to 500 mM; **Fig. 5.11 A and C**). Similarly, there was no difference in the LLPS behavior of NFAT5₁₃₂-

B and D). However, in the presence of 20 mM sorbitol, 25 μM NFAT5₁₃₂₋₂₅₃ failed to phase separate, as the condition was the threshold boundary of NFAT5₁₃₂₋₂₅₃, and the LLPS behavior was not stable. These results suggest that LLPS of both NFAT5 full NLS and NFAT5 AED+NLS is mainly triggered by electrostatic interactions, and environmental crowders, such as sorbitol, are not essential.



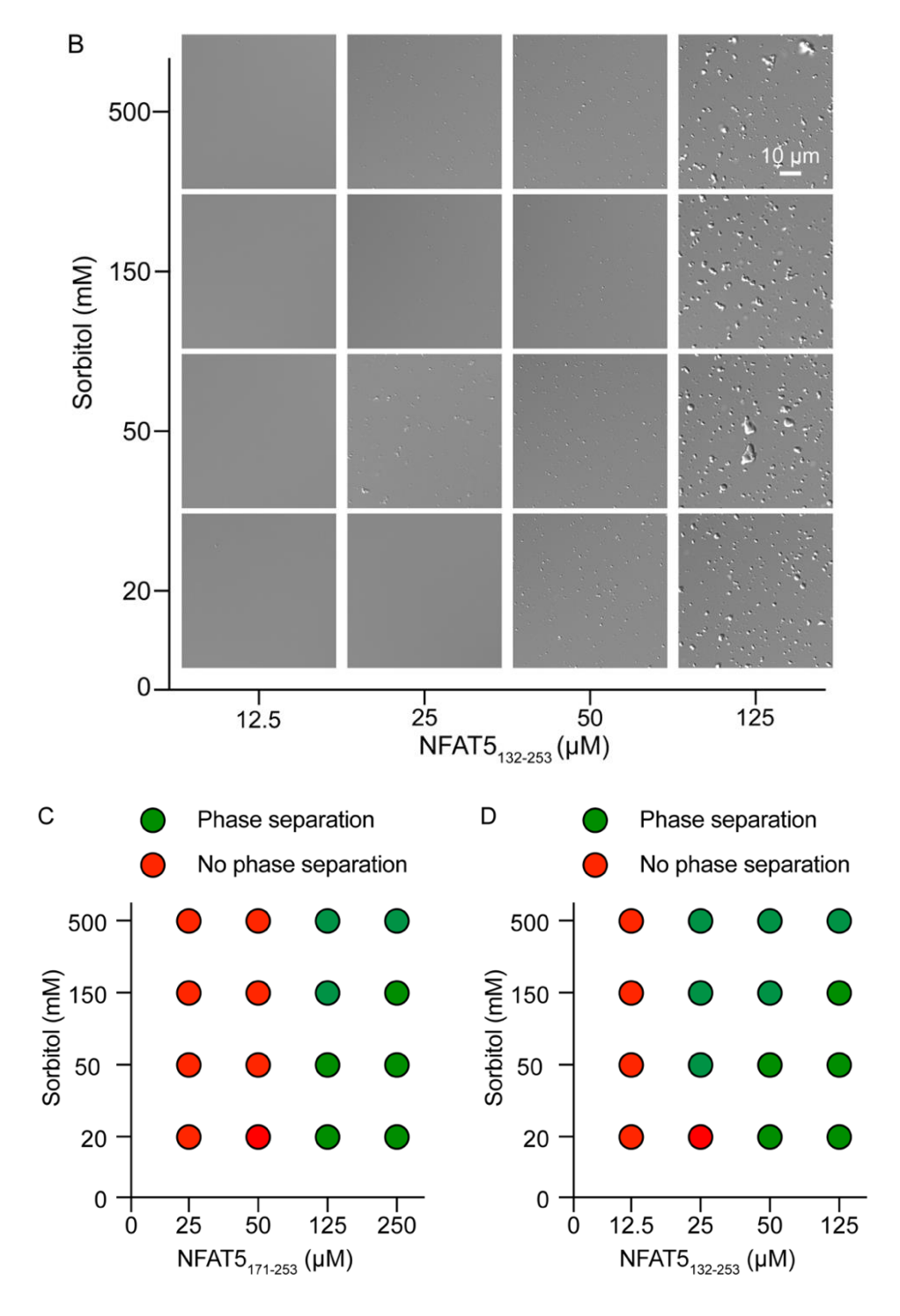


Fig. 5.11 Phase diagrams of NFAT5 constructs as a function of sorbitol with a fixed concentration of 100 mM NaCl. (A-B) Formation of NFAT5₁₇₁₋₂₅₃ droplets (A) and NFAT5₁₃₂₋₂₅₃ droplets (B) in buffers containing different concentrations of sorbitol with a fixed NaCl concentration of 100 mM. (C-D) Phase diagram of NFAT5₁₇₁₋₂₅₃ (C) and NFAT5₁₃₂₋₂₅₃ (D) as a function of sorbitol. A green circle denotes "phase separation,"

and a red circle denotes "no phase separation." All protein samples were freshly prepared, and their LLPS was induced by decreasing the concentration of NaCl from 500 mM to 100 mM. DIC images were captured to detect LLPS after standing for 5 minutes. Three fields were randomly selected, and if protein droplets were observed in all selected fields, the condition was assessed as "phase separation" and vice versa. Scale bars: $10 \, \mu m$.

5.1.9 The dynamics of phase separated NFAT5 AED+NLS and NFAT5 full NLS

Our findings suggest that NFAT5 AED+NLS and NFAT5 full NLS differ in material properties and LLPS boundary. To assess the mobility of NFAT5₁₇₁₋₂₅₃ (NFAT5 full NLS) and NFAT5₁₃₂₋₂₅₃ (AED+NLS), we conducted a fluorescence recovery after photobleaching (FRAP) assay.

Firstly, we investigated the exchange of macromolecules within the condensed phase. We point-photobleached NFAT5₁₃₂₋₂₅₃ droplets and found that the fluorescent intensity of its inner condensates recovered to 60% in 5 minutes, indicating the macromolecule mobility in the condensed phase (**Fig. 5.12 A and B**).

Next, we investigated the exchange of macromolecules between the condensed phase and the dilute phase. The condensed droplets of NFAT5 full NLS and NFAT5 AED+NLS with a diameter of approximately 3 µm were bleached, respectively. During

the first 3 minutes, both NFAT5₁₃₂₋₂₅₃ and NFAT5₁₇₁₋₂₅₃ exhibited similar rates of fluorescence recovery (**Fig. 5.12 C and D**). After 6 minutes, NFAT5₁₇₁₋₂₅₃ recovered nearly 80% of the fluorescent intensity, while NFAT5₁₃₂₋₂₅₃ only recovered about 60% (**Fig. 5.12 E**). These results indicate that both NFAT5 constructs can freely diffuse across the boundaries between the condensed and dilute phases, with NFAT5 AED+NLS possessing less mobility than NFAT5 full NLS.

In conclusion, the bi-directional signal exchange of NFAT5 AED+ full NLS indicates that the condensates' inner and outer phases are mobile. LLPS of NFAT5 full NLS and NFAT5 AED+ full NLS exhibits different mobility.

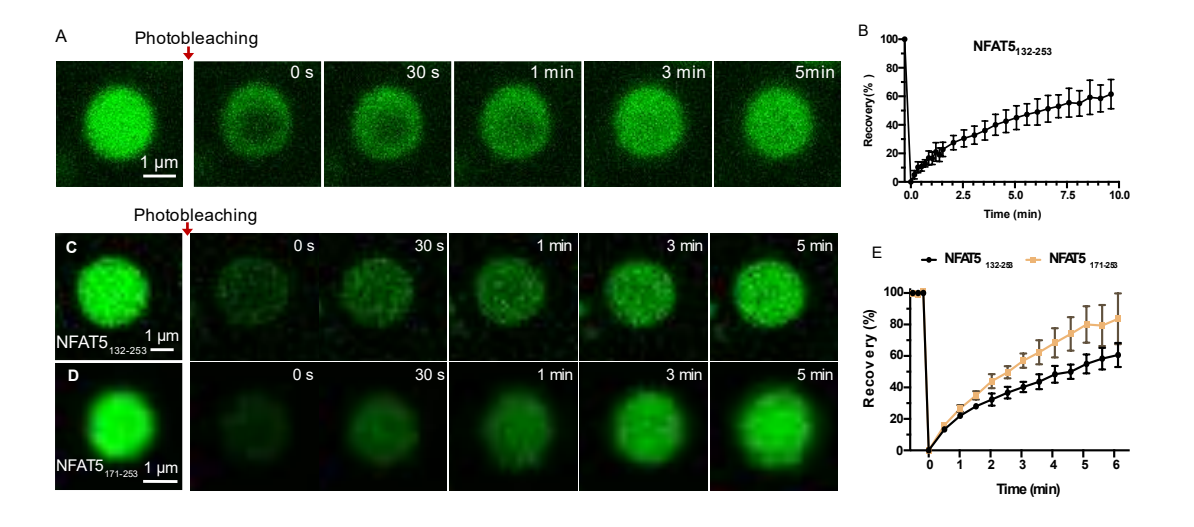


Fig. 5.12 LLPS of NFAT5 constructs exhibited high mobility. The results of the FRAP assay revealed the percentage of fluorescent signal recovery in the condensed phase of NFAT5₁₃₂₋₂₅₃ and NFAT5₁₇₁₋₂₅₃ at a concentration of 0.3 mM. LLPS was induced at 60 mM NaCl. (A) The fluorescent signal of point-bleached NFAT5₁₃₂₋₂₅₃ was monitored for 5 min. (B) The curves show the averaging of the signals from four

NFAT5₁₃₂₋₂₅₃ droplets with a diameter of around 3 μ m. The droplets were point-photobleached for FRAP. (C-D) The whole droplet of NFAT5₁₃₂₋₂₅₃ (C), and NFAT5₁₇₁₋₂₅₃ (D) was photobleached and the percentage of fluorescent recovery was recorded in 6 min, respectively. (E) The curves show the averaging of the signals from three droplets with a diameter of around 2 μ m. The scale bars are 1 μ m. All data were presented as mean \pm s.e.m.

In general, N-terminal NFAT5 containing cNLS undergoes LLPS. *In vitro* characterization of NFAT5 full NLS and NFAT5 AED+NLS LLPS reveals that NFAT5 undergoes LLPS via electrostatic interactions, exhibiting distinct material properties, LLPS boundaries, and mobilities.

5.2 NFAT5 undergoes phase separation in vivo

We found that NFAT5 full NLS and NFAT5 AED+NLS underwent LLPS *in vitro*. To further investigate the *in vivo* LLPS of NFAT5 and it factors, Dr. Ko's lab demonstrated NFAT5 LLPS in living cells.

5.2.1 Endogenous NFAT5 undergoes LLPS under varying tonicity

Stimulated emission depletion (STED) super-resolution imaging was utilized to visualize NFAT5 LLPS. The two-dimensional (2D) analysis demonstrated the presence

of foci in HeLa cells under isotonic, hypotonic, and hypertonic conditions (**Fig. 5.13**). Notably, condensed NFAT5 was observed in different locations within the cells in accordance with its nucleocytoplasmic shuttling. Specifically, under isotonic conditions, NFAT5 foci were distributed throughout the cells, while under hypertonic conditions, they exhibited nuclear localization. Under hypotonic conditions, NFAT5 foci were observed to localize to the cytoplasm.

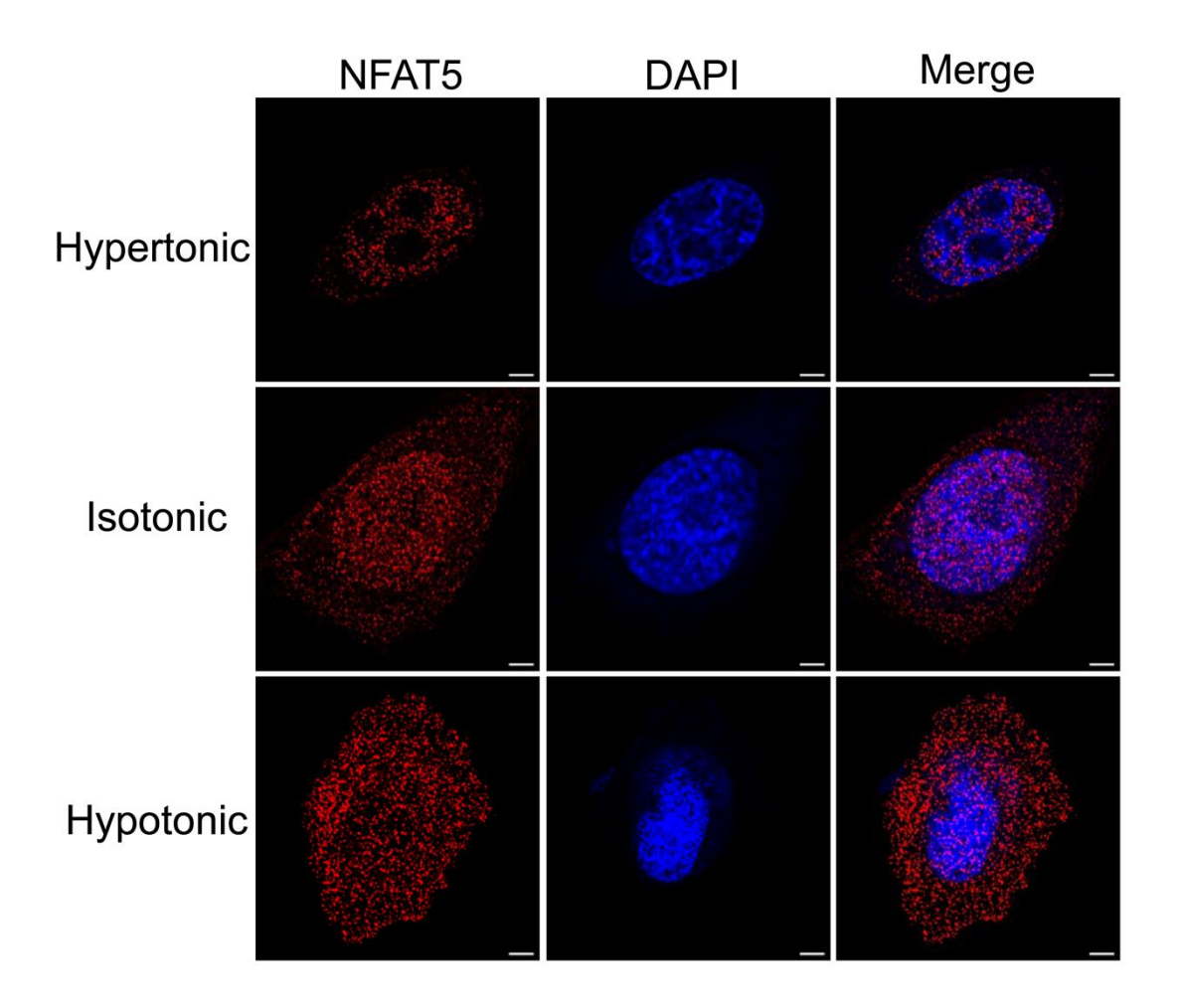


Fig. 5.13 STED monitored LLPS formation of endogenous NFAT5 under varying tonicity. After hypertonic, hypotonic, and isotonic treatments for 2 hours, HeLa cells were fixed and incubated with corresponding antibodies. NFAT5 was detected using an anti-NFAT5 antibody. Statistic data were presented as mean \pm s.e.m with results from 3

independent batches of experiments. ns, not significant; *, p<0.05; **, p<0.01; ***, p<0.001; ****, p<0.0001 using one-way ANOVA with Dunnett's multiple comparisons tests. Scale bar: 1 μ m.

In addition, we quantified endogenous NFAT5 puncta in HeLa cells under isotonic and hypotonic conditions and observed a significant increase in NFAT5-enriched puncta over time under hypotonic treatment (**Fig. 5.14**). These findings indicate that NFAT5 undergoes phase separation *in vivo*. In addition, hypotonicity promotes the puncta formation.

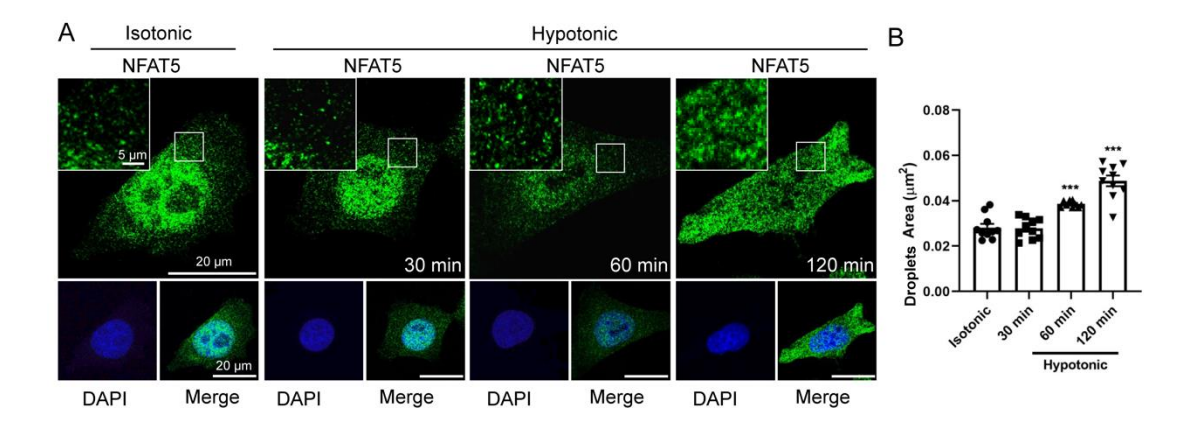


Fig. 5.14 LLPS formation of endogenous NFAT5 under changes of tonicity. After hypotonic, hypertonic and isotonic treatments, HeLa cells were fixed and incubated with corresponding antibodies. NFAT5 was detected using an anti-NFAT5 antibody. Statistic data were presented as mean \pm s.e.m with results from 3 independent batches of experiments. n.s., not significant; *, p<0.05; **, p<0.01; ***, p<0.001; ****, p<0.001 using one-way ANOVA with Dunnett's multiple comparisons tests. Scale bar: 20 μ m and 5 μ m, respectively.

5.2.2 Fusion of phase separated NFAT5₁₋₅₄₃-AcGFP exhibits liquid-like property

We then investigated the property of NFAT5-enriched puncta in living cells by transfecting NFAT5₁₋₅₄₃-AcGFP into HeLa cells. This truncated recombinant NFAT5 contains N-terminal AED (amino acids 132-253) that is responsive to nuclear export under hypotonicity, full NLS (amino acids 171-253) that is essential for nuclear import, and RHD domain (amino acids 264-581), a DNA binding domain. This protein is larger than 40 kDa and requires an active transport mechanism to move across the nuclear membrane (Cavazza & Vernos, 2016).

Similar to endogenous NFAT5, when cells were subjected to hypotonic conditions, ectopically expressed NFAT5₁₋₅₄₃-AcGFP underwent phase separation, forming two small puncta that rapidly fused into a larger punctum (**Fig. 5.15**). The result further supports our *in vitro* findings that phase-separated NFAT5 possesses liquid-like properties and confirms that NFAT5 undergoes LLPS.

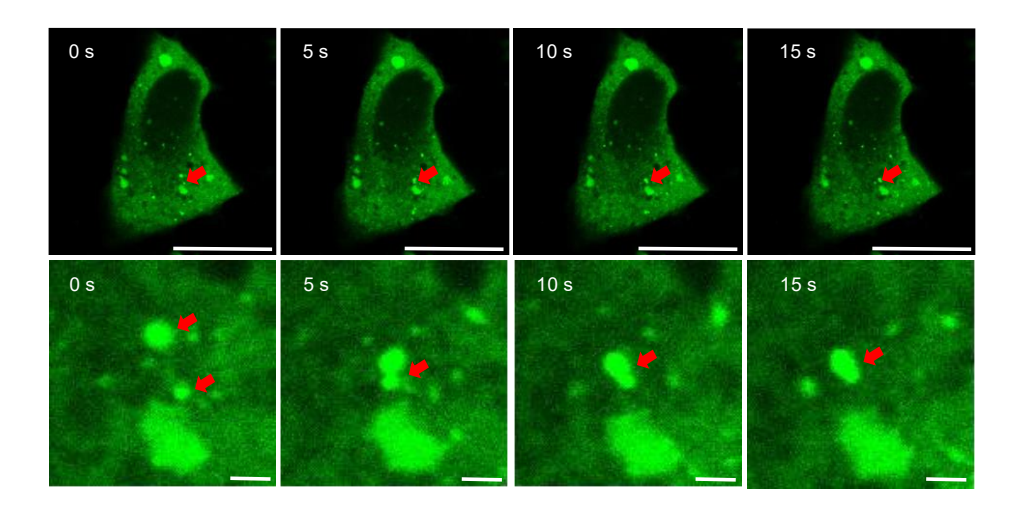


Fig. 5.15 NFAT5₁₋₅₄₃**-AcGFP droplets fusion.** HeLa cells were transfected into NFAT5₁₋₅₄₃-AcGFP and treated with the hypotonic medium for 2 hours. Fluorescence imaging was used to monitor the fusion of phase-separated NFAT5₁₋₅₄₃-AcGFP. Scale bar: 20 μm (upper) and 1 μm, respectively.

5.2.3 The liquidity of phase separated NFAT5₁₋₅₄₃-AcGFP was increased under hypotonicity

Our earlier findings indicate that hypotonicity affects the LLPS of NFAT5₁₋₅₄₃-AcGFP. To investigate the role of hypotonicity in regulating the LLPS of NFAT5₁₋₅₄₃-AcGFP, we monitored the exchange rate of condensed NFAT5₁₋₅₄₃-AcGFP using FRAP assay. After photo-bleaching, the NFAT5₁₋₅₄₃-AcGFP signals were recovered within one minute (**Fig. 5.16 A**). Under hypotonic conditions, the recovery speed of condensed NFAT5₁₋₅₄₃-AcGFP was much faster, with a higher recovery rate of 60%, compared to isotonic conditions (**Fig. 5.16 B**). These results reveal that hypotonicity increases the liquidity of NFAT5 LLPS.

In conclusion, our findings demonstrate that electrostatic interactions trigger the LLPS of NFAT5 in a tonicity-dependent manner. Meanwhile, hypotonicity increases the liquidity of the condensed liquid phase of NFAT5.

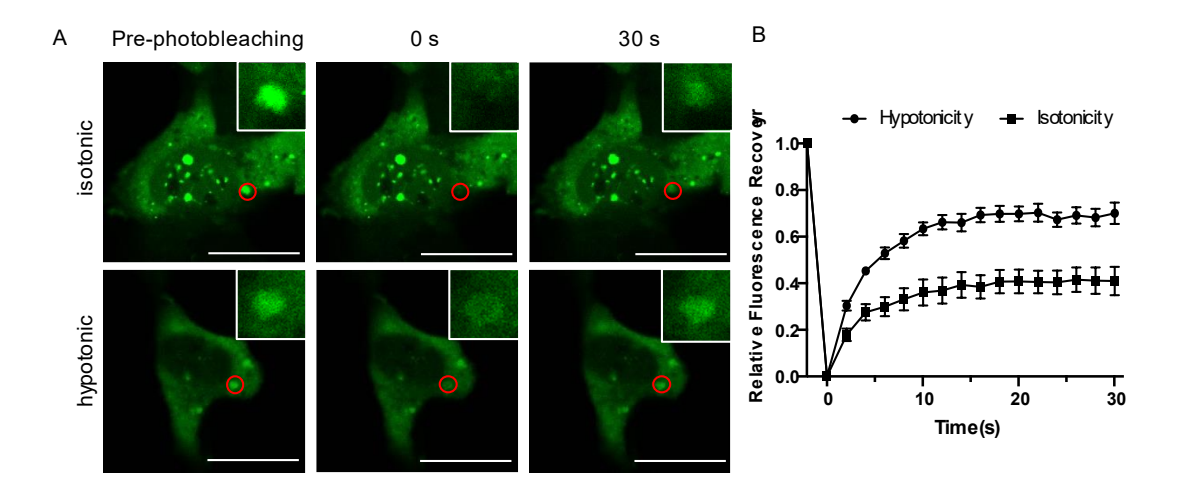


Fig. 5.16 NFAT5₁₋₅₄₃-AcGFP exhibits increased mobility under the hypotonic treatment. Cells were subjected to isotonicity and hypotonicity for 2 hours, respectively. After photobleaching, the fluorescent signal of ectopically expressed NFAT5₁₋₅₄₃-AcGFP was monitored for 1 min. All data were presented as mean \pm s.e.m. Scale bars: 20 μ m.

Chapter 6 KPNB1 reduces the liquidity of NFAT5 LLPS to facilitate its nuclear import

6.1 KPNB1 inhibits LLPS of NFAT5 AED+NLS in a concentration-dependent manner

According to previous research, the nuclear import receptor karyopherin-β2, also known as TNPO1, is a member of the KPNB family, and plays a role in regulating LLPS of RNA binding proteins with prion-like domains (Yoshizawa et al., 2018). Our earlier findings identified that KPNB1 is the nuclear import receptor for NFAT5, which undergoes LLPS. Building on this, we conducted further investigations to explore the role of KPNB1 in regulating the LLPS of NFAT5.

We mixed KPNB1 with phase-separated NFAT5 AED+NLS (amino acids 132-253) at various molar ratios and detected condensed NFAT5 AED+NLS droplets using fluorescence microscopy. In the absence of KPNB1, we observed that NFAT5 AED+NLS underwent LLPS (**Fig. 6.1 A, lane 1**). However, increasing the concentration of KPNB1 resulted in a significant decrease in the formation of condensed NFAT5₁₃₂₋₂₅₃ droplets (**Fig. 6.1 A**). Notably, when a molar ratio of 10% KPNB1 was mixed with phase-separated NFAT5₁₃₂₋₂₅₃, no fluorescence condensates were detected, indicating that KPNB1 interfered with the LLPS of NFAT5₁₃₂₋₂₅₃ (**Fig. 6.1 A**, compare **lane 1** and **lane 4**). Specifically, as the concentration of KPNB1

increased by 10-fold, from a molar ratio of 50 to 5 (NFAT5₁₃₂₋₂₅₃/KPNB1), the number of condensed droplets significantly decreased (**Fig. 6.1 B**).

DIC imaging revealed a morphological change in condensed NFAT5₁₃₂₋₂₅₃ droplets when KPNB1 was added (**Fig. 6.1 A**). The addition of KPNB1 disrupted the fusion of NFAT5₁₃₂₋₂₅₃ droplets and reduced their diameters, resulting in the disappearance of fused droplets and leaving only tiny single droplets (**Fig. 6.1 A**, compare **Lane1** and **Lane 3**).

In the next step, we conducted sedimentation experiments to investigate the effect of KPNB1 on the enrichment of NFAT5 AED+NLS in the condensed liquid phase. In the absence of KPNB1, nearly 40% of NFAT5₁₃₂₋₂₅₃ was detected in the condensed phase, whereas in the presence of KPNB1, condensed NFAT5₁₃₂₋₂₅₃ was dispersed in the solution (**Fig. 6.1 C and D**).

Furthermore, adding KPNB1 led to the rapid dispersion of the condensed liquid phase into a homogenous aqueous solution (**Fig. 6.1 E**). 3D reconstruction confirmed the inhibitory effect of KPNB1 on LLPS of NFAT5₁₃₂₋₂₅₃, as droplets of NFAT5₁₃₂₋₂₅₃ dispersed after an equal amount of KPNB1 was added (**Fig. 6.1 F**).

In summary, these results indicate that KPNB1 acts as a chaperone to modulate the LLPS of NFAT5, consistent with current understandings of the role of nuclear import receptors in regulating LLPS.

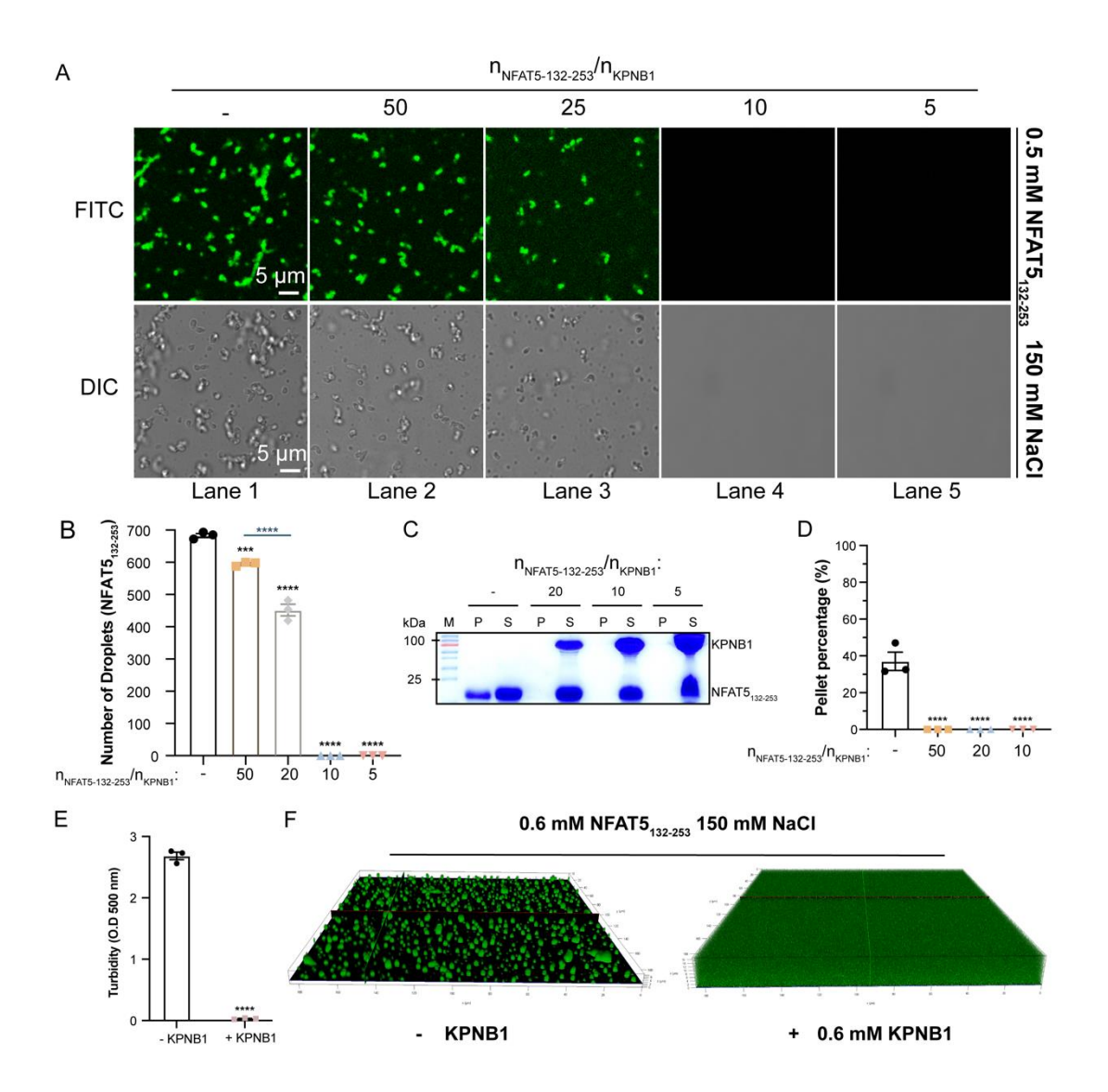


Fig. 6.1 KPNB1 inhibits LLPS NFAT5₁₃₂₋₂₅₃ in a concentration-dependent manner.

(A) Fluorescence and DIC imaging of NFAT5₁₃₂₋₂₅₃ puncta formation without or with different molar ratios of KPNB1. LLPS of 0.5 mM NFAT5₁₃₂₋₂₅₃ was induced by decreasing NaCl concentration from 500 mM to 150 mM. (B) Quantification of condensed NFAT5₁₃₂₋₂₅₃ formation in Figure A. (C) Sedimentation assay showing the

enrichment of condensed NFAT5₁₃₂₋₂₅₃ in the pellet (P) fraction at different molar ratios of KPNB1. M: marker; NFAT5₁₃₂₋₂₅₃: 13.4 kD; KPNB1: 97 kD. "P" and "S": the fractions of proteins recovered in the condensed phase (P) and dilute phase (S). (D) Quantification of sedimentation assay results. The fraction of "S" was normalized to 100%. The fractions of "P" were quantified from three independent repeats of the experiment. (E) Turbidity assay showing the difference in turbidity between the mixture of KPNB1 and NFAT5₁₃₂₋₂₅₃ and phase-separated NFAT5₁₃₂₋₂₅₃. KPNB1 was mixed with NFAT5₁₃₂₋₂₅₃ at a 1/1 molar ratio. The concentration of NFAT5₁₃₂₋₂₅₃ was 0.5 mM, and the NaCl concentration was 150 mM. Turbidity was measured at UV-Vis 500 nm. (F) 3D reconstruction of LLPS of 0.6 mM NFAT5₁₃₂₋₂₅₃ with or without KPNB1 in 150 mM NaCl. All statistical data were presented as mean ± s.e.m with results from 3 independent batches of corresponding experiments. n.s., not significant; *, p<0.05; **, p<0.01; ***, p<0.001; ****, p<0.001; ****, p<0.0001 using one-way ANOVA with Dunnett's multiple comparisons test. Scale bars: 5 µm.

6.2 KPNB1 reduces the liquidity of NFAT5 LLPS in vivo

After confirming the effect of KPNB1 on the LLPS of NFAT5 in vitro, Dr. Ko's lab investigated its regulation of the LLPS of endogenous NFAT5 in living cells. A gradual decrease in the LLPS of endogenous NFAT5 was observed after prolonged hypertonic treatment (**Fig. 6.2 A and B**). Knocking down KPNB1 abolished the nuclear localization of NFAT5 and resulted in increased condensed NFAT5 droplets (**Fig. 6.2 C**)

and D). These results corroborate our conclusion that KPNB1 is the exclusive nuclear import receptor for NFAT5 and indicate that KPNB1 can reduce the LLPS of NFAT5.

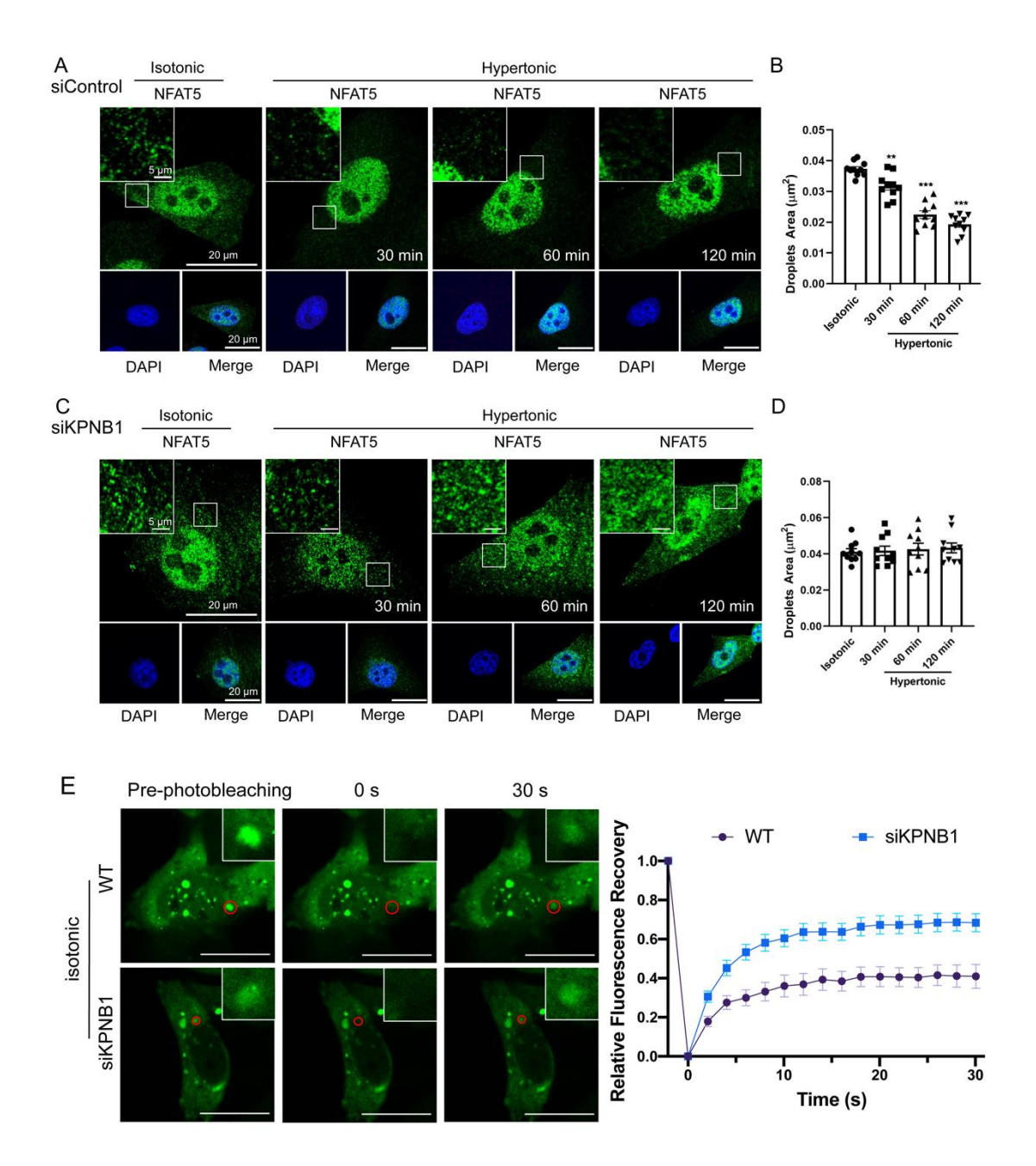


Fig. 6.2 KPNB1 inhibits LLPS of NFAT5 in vivo. (A and C) LLPS formation of endogenous NFAT5 with (C) or without (A) KPNB1 siRNA knockdown, under isotonicity and hypertonicity, respectively. After hypertonic and isotonic treatments, HeLa cells were fixed and incubated with corresponding antibodies. NFAT5 was

detected using an anti-NFAT5 antibody. Cells were subjected to isotonicity and hypotonicity for 2 hours, respectively. (B and D, right) Quantification of LLPS formation of endogenous NFAT5. (E) FRAP demonstrated the effect of KPNB1 on the LLPS of NFAT5₁₋₅₄₃-AcGFP. After photobleaching, the fluorescent signal of ectopically expressed NFAT5₁₋₅₄₃-AcGFP was monitored for 1 min. Statistic data were presented as mean ± s.e.m with results from 3 independent batches of experiments. n.s., not significant; *, p<0.05; **, p<0.01; ***, p<0.001; ****, p<0.0001 using one-way ANOVA with Dunnett's multiple comparisons test. Scale bars: 20 μm and 5 μm.

In the next step, the impact of KPNB1 on the liquidity of condensed NFAT5₁₋₅₄₃-AcGFP was investigated. As described in Chapter 5, ectopically expressed NFAT5₁₋₅₄₃-AcGFP was photobleached, and the fluorescent intensity was monitored. In the presence of KPNB1, the mobility of NFAT5 condensates only recovered to 40% (**Fig. 6.2 E, WT**). When KPNB1 was knocked down, however, the mobility of NFAT5 condensates was significantly increased, and its fluorescent intensity was recovered to more than 60% with a faster recovery speed (**Fig. 6.2 E**). These finds indicate that KPNB1 regulates the LLPS of NFAT5 by reducing the liquidity of NFAT5-enriched droplets. Furthermore, the findings reveal a relationship between the nuclear import activity of NFAT5 and its LLPS behavior.

Chapter 7 Structural study of the KPNB1-NFAT5 $_{\rm NLS}$ complex to delineate the molecular mechanism of KPNB1-mediated nuclear import of NFAT5

7.1 Sample preparation of KPNB1-NFAT5 complex for cryo-EM studies

KPNB1 and NFAT5 full NLS (amino acid 171-253) were purified separately following the protocols described in the Methods section. To form the KPNB1-NFAT5 full NLS complex, KPNB1 was mixed with excessive amount of NFAT5 full NLS and passed through the gel filtration column. A peak eluted at 42 ml and was confirmed to be the KPNB1-NFAT5 full NLS complex by SDS gel (**Fig. 7.1**). This sample was not homogenous enough to obtain a high quality cryo-EM map. The cryo-EM density map showed very low resolution with no clear signal for NFAT5.

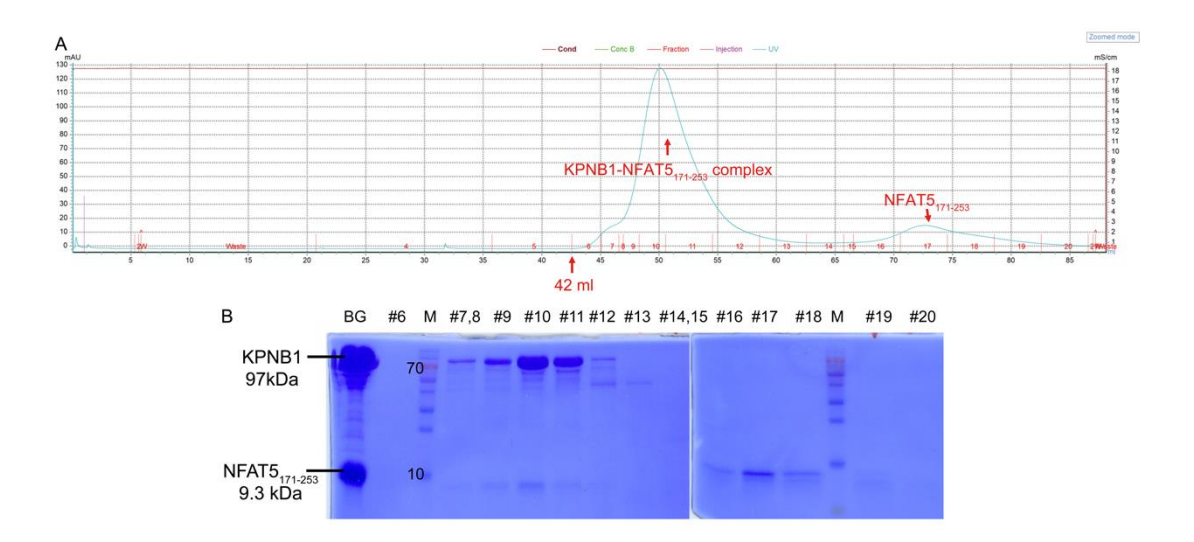


Fig. 7.1 Characterization of KPNB1-NFAT5 full NLS complex by SDS-PAGE analysis. (A) The profile of gel filtration of KPNB1-NFAT5₁₇₁₋₂₅₃ complex. (B) SDS-

PAGE analysis of KPNB1-NFAT5₁₇₁₋₂₅₃ complex. "BG": the samples before loading to the size exclusion column; "M": Marker; "#6" "#7,8"- "#20": collected fractions.

We reason KPNB1 is highly dynamic and as a result the KPNB1-NFAT5 complex may not be stable enough for Cryo-EM analysis. A previous study showed that crosslinking was effective to stabilize the IPO7-KPNB1-Histone complex for Cryo-EM analysis (Ivic et al., 2019). We decided to use this approach as well. KPNB1 mixed with 3 molar excesses of NFAT5 full NLS (amino acid 171-253) was isolated by gel filtration and single peak was eluted at 42 ml and was analysed on SDS-PAGE (Fig. **7.2** A). The complex was cross-linked by incubating with 0.1% glutaraldehyde for 2 min at 37 °C. Cross-links were checked by SDS-PAGE (Fig. 7.2 A). The sample was subjected to gel filtration to remove aggregates. The crosslinked KPNB1-NFAT5 complex was eluted as a single peak at 42 ml with the molecular weight confirmed by SDS-PAGE analysis (Fig. 7.2 B and C). The purified sample was then diluted to a concentration of 80 µM from the initial concentration of 130 µM for cryo grid preparation. After glow discharging the EM grids, 3 µl of the diluted sample was applied onto the carbon side and blotted for 4.5 seconds before plunge-freezing. Data collection was performed using a 300keV Titan Krios microscope with a K3 camera, and a total of 4620 movies were collected.

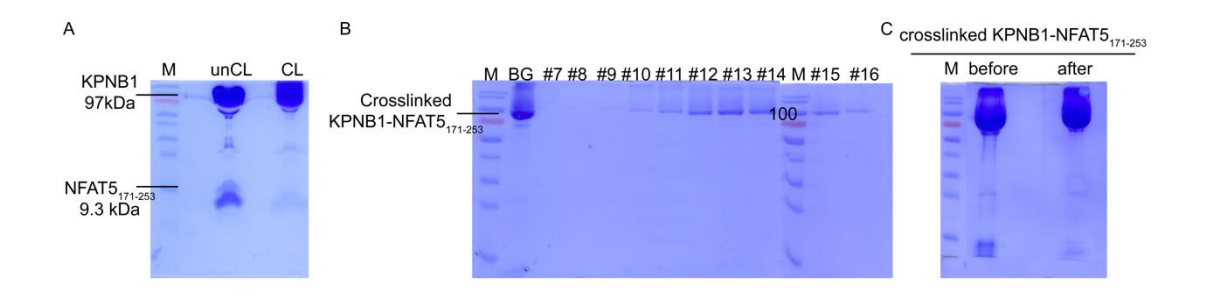


Fig. 7.2 Characterization of cross-linked KPNB1-NFAT5 full NLS complex by SDS-PAGE analysis. SDS-PAGE analysis of KPNB1-NFAT5₁₇₁₋₂₅₃ complex (A): before ("unCL") and after crosslinking ("CL"); gel filtration of cross-linked KPNB1-NFAT5₁₇₁₋₂₅₃ complex (B); cross-linked KPNB1- NFAT5₁₇₁₋₂₅₃ complex (C): before and after gel-filtration.

7.2 Cryo-EM structure determination of the KPNB1-NFAT5 complex

The Cryo-EM map of KPNB1 and NFAT5 complex was obtained via the process illustrated in Fig. 7.3 A. Firstly, 4620 movies were pre-processed by motion correction and CTF estimation in CryoSPARC v3.1. Blob picker was then done to select 3,585,588 particles with a diameter of approximately 130 Å. Subsequently, 2D classification and Ab-initio reconstruction were performed to remove junk particles and build up initial 3D maps. The resulting particle set (1278986 particles) underwent rounds of heterogenous refinements to distinguish differences between the various 3D maps. Particles were screened to identify those containing a complete KPNB1 molecule with NFAT5 bound, resulting in a final set containing ~152k particles. Homogenous refinement was performed to obtain a 4.39 Å map, which was further optimised to reach a 4.09 Å resolution at a Fourier Shell Correlation (FSC) threshold of 0.143 by local resolution refinement and non-uniform refinement.

As reviewed in numerous structural analyses, KPNB1 forms an extended superhelical structure consisting of 19 HEAT repeats (Cingolani et al., 2002; Cingolani et al., 1999; Mitrousis et al., 2008; Vetter et al., 1999). KPNB1 exhibits a high degree of flexibility and acts like a molecular spring to "cradle" around diverse substrates for

specific KPNB1-substrate interactions (Cingolani et al., 2002; Cingolani et al., 1999; Mitrousis et al., 2008; Vetter et al., 1999). Our Cryo-EM density map revealed a similar superhelical structure, with the concave surface possessing a higher local resolution of ~ 3.8 Å than the convex surface at ~ 4.8 Å resolution (**Fig. 7.3 C**). Additionally, the N-terminal end of the superhelical structure shows better solution than the C-terminal end (residue 1-570 vs 570-876). In fact, the density becomes rather poor for the N-terminal end starting at residue 680 (**Fig. 7.4 A**). This suggests that the C-terminal end is highly flexible and unlikely to engage NFAT5, which is consistent with our previous ITC data.

When we docked the atomic model of KPNB1 into the Cryo-EM map, we observed extra density at a contour level of 0.042 by the concave side of the superhelical structure, which likely represents the cNLS (residue 199-216) of NFAT5 (Fig. 7.4 A). However, this density gradually faded as the contour increased to 0.154, possibly due to the flexible nature of the unstructured NFAT5-cNLS. The extra density spans across HEAT repeat 8-12 and consists of two distinct parts. One part is a linear-shaped density running parallel to the helix of the 8th HEAT repeat (Fig. 7.4 B). The other part is a globular helix proximal to the highly conserved acidic loop (TKQDENDDDDDW) located within HEAT repeat 8-12 (Fig. 7.4 B). Interestingly, the NFAT5-contacting region of KPNB1 is covered by numerous acidic residues, which is electrostatically complementary to the positively charged cNLS (residue 199-216) of NFAT5. The electrostatic map of the complex supports the idea that the electrostatic complementarity may be a major factor to favour KPNB1-NFAT5 interaction (Fig. 7.4 C).

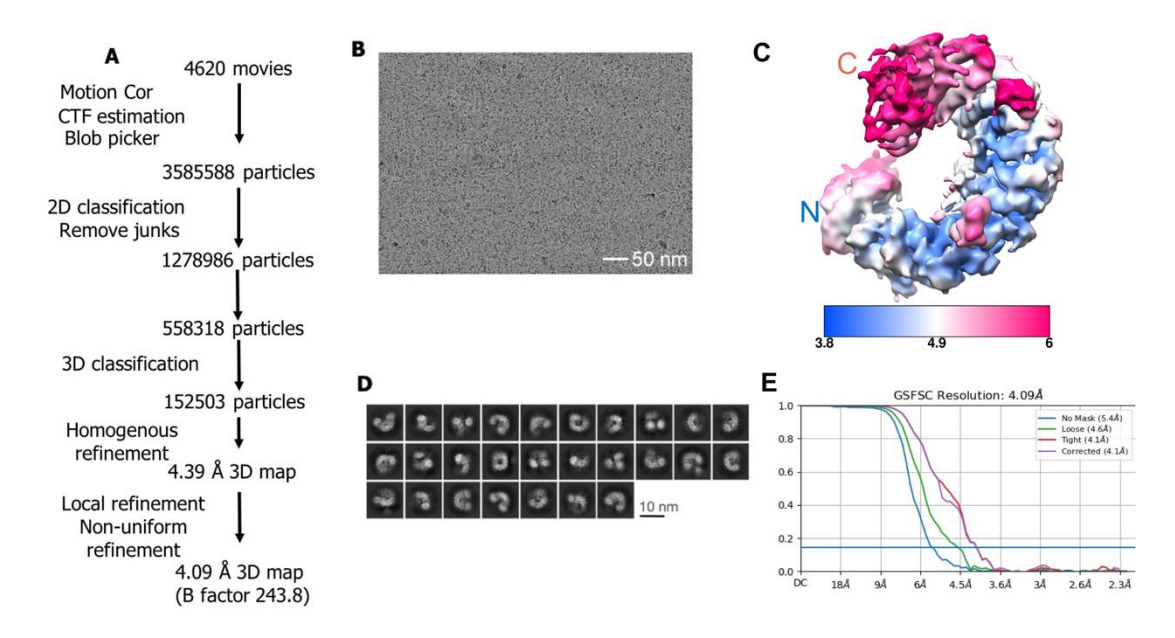


Fig. 7.3 Image analysis of KPNB1 and NFAT5 construct complex. (A) Summary of image processing workflow in CryoSPARC v3.1. (B) A representative microgram, scale bar 50 nm. (C) Local resolution estimation analyzed by CryoSPARC v3.1. (D) Representative 2D class averages from CryoSPARC v3.1 (E) Fourier shell correlation curve at different conditions.

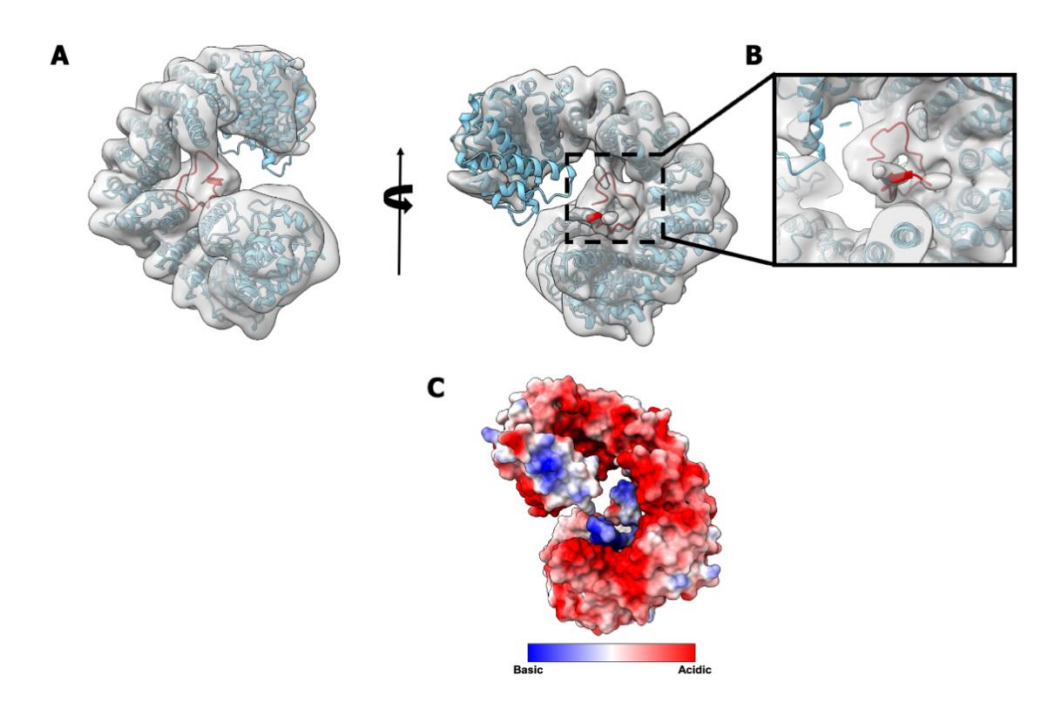


Fig. 7.4 Structure of KPNB1 and NFAT5 construct complex. (A) different views of the structure of KPNB1 fitting into the Cryo-EM map with NFAT5 construct cradled

inside. KPNB1 is colored in sky blue, while NFAT5 truncate colored in red. (B) Magnified view of the extra density after fitting of KPNB1 into Cryo-EM map with NFAT5 (residue 199-220) docking. (C) Electrostatic map of the complex. The acidic and basic residues are shown in red and blue respectively.

7.3 The KPNB1-NFAT5 structure reveals that the binding site for NFAT5 overlaps with that for the IBB domain

Macromolecular transport is a critical biological process in eukaryotic cells that involves the movement of molecules between the cytoplasm and the nucleus. The transport process is facilitated by a heterodimer of KPNB1 and KPNA (Cingolani et al., 1999). According to previous reports, KPNA is responsible for recognizing cargo proteins that contain a signature nuclear localization signal (NLS) in their sequence, while KPNB1 interacts with the nuclear pore complex for nuclear entry (Cingolani et al., 1999). KPNA1, a 60 kDa protein, is made up of a C-terminal NLS-binding domain and a flexible linker that connects it to an N-terminal importin-beta-binding (IBB) domain. Essentially, it was previously understood that the interaction between KPNB1 and the N-terminal aIBB domain of KPNA1 facilitates cargo translocation into the nucleus.

The atomic structures of homology IBB and KPNB1 have been resolved using X-ray Crystallography and uploaded in the protein data bank (PDB code: 2q5d and 1qgk), albeit the folding and architecture highly resemble each other. Using 1qgk as a model compared with the binding sites of NFAT5 and KPNB1 (**Fig. 7.5**), the IBB domain intimately associates with the concave surface of KPNB1, with the amino-end extended

moiety binding to HEAT repeat 7-11 and the carboxy-end helix interacting with HEAT repeat 12-19. Similar to NFAT5, the IBB domain is rich in basic residues complementary to negatively charged KPNB1 inner surface (Mitrousis et al., 2008).

A comparison of the KPNB1-NFAT5 and KPNB1-aIBB structures reveal that aIBB and NFAT5 suggests some sharing binding sites (**Fig. 7.5 B**). Even so, the C-terminal part of KPNB1 in these two structures adopt distinct conformation, as the C-termini of KPNB1 has an approximately 15-degree bending from the NFAT5 complex to the aIBB complex. This may be due to the effects from the interactions of the carboxy-terminal helix of aIBB with the C-terminal HEAT repeats of KPNB1. It's noteworthy that the IBB helix alone is sufficient to facilitate the complex formation, notwithstanding the binding affinity being reduced significantly (Rollenhagen et al., 2003). Interestingly, the N-terminal extended moiety of aIBB fits reasonably well to the density for NFAT5 after docking the IBB complex into the Cryo-EM map of NFAT5 and KPNB1 (**Fig. 7.5 A**). It has been reported that the N-terminal extended moiety interacts with the negatively charged residues in KPNB1 HEAT repeat 7-11 as well as the acidic loop in HEAT repeat 8 including the strictly conserved W342 (Mitrousis et al., 2008). Therefore, we speculate that the binding site for NFAT5 may at least partly resemble the IBB domains.

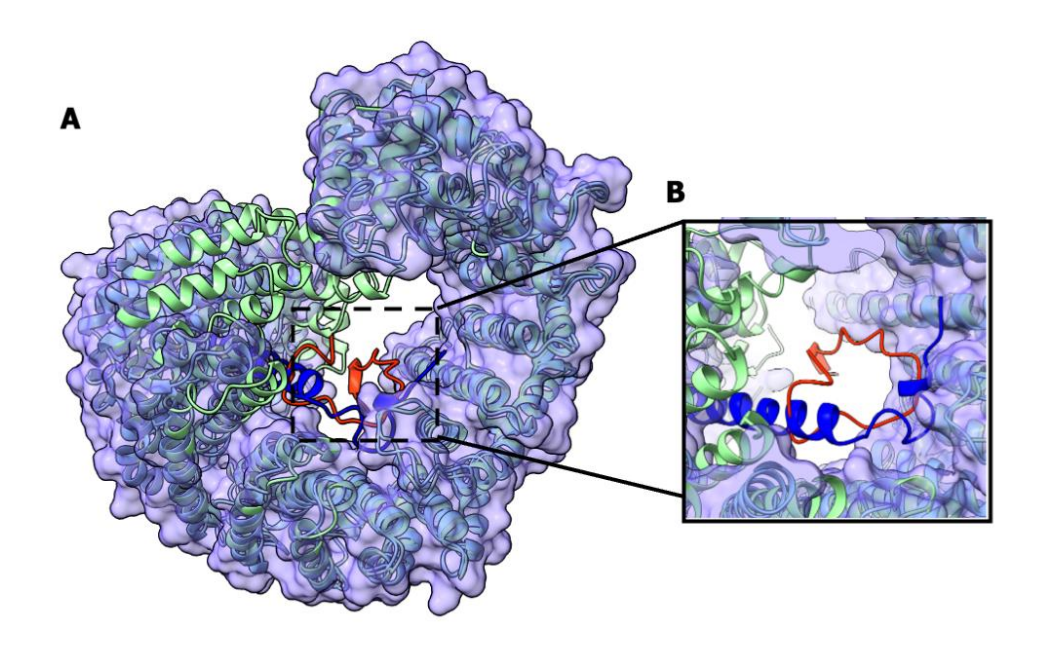


Fig. 7.5 Comparison study of the two KPNB1 structures in complex with NFAT5 and aIBB. (A) Alignment of NFAT5 and aIBB complexes at the N-terminal end of KPNB1. NFAT5 complex's KPNB1 is coloured sky blue with a purple surface. aIBB complex's KPNB1 is coloured flora. (B) Magnified view highlighting the NFAT5 and aIBB, which are coloured blue and red respectively. The acidic loop of KPNB1 is coloured yellow. aIBB complex PDB: 1qgk.

7.4 The KPNB1-NFAT5 structure reveals that the binding site for NFAT5 also overlaps with that for Ran-GTP

The shuttling of KPNB1 between the nucleus and cytoplasm is regulated by the small Ras-like GTP-binding protein, which can switch between a GTP- and GDP-bound form via GTP hydrolysis and nucleotide exchange (Renault et al., 1998). Importantly, the GTP-bound state Ran (Ran-GTP) is found at higher levels in the nucleus than in the cytoplasm. Once KPNB1 has translocated into the nucleus via the nuclear pore complex, cargo is displaced by Ran-GTP to form a KPNB1 and Ran-GTP

complex, which can then be exported outside the nucleus. Subsequent hydrolysis of GTP in the cytoplasm triggers the disassembly of Ran-GDP and KPNB1, allowing another cycle of nuclear import to occur.

Notably, binding analysis has shown that the N-terminal region of KPNB1 is essential for the binding of Ran-GTP, and that the first 364 residue of KPNB1 are sufficient to elicit a high binding affinity to Ran-GTP (Kutay et al., 1997). This has been confirmed by the crystallography structure of Ran-GDP in complex with a KPNB1 truncate of HEAT repeat 1-10 (PDB code: 1ibr). Like the IBB domains and NFAT5, Ran packs against the internal surface of the cradle-shaped KPNB1 and forms two major contact areas, with the first covering the concave face of the first three HEAT repeats of KPNB1, and the second located at the HEAT repeat 7 and the conserved acidic loop of HEAT repeat 8.

The structures of KPNB1 complexes with NFAT5 and Ran-GTP align well, except for the 8th HEAT repeat of the NFAT5-complexed KPNB1, which points more outward compared to the KPNB1 truncate (**Fig. 7.6 B**). Notably, the binding surface of Ran-GTP at the acidic loop of HEAT repeat 8 coincides with the interaction sites of NFAT5, providing a potential explanation for the slight structural difference between the two complexes. Moreover, **Fig. 7.6 A** shows that Ran-GTP occupies part of the extra density for NFAT5 when the Ran-GTP complex is docked into the Cryo-EM map of NFAT5 complex. These observations suggest that competition between Ran-GTP and NFAT5 could occur after the nuclear translocation of KPNB1, leading to the unloading of NFAT5 upon the formation of the Ran-GTP complex.

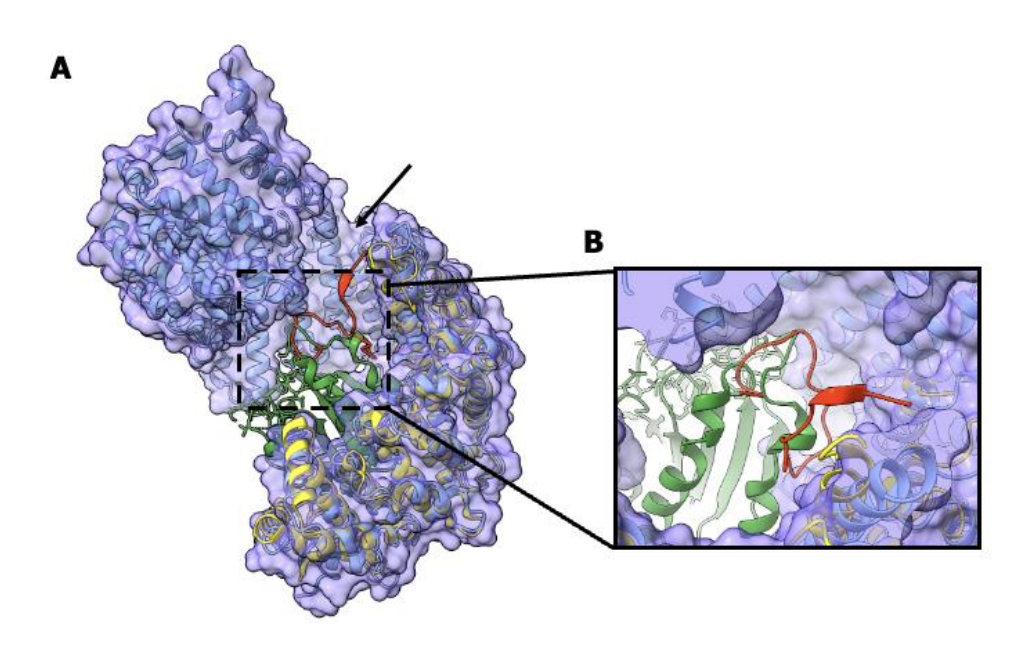


Fig. 7.6 Comparison study of the two KPNB1 structures in complex with NFAT5 and Ran-GTP. (A) Alignment of NFAT5 and Ran-GTP complexes at the N-terminal end of KPNB1. NFAT5 complex's KPNB1 is coloured sky blue with a purple surface. Ran-GTP complex's KPNB1 is coloured Yellow. (B) Magnified view highlighting the NFAT5 and Ran-GTP, which are coloured Green and red respectively. Arrow indicates the orientation difference at the 8th HEAT repeat of the two complexes. Ran-GTP complex PDB: 1ibr.

7.5 NFAT5 adopts a similar binding mode to PTHrP_{ncNLS}

The structure of KPNB1 is composed of 19 HEAT repeat superhelices arranged in an elongated, worm-like shape. Although the secondary structure of KPNB1 is well-defined, the overall architecture is highly flexible, which is necessary for nuclear import facilitated by cargo proteins such as transcription factors. This flexibility is due to the linear architecture of KPNB1 lacking a globular hydrophobic core, which allows it to conform to different binding partners with increased conformational freedom. Moreover, the diverse conformations of KPNB1 have been confirmed by high-

resolution X-ray crystallography and Cryo-EM analysis. Numerous structures of KPNB1 in complex with various substrates have been resolved at the atomic level. For example, the structures of KPNB1 truncates binding to ncNLS of parathyroid hormone-related protein (PTHrP) (PDB code: 1m5n) and Ran-GTP were solved using X-ray crystallography with resolutions of 2.9 Å and 2.3 Å, respectively. Additionally, the atomic structure of histone and full-length KPNB1 (PDB code: 6n89) was determined from a ~7.5 Å Cryo-EM map, which is the only KPNB1 structure from Cryo-EM so far, and the low resolution of this map may be due to the intrinsic flexible nature of KPNB1.

The folding of various KPNB1 structures is diverse depending on the associated substrates, albeit all of them adopt a 'close' conformation. To better capture the conformational differences, Fig. 7.7 aligns the KPNB1-NFAT5 complex with various KPNB1 complexes by anchoring to the N-terminal heat repeats and examining the discrepancy of the alignment. As predicted, some complexes appear to 'grab' the cargo more tightly, while others have their C-terminal end pointing in a different direction. Some regions of the structure, including the acidic loop and the tallest 8th heat repeat, are more flexible and adopt different orientations in the KPNB1 complexes. The functional implications of these conformational differences remain to be elucidated. Specifically, the first ten heat repeats adopt a highly similar conformation in both truncated and full-length KPNB1, despite different binding substrates, as shown in Fig. 7.7 A and B. For the C-terminal heat repeats, obvious conformational differences were observed, possibly due to the diverse binding modes to their substrate (Fig. 7.7 C). Interestingly, the atomic structure of KPNB1-NFAT5 NLS is resolved by Cryo-EM with

a C-terminal end vastly diverse from that of another Cryo-EM structure, KPNB1-histone. Instead, the overall conformation of KPNB1-NFAT5 NLS is much more similar to KPNB1-aIBB.

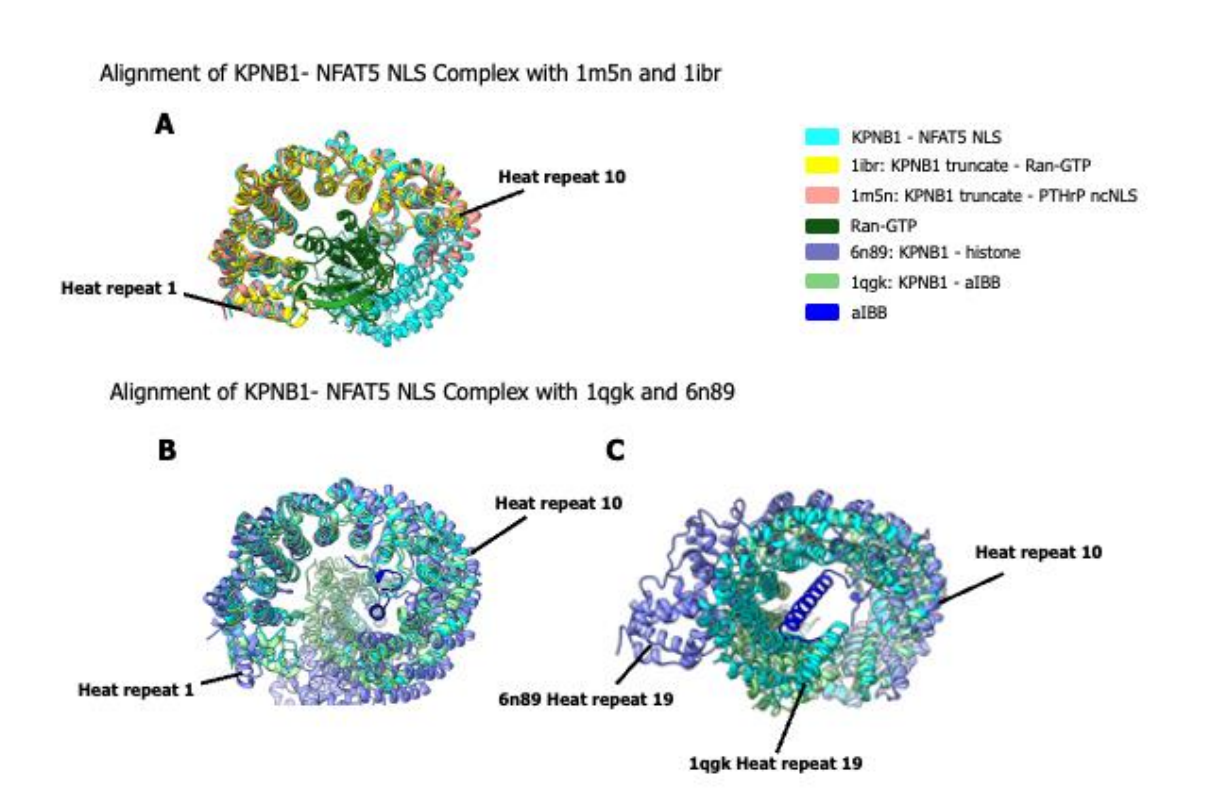


Fig. 7.7 Structural analysis on KPNB1 binding to different ligands. (A) Alignment of the structure of full-length KPNB1-NFAT5 NLS to that of the two truncated KPNB1 complexes. The first 10 heat repeats are highlighted. (B) Alignment of the structure of full-length KPNB1-NFAT5 NLS to that of the full-length KPNB1 in complex with histone and aIBB. The first 10 heat repeats are highlighted. (C) The C-terminal heat repeats of the same alignment of (B) are highlighted.

Chapter 8 Structure-based biochemical studies to delineate the molecular mechanism of tonicity-driven nuclear import of NFAT5

8.1 Competitive binding assay confirms that NFAT5 and RanGTP bind to overlapping sites on KPNB1

According to our findings, the nuclear import receptor KPNB1 binds to NFAT5, leading to its nuclear localization. Cryo-EM structure of the KPNB1-NFAT5_{cNLS} complex revealed that RanGTP and NFAT5_{cNLS}, two cargoes of KPNB1, bind to an overlapping site on KPNB1. To confirm the binding site, we performed competition binding assays. Initially, We measured the binding affinity of RanQ69L, a constitutively active model of RanGTP, with KPNB1 (Chen et al., 2017). Unexpectedly, RanQ69L showed no interaction with KPNB1 (Fig. 8.1).

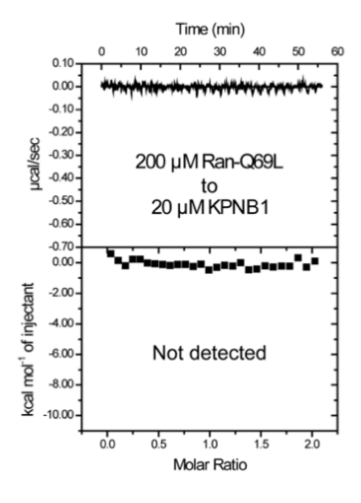


Fig. 8.1 Characterization of the interaction between RanQ69L and KPNB1. 200 μ M RanQ69L was titrated to 20 μ M KPNB1.

After nucleotide exchange using a non-hydrolyzable analog of guanosine triphosphate (GTP), GppNHp, we determined that RanQ69L-GppNHp bound to KPNB1 with a binding affinity of Kd \sim 63.69 nM (**Fig. 8.2 A**). Subsequently, we incubated 35 μ M RanQ69L-GppNHp with 20 μ M KPNB1 for 5 minutes before titrating 200 μ M NFAT5_{cNLS}. The ITC results revealed a weak interaction between NFAT5_{cNLS} and RanQ69L-GppNHp saturated KPNB1 (Kd \sim 56.82 μ M) compared to the control where NFAT5_{cNLS} bound to KPNB1 with a binding affinity of Kd \sim 2.78 μ M (**Fig. 8.2 compare B and C**).

ITC measurements provided additional evidence supporting our Cryo-EM structure, as they confirmed that RanGTP and NFAT5 bound to KPNB1 competitively at an overlapping binding surface. It is in line with the mechanism by which RanGTP induces cargo release.

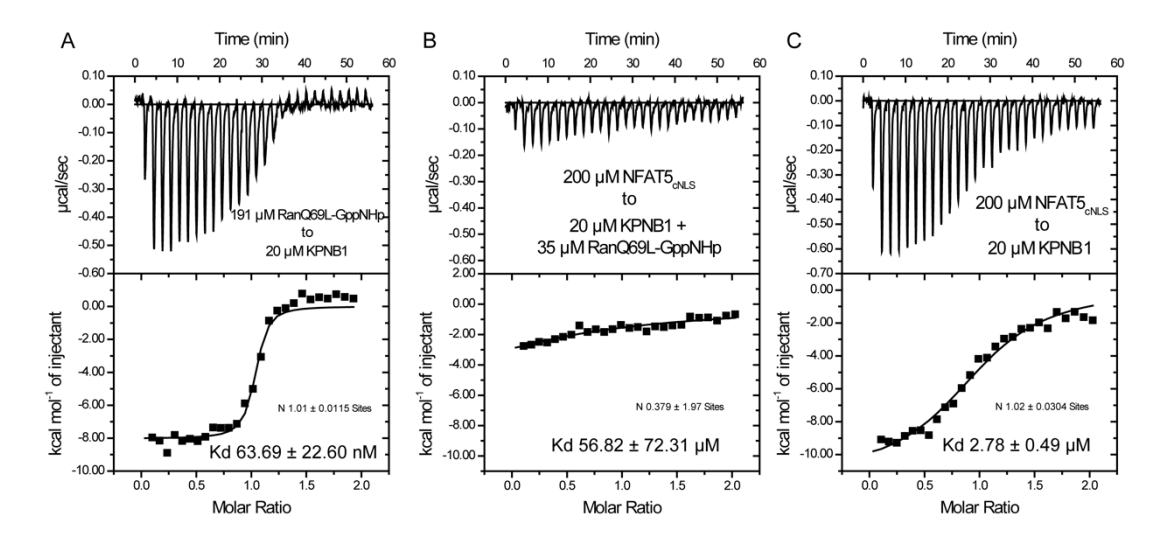


Fig. 8.2 The competition for binding to KPNB1 by RanQ69L-GppNHp and NFAT5_{cNLS}. (A) Interaction of RanQ69L-GppNHp with KPNB1. (B) ITC to investigate

the interaction of synthetic NFAT5_{cNLS} and KPNB1 saturated by RanQ69L-GppNHp.

(C) ITC to investigate the interaction of synthetic NFAT5_{cNLS} and KPNB1.

8.2 The conserved acidic loop in KPNB1 is required for binding to NFAT5_{cNLS}

Our Cryo-EM structure of the KPNB1-NFAT5_{cNLS} complex highlighted the importance of amino acids in KPNB1's 8th HEAT repeat acidic binding groove. This region of KPNB1 that interacts with NFAT5 is characterized by numerous acidic residues that are electrostatically complementary to the positively charged cNLS (amino acids 199-216) of NFAT5. Previous research demonstrated the involvement of KPNB1-D288 in interactions with parathyroid hormone-related protein (PTHrP)-ncNLS (Cingolani et al., 2002), IBB-R13 (Cingolani et al., 1999), and Ran-R140 (Vetter et al., 1999). Therefore, we conducted mutagenesis screening of the acidic residues in the 8th HEAT repeat of KPNB1 to evaluate their contribution to NFAT5 binding.

These double-mutants were generated by replacing D288, E289, D292 and E296 with either alanine or lysine, including KPNB1-D288A_E289A, KPNB1-D288K_E289K, KPNB1-E289A_D292A, KPNB1-E289K_D292K, KPNB1-D292A_E296A and KPNB1-D292K_E296K. They were well expressed and purified to homogeneity.

We measured the affinity of these mutants to NFAT5_{cNLS} using ITC. The wild-type KPNB1 had an affinity to NFAT5_{cNLS} in the micromolar range (\sim 0.56 μ M; Fig. 8.3 A). The D288A_E289A mutation caused an increase in the Kd value by approximately 3-4 folds (Kd \sim 1.94 μ M; Fig. 8.3 compare A and B). Furthermore, the D288K_D289K mutation showed a \sim 40-fold increased Kd value (Kd \sim 20.37 μ M; Fig. 8.3 compare A and C). These results suggest that residues D288 and E289 contribute to the binding of NFAT5_{cNLS}.

However, alanine substituted E289_D292 and D292_E296 barely changed the affinity (Kd \sim 0.76 μ M; **Fig. 8.3 compare D and F with A**). E289K_D292K and D292K_E296K mutants showed a slightly decreased binding affinity (Kd \sim 2.14 μ M, \sim 2.16 μ M; **Fig. 8.3 compare E and G with A**). These measurements suggest that D292 and E296 have a relatively minor contribution to the interaction between NFAT5 and KPNB1

These ITC measurements indicate that D288 of KPNB1 plays a vital role in the interaction between NFAT5_{cNLS} and KPNB1, while E289 plays a minor role. The two residues may function as a critical tether in stabilizing the relative position of NFAT5_{cNLS}.

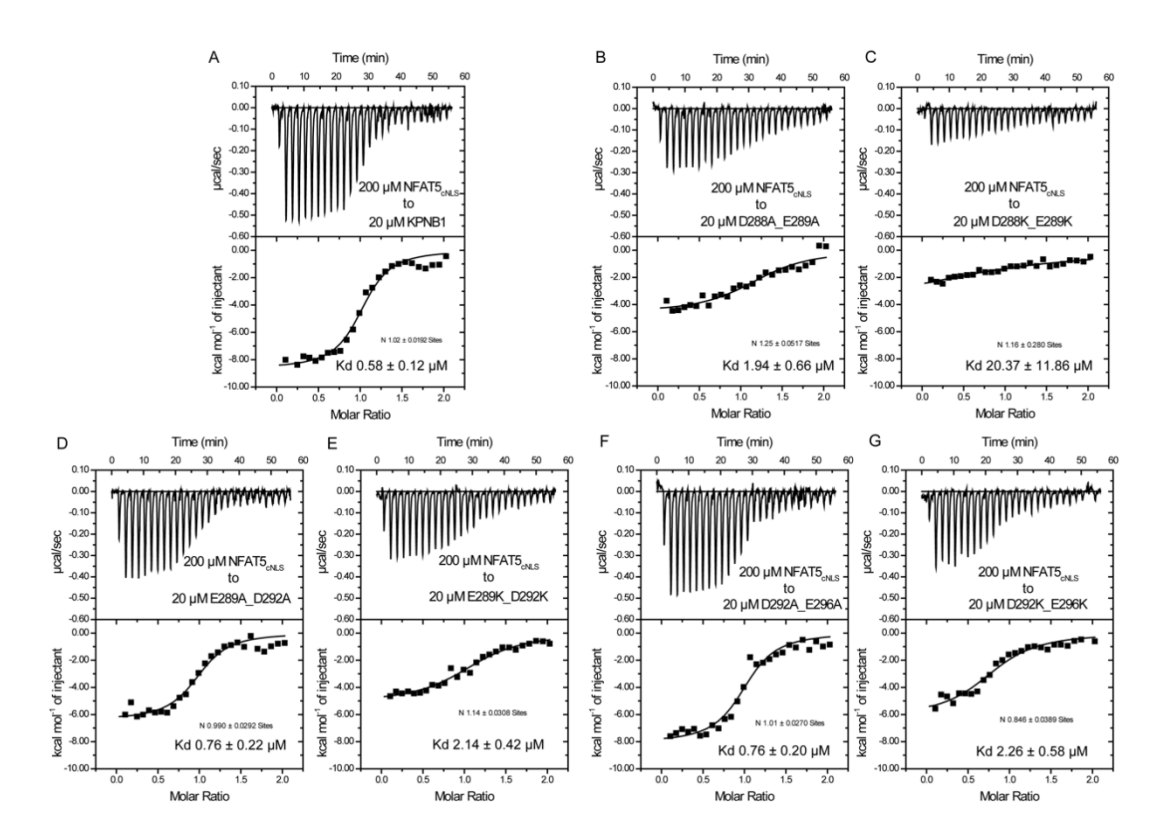


Fig. 8.3 Characterization of the interaction between NFAT5_{cNLS} and KPNB1 mutants. 200 μ M synthetic peptide NFAT5_{cNLS} was titrated to 20 μ M KPNB1 and its double mutants, respectively.

8.3 Key residues that contribute to KPNB1-KPNA1_{IBB} complex are essential for KPNB1-NFAT5_{cNLS} complex

Our Cryo-EM structure of the KPNB1-NFAT5_{cNLS} complex highlighted the importance of amino acids in the basic concave surface of KPNB1, including residues W342, W430 and W472. Notably, W472 and W430 are strictly conserved across different species, underscoring their functional importance in KPNB1. Additionally, these two residues have been found to impact the binding affinity between KPNB1 and KPNA1-IBB (Mitrousis et al., 2008).

To investigate the role of these amino acids, we generated KPNB1 single mutants by substituting W342, W430 and W472 with either alanine or lysine. Specifically, KPNB1-W342A, KPNB1-W430K and KPNB1-W472K were well expressed and purified to homogeneity.

We measured the affinity of these mutants to NFAT5_{cNLS} using ITC. In comparison to the wild-type KPNB1 (\sim 0.56 μ M; **Fig. 8.3 A**), alanine substituted W342A barely changed the affinity (\sim 0.55 μ M; **Fig. 8.4 A**). However, KPNB1-W430K and KPNB1-W472K showed decreased binding affinities (Kd \sim 7.63 μ M, \sim 2.94 μ M; **Fig. 8.4 B and** C), suggesting the crucial role of W430 and W472 in the interaction between KPNB1 with NFAT5_{cNLS}.

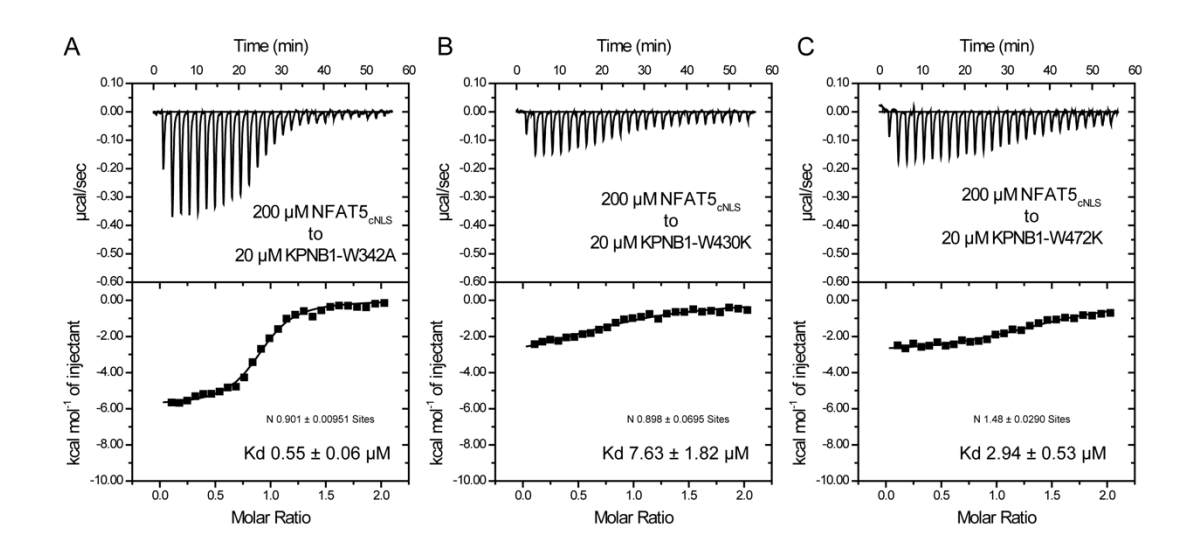


Fig. 8.4 Characterization of the interaction between NFAT5_{cNLS} and KPNB1 mutants. 200 μ M synthetic peptide NFAT5_{cNLS} was titrated to 20 μ M KPNB1 mutants respectively.

8.4 The hydrophobic binding surface in KPNB1 is required for binding to NFAT5_{cNLS}

In the vicinity of NFAT5_{cNLS}, our Cryo-EM structure analysis revealed the presence of residues V350, M353, and L354 within a hydrophobic binding surface of KPNB1. To investigate the functional significance of these amino acids, we generated KPNB1 double mutants with alanine substitutions at V350, M353, and L354. Specifically, we obtained KPNB1-V350A_M353A and KPNB1-M353A_L354A mutants, which were successfully expressed and purified to homogeneity.

We assessed the binding affinity of these mutants to NFAT5_{cNLS} by ITC. In comparison to the wild-type KPNB1 (Kd \sim 0.56 μ M; **Fig. 8.3 A**), the alanine substitution of KPNB1-V350A_M353A showed a slightly decreased binding affinity (Kd \sim 1.48 μ M; **Fig. 8.5 A**). Furthermore, the M353K_L354K mutation showed a \sim 14-fold increased Kd value (Kd \sim 7.30 μ M; **Fig. 8.5 B**).

These findings unequivocally emphasize the crucial role of V350, M353 and L354 in the interaction between KPNB1 and NFAT5 $_{cNLS}$.

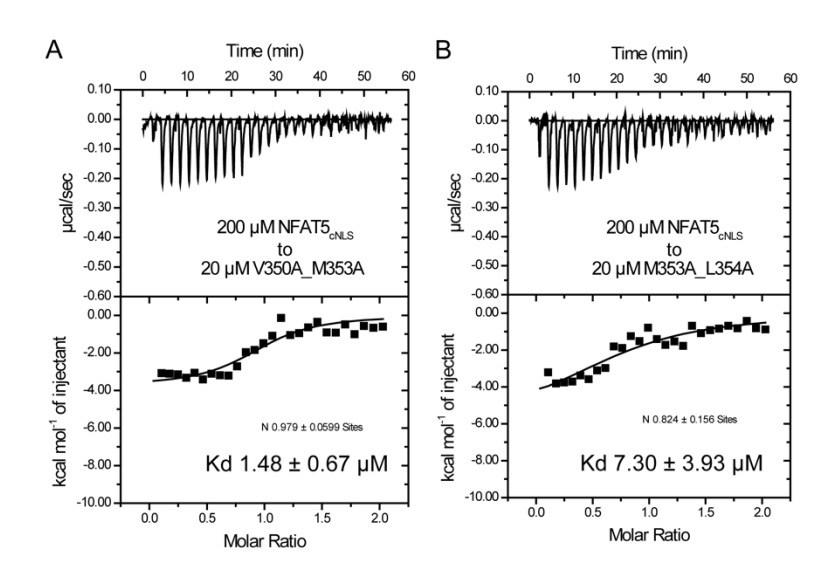


Fig. 8.5 Characterization of the interaction between NFAT5_{cNLS} and KPNB1 mutants. 200 μ M synthetic peptide NFAT5_{cNLS} was titrated to 20 μ M KPNB1 double mutants respectively.

8.5 NFAT5 LLPS is mediated by positively charged residues within the cNLS

Dr. Ko's previous data showed that the positively charged residues R202_K203R_R204 at cNLS domain is necessary for NFAT5 nuclear import activity (Section 4.2, Fig. 4.3), and NFAT5 AED+NLS undergoes LLPS. To investigate the role of cNLS in NFAT5 LLPS, we created three double- or triple-mutants in which arginine and lysine residues were replaced with alanine (Fig. 8.6 A). All three mutants were well expressed in *E.coli* and purified using the same protocol as the wild-type (WT) NFAT5 AED+NLS (amino acids 132-253).

Under 100 mM NaCl, we observed fluorescence-labeled condensed droplets of NFAT5₁₃₂₋₂₅₃. In comparison, we did not observe any condensate formation of the three

mutants (R199A_K200A, R202A_K203A_R204A and R214A_R215A) of NFAT5 AED+NLS (NFAT5₁₃₂₋₂₅₃) under the same conditions (**Fig. 8.6 B**). Further analysis of the component in the condensed phase using sedimentation assay revealed that, except for WT, the three mutants were distributed as a single homogeneous solution (**Fig. 8.6 C and D**). In addition, the solutions of the three mutants were transparent when compared to the turbidity observed in the WT solution, confirming that NFAT5 AED+NLS -R199A_K200A, NFAT5 AED+NLS -R202A_K203A_R204A, and NFAT5 AED+NLS-R214A R215A failed to undergo LLPS (**Fig. 8.6 D**).

These findings suggest that positively charged amino acids in the cNLS domain are necessary for nuclear import and NFAT5 LLPS.

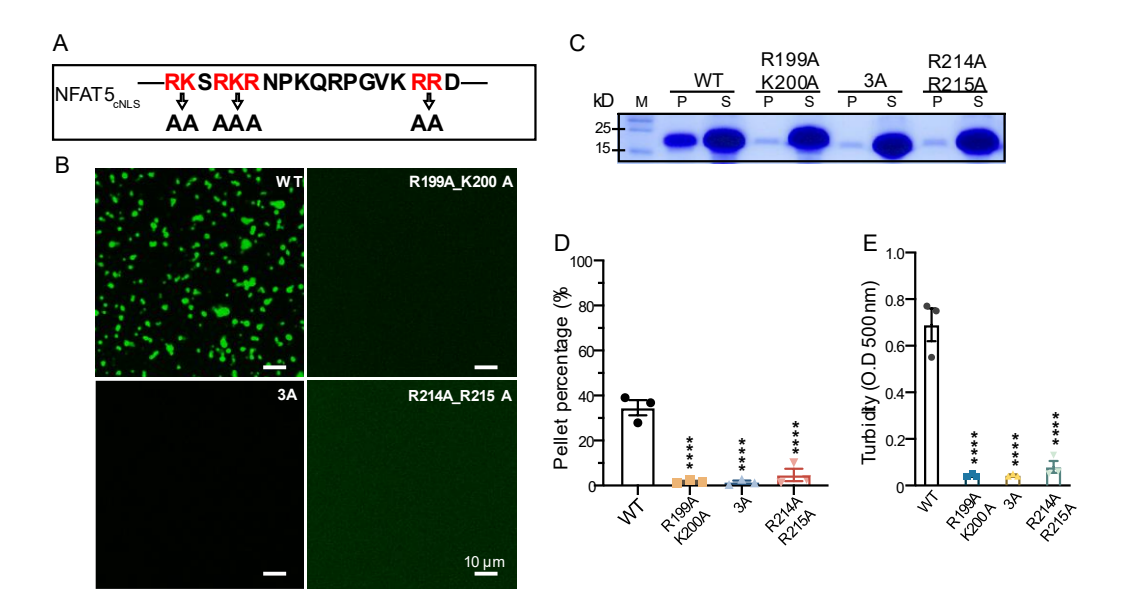


Fig. 8.6 K/R-rich bipartite cNLS is required for LLPS of NFAT5. (A) Scheme diagram depicting the sequence of NFAT5_{cNLS}. The highlighted positively charged bipartite cNLS (R199_K200; 3A: R202_K203_R204 and R214_R215) were mutated

to alanine. (B) Fluorescence imaging of LLPS at 100 mM NaCl. 0.6 mM NFAT5₁₃₂₋₂₅₃ and its mutants were labeled by Alexa 488 fluorophore. (C) SDS-PAGE analysis of the component in pellet fractions and supernatant fractions. M: marker; NFAT5₁₃₂₋₂₅₃ (WT), R199A_K200A and R214A_R215A: 13.4 kDa; R202A_K203A_R204A (3A): 13.2 kDa; "P" and "S": the fractions of proteins recovered in the condensed phase (P) and dilute phase (S). (D) Quantification of LLPS enrichment. The fraction of "P" was normalized with the "S" fraction from three independent repeated experiments. (E) Turbidity assay to demonstrate differences in turbidity among four proteins when protein concentration was 0.6 mM and NaCl concentration was 100 mM. The turbidity was measured at 500 nm UV-Vis. Statistics were presented as mean ± s.e.m. for three independent batches of experiments. *, p<0.05; **, p<0.01; ***, p<0.001 using one-way ANOVA with Dunnett's multiple comparisons test. The scale bar is 10 μm.

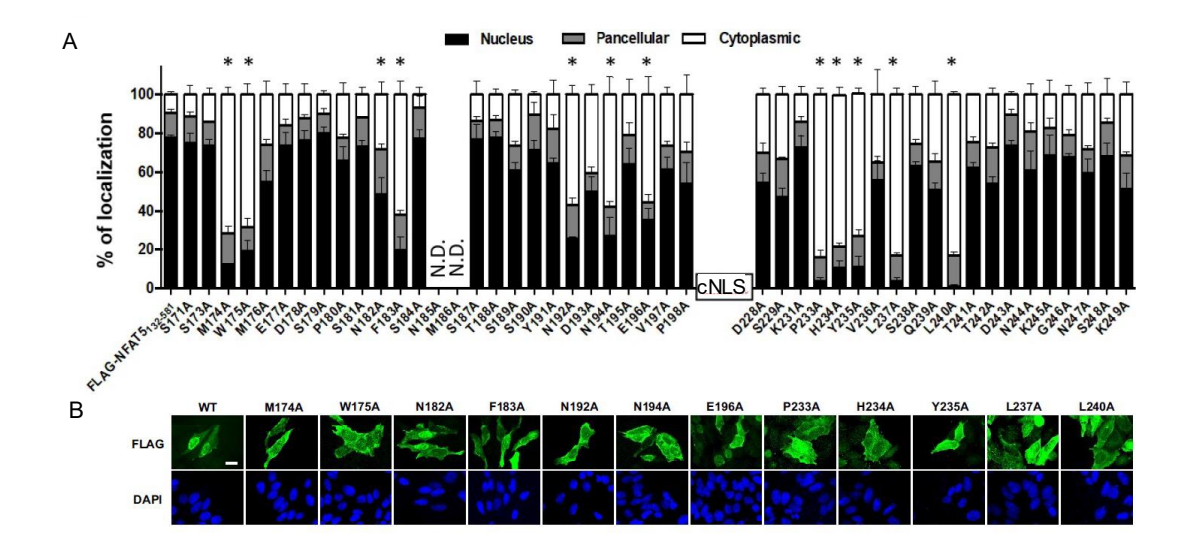
8.6 NFAT5 LLPS is mediated by multiple residues within the full NLS

Functional mapping of pivotal NFAT5 residues for nuclear import activity

Dr. Ko's lab conducted comprehensive alanine-scanning mutagenesis to identify the pivotal amino acid residues essential for the nuclear import activity of NFAT5 *in vivo*. FLAG-NFAT5₁₃₂₋₅₈₁ containing the AED domain required for nuclear export, the full NLS domain identified as essential for nuclear import, and the RHD domain, a

DNA binding domain, was used as a template for mutagenesis. Due to its size that exceeded 40 kDa, this protein required an active transport mechanism for translocation across the nuclear membrane.

The result indicated that the substitution of specific amino acids with alanine, such as M174, W175, N182, F183, N192, N194, or E196 (located proximal to the cNLS) and P233, H234, Y235, L237, or L240 (located distal to the cNLS), under hypertonic conditions significantly abolished NFAT5 nuclear localization (**Fig. 8.7**). This suggests the indispensability of these specific amino acid residues in facilitating the nuclear import of NFAT5.



NFAT5₁₃₂₋₅₈₁ **mutants.** (A) Quantitative analysis of fluorescence signal subcellular localization in HeLa cells expressing alanine-substituted FLAG-NFAT5 mutants. Cells were fixed with paraformaldehyde, stained with DAPI, and imaged using confocal

microscopy 24 hours after transfection of FLAG-NFAT5₁₃₂₋₅₈₁ carrying the indicated mutation under isotonic conditions. At least 100 cells were scored for each condition. The results are presented as the mean \pm s.e.m. of three independent experiments. * represents a significant reduction in nuclear FLAG signal compared to cells expressing FLAG-NFAT5₁₃₂₋₅₈₁, p<0.0001, by one-way ANOVA with Bonferroni's multiple comparison test as a post-test. (B) Representative fluorescence images of fixed HeLa cells expressing indicated recombinant NFAT5 mutants under hypertonicity. The scale bar is 30 μ m.

Alanine mutagenesis enhances NFAT5 LLPS by reducing liquidity

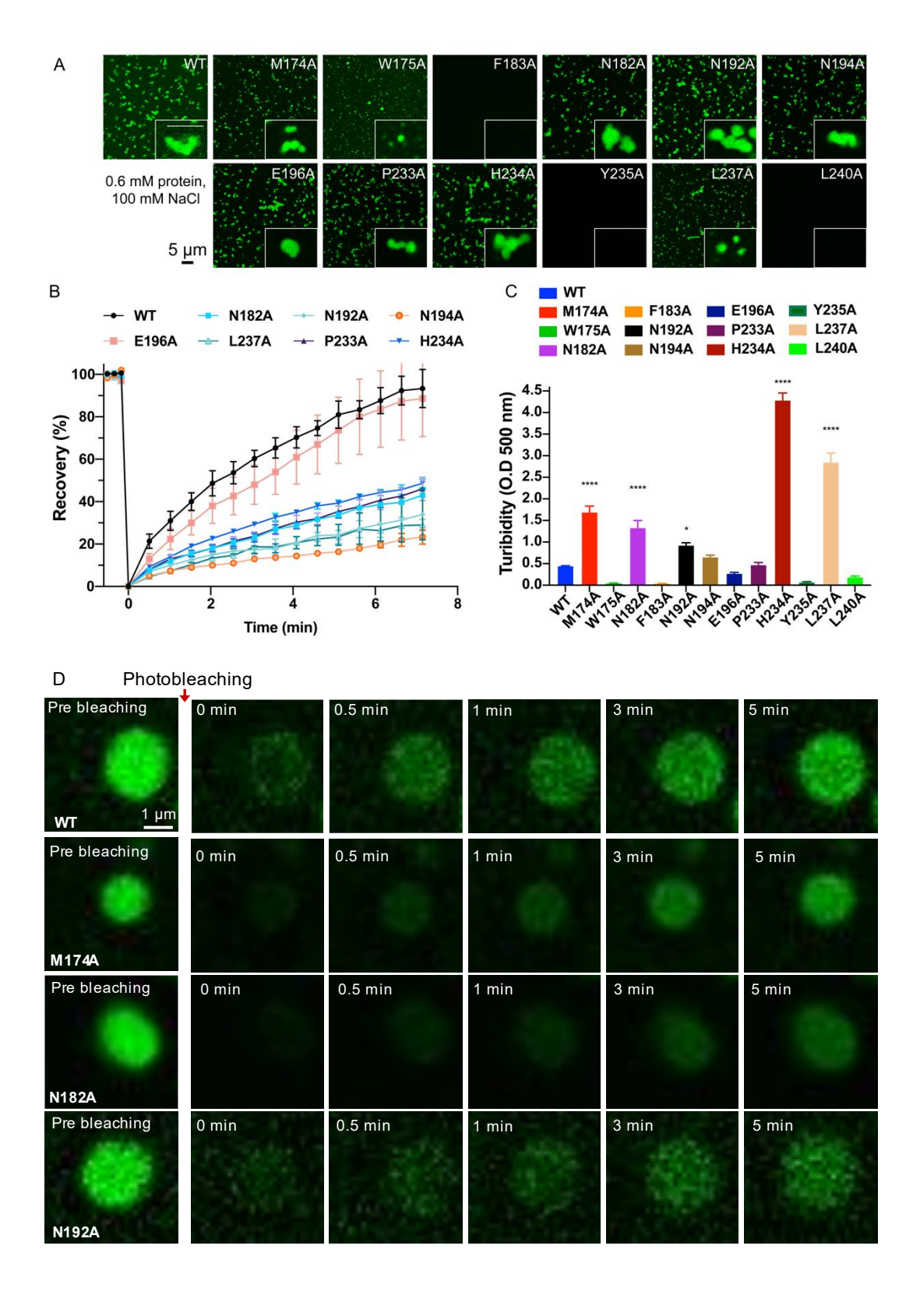
To elucidate the relationship between the essential amino acids screened for nuclear import and the LLPS of NFAT5, we generated alanine mutants using NFAT5 AED+NLS as a template and purified them using the same protocol as used in the wild type.

We assessed the formation of condensed droplets formation of these alanine-substituted NFAT5 AED+NLS mutants and found that most fluorescence-labeled alanine mutants were enriched in condensed droplets, except for F183A, Y235A, and L240A (**Fig. 8.8 A**). However, among the condensed mutants, the morphology of condensed droplets of W175A and E196A (proximal to the cNLS) exhibited soft material properties, whereas the others were as firm as the wild type.

To rule out the possibility that the condensed liquid phase of alanine mutagenesis was different in molecules exchange, we conducted FARP experiments. E196A, similar to the wild-type NFAT5₁₃₂₋₂₅₃, recovered over 80% of the fluorescent intensity after photobleaching, indicating that the mobility in the condensed phase remained unchanged (**Fig. 8.8 B and D**). On the other hand, the fluorescent signal of N182A, N192A, N194A, L237A, P233A, and H234A exhibited a lower recovery rate at > 40%. Specifically, N194A recovered only 20% after photobleaching (**Fig. 8.8 B and D**). All alanine mutants were recovered with a lower recovery speed than the wild type, suggesting decreased mobility (**Fig. 8.8 D**).

Consistent with these results, except for F183A, Y235A, and L240A, the solutions of other mutants turned opalescent immediately when the NaCl concentration was decreased (**Fig. 8.8 C**).

In summary, alanine mutagenesis of NFAT5 abolished its nuclear localization activity but enhancing LLPS through decreasing the liquidity. The amino acids that are indispensable for nuclear import activity are also critical for the LLPS of NFAT5.



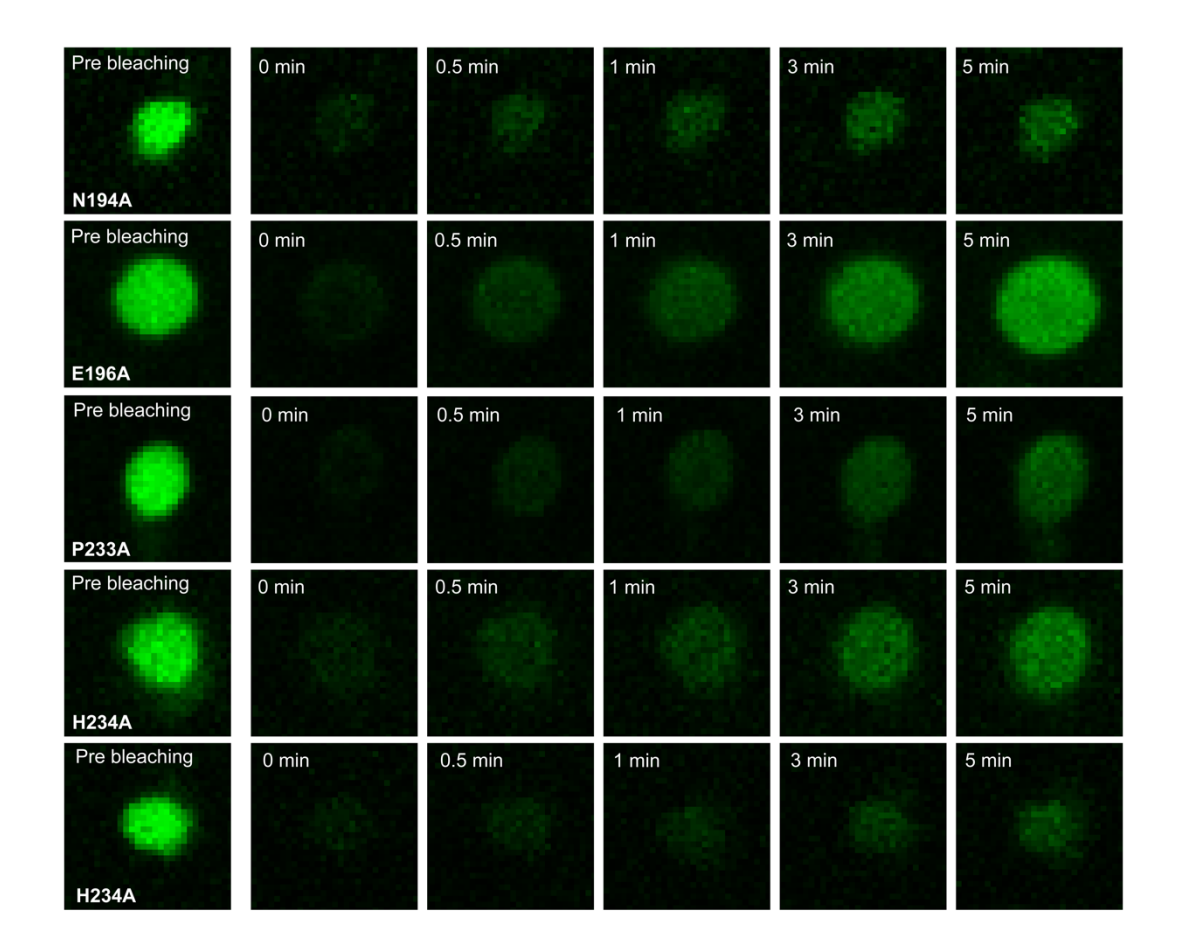


Fig. 8.8 Alanine mutagenesis improves NFAT5 LLPS. (A) Fluorescence droplets formed at 100 mM NaCl by 0.6 mM NFAT5₁₃₂₋₂₅₃ and its corresponding alanine mutants. (B) FRAP of phase-separated alanine mutants compared to NFAT5₁₃₂₋₂₅₃ wild type. (C) UV-Vis 500 nm turbidity measurements of solutions containing corresponding proteins. (D) Fluorescence imaging demonstrating the fluorescent intensity recovery of NFAT5₁₃₂₋₂₅₃ and its alanine mutagenesis. Statistic data were presented as mean \pm s.e.m with results from 3 independent batches of experiments. n.s., not significant; *, p<0.05; ***, p<0.01; ****, p<0.001; *****, p<0.0001 using one-way ANOVA with Dunnett's multiple comparisons test. Scale bars are 5 μm (A) and 1 μm (D), respectively.

8.7 NFAT5 LLPS is disrupted by tonicity-driven phosphorylation in the AED+NLS region

The role of tonicity-driven phosphorylation in regulating the nucleocytoplasmic transport of NFAT5 has been extensively investigated. Phosphorylation at T135 and Y143 of NFAT5 has been shown to significantly enhance its transcription and transactivation activities and increase its nuclear abundance (Gallazzini et al., 2011; Irarrazabal et al., 2010; Zhou et al., 2010). To explore the relationship between nucleocytoplasmic transport and LLPS of NFAT5, we generated two phosphomimetics using NFAT5 AED+NLS (amino acids 132-253) as the template. T135E and Y143E mutants of NFAT5 AED+NLS were purified using the same protocol as the WT.

As depicted in **Fig. 8.9 A**, NFAT5 AED+NLS-T135E and NFAT5 AED+NLS-Y143E failed to form condensed droplets compared to the wild type. The two phosphomimetics could not form any condensed phase (**Fig. 8.9 B and C**). Moreover, the solutions of the two phosphomimetics remained clear aqueous solutions with decreasing NaCl concentration (**Fig. 8.9 D**). Our findings suggest that tonicity-driven phosphorylation of NFAT5 AED+NLS impedes its LLPS.

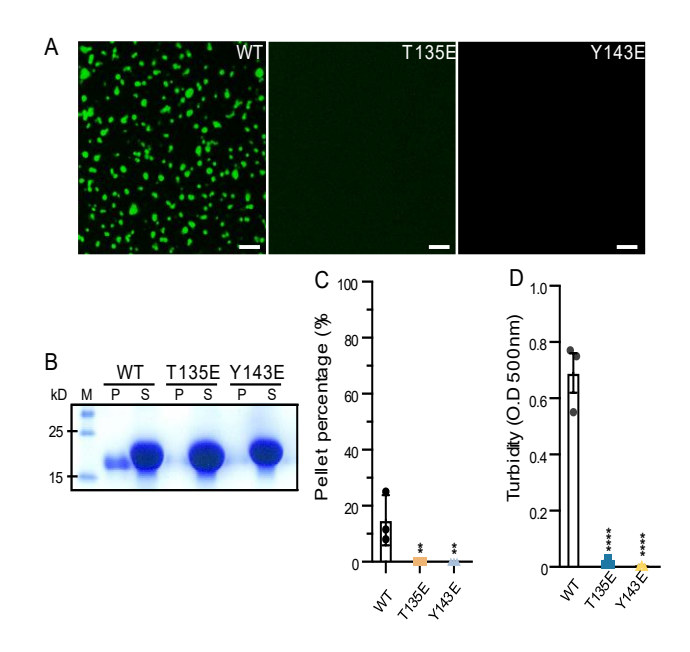


Fig. 8.9 Tonicity-driven phosphorylated sites are important for the LLPS of NFAT5. (A) Fluorescence imaging of 0.6 mM condensed NFAT5₁₃₂₋₂₅₃ and its mutants in 100 mM NaCl. Fluorophore Alexa 488 was used for LLPS imaging. (B) SDS-PAGE analysis of the component in pellet fractions and supernatant fractions. M: marker; NFAT5₁₃₂₋₂₅₃ (WT), T135E and Y143E: 13.4 kDa. "P" and "S": the fractions of proteins recovered in the condensed phase (P) and dilute phase (S). (C) LLPS enrichment quantification. The fraction of "P" was normalized with the "S" fraction from three independent repeated experiments. (D) Turbidity assay demonstrating the differences in turbidity among four proteins when the protein concentration was 0.6 mM, and the NaCl concentration was 100 mM. The turbidity was measured at 500 nm UV-Vis. Statistics were presented as mean ± s.e.m. for three independent batches of experiments. *, p<0.05; **, p<0.01; ***, p<0.001; ****, p<0.0001 using one-way ANOVA with Dunnett's multiple comparisons test. The scale bar is 10 μm.

Chapter 9 Conclusions and discussions

NFAT5 is the only mammalian tonicity-regulated transcription factor. It is responsible for mounting a rapid response, usually within 10-30 minutes, to rescue cells from the deleterious and irreversible damage of hypertonicity. NFAT5 fulfills this task by undergoing tonicity-driven nuclear import so that it quickly accumulates in the nucleus to orchestrate a transcription program of osmo-adaptive response. Our studies here uncover several novel aspects of this process to improve our knowledge of NFAT5.

9.1 Nuclear import of NFAT5 depends solely on KPNB1 and a ncNLS

For the nuclear import process, a cargo can be transported by two types of transport machineries. The classical import machinery consists of an KPNA-KPNB1 heterodimer, with KPNA serving as the adaptor that recognizes the NLS on the cargo molecule and KPNB1 serving as the receptor to transport the trimeric KPNA-KPNB1-cargo complex through the nuclear pore complexes in the cytoplasm-to-nucleus direction. The second type of import machinery does not use KPNA as the adaptor. Instead, an KPNB molecule serves as both the adaptor and the receptor by binding to the NLS on the cargo molecule directly and carrying the dimeric KPNB-cargo complex through the nuclear pores.

The type of nuclear import machinery (i.e. KPNA-KPNB1 vs. KPNB-only) is determined by the NLS on the cargo molecule. Majority of nucleus-destined cargo molecules contain a classical K/R-rich NLS (cNLS) that is specifically recognized by one of the many KPNA members for fast and efficient nuclear import by the KPNA-KPNB1 machinery. For cargos transported by KPNB-only machinery, their NLSs are not the cNLS type and instead very diverse in terms of sequence and binding mode to KPNB members. Currently, the nuclear import machinery for some of the over 2,000 nucleus-destined proteins are yet to be identified.

Here our siRNA studies show that the tonicity-driven nuclear import process of NFAT5 depends only on KPNB1. Additionally, the full NLS of NFAT5 is a very long segment (residues 171 to 253) that contains a K/R-rich bipartite cNLS flanked by flexible loops at both the N- and C-terminal ends. This finding assigns NFAT5 to a small but expanding group of cargo molecules such as histones, PTHrP and SREBP that employ the KPNB1-only machinery route.

9.2 The KPNB1-NFAT5 structure reveals a unique binding site that overlaps with RanGTP and IBB

KPNB1 is a large-sized molecule that forms a super-helical structure with its 19 HEAT repeats. As a result, the concave side of KPNB1 forms an extended binding surface that can accommodate a variety of substrates. This binding surface is populated

by many acidic residues including aspartate and glutamate, which can form electrostatically favorable interactions with K/R-rich NLS substrates.

Extensive studies have revealed how KPNB1 recognizes two key binding partners, namely RanGTP and IBB. KPNB1 binds to Ran-GTP three distinct binding sites: N-terminal site (HEAT repeat 1-3), region nearby acidic loop, and C-terminal site (HEAT repeat 13-15). And the IBB intimately associates with the concave surface of KPNB1, with the amino-end extended moiety binding to HEAT repeat 7-11 and the carboxyend helix interacting with HEAT repeat 12-19.

Here our structure shows that NFAT5 binds to a region on KPNB1 that overlaps with both RanGTP and IBB. Additionally, our mutational studies show that D288, M350, L354 and W472 of KPNB1 play vital roles in the interaction between NFAT5_{cNLS} and KPNB1, while E289 and W430 play minor roles. These findings offer mechanistic details to explain how KPNB1 is solely responsible for the nuclear import of NFAT5 while KPNAs are not needed. Our results also explain how the KPNB1-mediated nuclear import of NFAT5 is RanGTP-dependent.

Notably, our structure and biochemical studies reveal a moderate binding affinity between KPNB1 and NFAT5. The Kd values measured by *in vitro* ITC experiments are within 0.5- 4.6 µM range. The Cryo-EM structure of the KPNB1-NFAT5 complex shows limited density that accounts only for the short cNLS segment but not the full

NLS. Such moderate binding affinity is not common as most cargo molecules bind to their cognate KPNA or KPNB very tightly to ensure efficient nuclear import. We propose this feature could be beneficial for tonicity regulation as it may render the basal level of NFAT5 nuclear import relatively low and thus susceptible to enhancement by tonicity.

9.3 The NFAT5 NLS undergoes tonicity-regulated LLPS

DNA-binding transcription factors (TF) typically consist of DNA binding domain and one or more separate activation domains (AD), which are intrinsically disordered regions (IDRs). Some of IDR-IDR interactions facilitate the formation of LLPS in biomolecular condensates, for instance, the embryonic stem cell (ESC) pluripotency TF OCT4 (Boija et al., 2018). Previous studies have reported that nuclear import receptors, such as TNPO1 for FUS, can interfere with the LLPS of cargo proteins (Gonzalez et al., 2021; Yoshizawa et al., 2018).

Here, we confirm that N-terminal NFAT5 is IDR that undergoes LLPS, which are triggered by electrostatic interactions. NFAT5 LLPS is adapted to various isotonic conditions and accumulates in different locations of the cells in response to isotonic, hypotonic, and hypertonic treatments. Notably, stressed conditions trigger the formation of NFAT5 liquid condensates, and hypotonicity enhances their enrichment,

suggesting that NFAT5 LLPS serves as a "storage room" for NFAT5 by limiting its distribution.

These findings demonstrate a correlation between LLPS and NFAT5 nucleocytoplasmic transport and explain the role of the N-terminal and C-terminal proximity of NFAT5_{cNLS} in mediating nuclear import. We conclude that condensed NFAT5 promotes the formation of the KPNB1-NFAT5 complex, which explains for how KPNB1 can effectively import NFAT5 despite having a micromolar affinity when cells are subjected to hypertonicity.

We use the following formula Kd=([L][R])/[LR] to explain our conclusion. [L] is the concentration of free cargo (NFAT5); [R] is the concentration of free receptor (KPNB1); [LR] is the concentration of ligand-receptor complex, the KPNB1-NFAT5 complex in the cytoplasm under hypotonic conditions. Under hypertonicity, the transcription of NFAT5 and enrichment of NFAT5 LLPS were increased significantly, increasing [L]. The expression of KPNB1 is not affected by tonicity, and [R] remains unchanged. When NFAT5 is imported into the nucleus, [LR] in the cytoplasm decreases. Even with a low binding affinity, high [L] triggers the formation of LR (the KPNB1-NFAT5 complex). Eventually, NFAT5 is imported into the nucleus.

Our findings on KPNB1's role in modulating the LLPS of NFAT5 are consistent with the reported research. The electrostatic surface potential of KPNB1 can hinder the self-association of its cargo, thereby reducing its LLPS.

Our study reveals that the cNLS of NFAT5, which is critical for its nuclear import activity, is also critical for LLPS. The RKR₂₀₂₋₂₀₄AAA mutant of NFAT5 abolishes its nuclear import and blocks the direct interaction with KPNB1. Furthermore, KR-rich cNLS is necessary for NFAT5 LLPS, highlighting the importance of electrostatic interactions. These findings support our conclusion that LLPS of NFAT5 serves as a "buffering system" to compensate for its deficiency of weak binding affinity to KPNB1 and contribute to its effective nuclear import.

Previous research has revealed that LLPS is essential in orchestrating cell signaling across time and space (Su et al., 2021). The nuclear import ability is activated by phosphorylated NFAT5-T135, which is directly phosphorylated by cyclin-dependent kinase 5 (CDK5), and NFAT5-Y143, of which phosphorylation is involved in phospholipase C-γ1 (PLC-γ1) and a tyrosine kinase, cellular-abelsongene (c-Abl) (Gallazzini et al., 2011; Gallazzini et al., 2010; Irarrazabal et al., 2010). Besides, p38 and ERK1/2 are involved in the tonicity-driven activation of NFAT5 in response to both hypertonicity and hypotonicity (Zhou, 2016). The pleiotropic effects of these kinases and phosphatases raise the question of how they can selectively signal to NFAT5 in the context of hypertonicity. LLPS may be essential in the selective signaling of NFAT5 in

response to hypertonicity, which activates the nuclear import ability of NFAT5 through PTMs of T135 and Y143. We observe that NFAT5 phosphomimetics fail to undergo LLPS, suggesting that the distinct liquidity of NFAT5 condensates in response to tonicity plays a role in the selective enrichment of kinases.

Finally, alanine mutagenesis eliminates the nuclear import of NFAT5, and condensed alanine mutagenesis exhibits decreased liquidity. This result could be explained in two ways: either NFAT5 condensates with reduced liquidity act as sequestration, blocking the association of kinases and NFAT5, resulting in PTM depletion, or NFAT5 condensates with lower dynamics cause a loss of NFAT5 enrichment, which cannot compensate for the low binding affinity between KPNB1 and NFAT5, ultimately leading to the increased dissociation of the KPNB1-NFAT5 complex and abolishing the nuclear import.

9.4 Broader implications and plans for future studies

NFAT family members share a similar domain structure: N-terminal regulatory domain containing a cNLS domain, a highly conserved Rel homology domain (RHD) that is the DNA binding domain, and a C-terminal transactivation domain (AD) with little sequence conservation. Similar to NFAT5, the nuclear import machinery of NFAT1-4 needs the interference of nuclear import receptors. Our findings are also applicable for other TFs.

Previously reported NFAT5-DNA complex has unusually high binding stability due to the classical "butterfly" binding model (Li et al., 2022). Y220, R217, E223, and R226 of NFAT5 N-terminal IDR have significant interactions with DNA (Li et al., 2022). Our data demonstrate that after being imported into the nucleus under hypertonicity, NFAT5 still undergoes LLPS in the nucleus. Additionally, our preliminary EMSA data suggest that NFAT5 N-terminal fragments without the DNA binding domain (RHD) bind to random DNA while undergoing LLPS. These findings imply that NFAT5 may increase its transcriptional efficiency via LLPS. Moreover, this possibility is bolstered by the fact that under hypertonic conditions, NFAT5 forms clusters in the nucleus and folds into chromatin domains to coordinate gene expression better. This behavior is similar to CTCF, which has been reported to undergo LLPS (Zhou et al., 2022). We also observe that reducing KPNB1 expression leads to the increased liquidity of condensed NFAT5 under hypertonic conditions. However, the mechanism underlying the effect of KPNB1 on the liquidity of condensed NFAT5 remains unclear. Further investigation is needed to elucidate the interplay between KPNB1 and NFAT5 LLPS.

Despite the fact that KPNB1 can break the LLPS of NFAT5, NFAT5 can still undergo LLPS under isotonic, hypotonic, and hypertonic conditions. Under the hypotonic condition, KPNB1 does not reduce NFAT5 LLPS, which enriches NFAT5 condensates in the cytoplasm. What is the factor in the interaction between KPNB1 and condensed NFAT5? To understand the regulation of this interaction, we need to

investigate the nuclear export mechanism of NFAT5, which is currently unknown. Once we establish the nuclear export mechanism, we can explore how it relates to the LLPS of NFAT5.

References

- Baade, I., Hutten, S., Sternburg, E. L., Pörschke, M., Hofweber, M., Dormann, D., & Kehlenbach, R. H. (2021). The RNA-binding protein FUS is chaperoned and imported into the nucleus by a network of import receptors. *Journal of biological chemistry*, 296, 100659. https://doi.org/https://doi.org/10.1016/j.jbc.2021.100659
- Boehning, M., Dugast-Darzacq, C., Rankovic, M., Hansen, A., Yu, T., Marie-Nelly, H., McSwiggen, D., Kokic, G., Dailey, G., & Cramer, P. RNA polymerase II clustering through CTD phase separation.
- Boija, A., Klein, I. A., Sabari, B. R., Dall'Agnese, A., Coffey, E. L., Zamudio, A. V., Li, C. H., Shrinivas, K., Manteiga, J. C., Hannett, N. M., Abraham, B. J., Afeyan, L. K., Guo, Y. E., Rimel, J. K., Fant, C. B., Schuijers, J., Lee, T. I., Taatjes, D. J., & Young, R. A. (2018). Transcription Factors Activate Genes through the Phase-Separation Capacity of Their Activation Domains. *Cell*, 175(7), 1842-1855.e1816. https://doi.org/10.1016/j.cell.2018.10.042
- Burg, M. B., Ferraris, J. D., & Dmitrieva, N. I. (2007). Cellular response to hyperosmotic stresses. *Physiological reviews*, 87(4), 1441-1474.
- Burg, M. B., Kwon, E. D., & KÜltz, D. (1997). REGULATION OF GENE EXPRESSION BY HYPERTONICITY. *Annual Review of Physiology*, 59(1), 437-455. https://doi.org/10.1146/annurev.physiol.59.1.437
- Cavazza, T., & Vernos, I. (2016). The RanGTP Pathway: From Nucleo-Cytoplasmic Transport to Spindle Assembly and Beyond [Mini Review]. *Frontiers in Cell and Developmental Biology*, 3. https://doi.org/10.3389/fcell.2015.00082
- Celetti, G., Paci, G., Caria, J., VanDelinder, V., Bachand, G., & Lemke, E. A. (2019). The liquid state of FG-nucleoporins mimics permeability barrier properties of nuclear pore complexes. *Journal of Cell Biology*, 219(1). https://doi.org/10.1083/jcb.201907157
- Chen, W.-S., Chen, Y.-J., Huang, Y.-A., Hsieh, B.-Y., Chiu, H.-C., Kao, P.-Y., Chao, C.-Y., & Hwang, E. (2017). Ran-dependent TPX2 activation promotes acentrosomal microtubule nucleation in neurons. *Scientific reports*, 7(1), 42297. https://doi.org/10.1038/srep42297
- Cheung, C. Y., & Ko, B. C. (2013). NFAT5 in cellular adaptation to hypertonic stress–regulations and functional significance. *Journal of molecular signaling*, 8(1), 1-9.
- Chong, P. A., & Forman-Kay, J. D. (2016). Liquid–liquid phase separation in cellular signaling systems. *Current opinion in structural biology*, 41, 180-186.
- Chook, Y. M., & Süel, K. E. (2011). Nuclear import by karyopherin-βs: Recognition and inhibition. Biochimica et Biophysica Acta (BBA) - Molecular Cell Research, 1813(9), 1593-1606. https://doi.org/https://doi.org/10.1016/j.bbamcr.2010.10.014
- Cingolani, G., Bednenko, J., Gillespie, M. T., & Gerace, L. (2002). Molecular basis for the recognition of a nonclassical nuclear localization signal by importin beta. *Mol Cell*, 10(6), 1345-1353. https://doi.org/10.1016/s1097-2765(02)00727-x
- Cingolani, G., Petosa, C., Weis, K., & Müller, C. W. (1999). Structure of importin-β bound to the IBB domain of importin-α. *Nature*, *399*(6733), 221-229.
- Cook, A., Bono, F., Jinek, M., & Conti, E. (2007). Structural biology of nucleocytoplasmic transport. *Annu. Rev. Biochem.*, 76, 647-671.

- Copp, J., Wiley, S., Ward, M. W., & van der Geer, P. (2005). Hypertonic shock inhibits growth factor receptor signaling, induces caspase-3 activation, and causes reversible fragmentation of the mitochondrial network. *Am J Physiol Cell Physiol*, 288(2), C403-415. https://doi.org/10.1152/ajpcell.00095.2004
- Desai, B. N., Myers, B. R., & Schreiber, S. L. (2002). FKBP12-rapamycin-associated protein associates with mitochondria and senses osmotic stress via mitochondrial dysfunction. *Proceedings of the National Academy of Sciences*, 99(7), 4319-4324.
- Di Ciano, C., Nie, Z., Szászi, K., Lewis, A., Uruno, T., Zhan, X., Rotstein, O. D., Mak, A., & Kapus, A. (2002). Osmotic stress-induced remodeling of the cortical cytoskeleton. *American Journal of Physiology-Cell Physiology*, 283(3), C850-C865.
- Dmitrieva, N. I., Cai, Q., & Burg, M. B. (2004). Cells adapted to high NaCl have many DNA breaks and impaired DNA repair both in cell culture and in vivo. *Proceedings of the National Academy of Sciences*, 101(8), 2317-2322.
- Dmitrieva, N. I., Michea, L. F., Rocha, G. M., & Burg, M. B. (2001). Cell cycle delay and apoptosis in response to osmotic stress. *Comparative Biochemistry and Physiology Part A: Molecular & Integrative Physiology*, 130(3), 411-420.
- Dustin, M. L., & Muller, J. (2016). Liquidity in immune cell signaling. Science, 352(6285), 516-517.
- Forwood, J. K., & Jans, D. A. (2002). Nuclear import pathway of the telomere elongation supressor TRF1: Inhibition by importin α. *Biochemistry*, 41(30), 9333-9340.
- Frey, S., & Görlich, D. (2009). FG/FxFG as well as GLFG repeats form a selective permeability barrier with self-healing properties. *The EMBO journal*, 28(17), 2554-2567. https://doi.org/https://doi.org/10.1038/emboj.2009.199
- Gallazzini, M., Heussler, G. E., Kunin, M., Izumi, Y., Burg, M. B., & Ferraris, J. D. (2011). High NaCl–induced activation of CDK5 increases phosphorylation of the osmoprotective transcription factor TonEBP/OREBP at threonine 135, which contributes to its rapid nuclear localization. *Molecular biology of the cell*, 22(5), 703-714. https://doi.org/10.1091/mbc.e10-08-0681
- Gallazzini, M., Yu, M.-J., Gunaratne, R., Burg, M. B., & Ferraris, J. D. (2010). c-Abl mediates high NaCl-induced phosphorylation and activation of the transcription factor TonEBP/OREBP. *The FASEB Journal*, *24*(11), 4325-4335. https://doi.org/https://doi.org/10.1096/fj.10-157362
- Garcia-Perez, A., & Burg, M. B. (1991). Renal medullary organic osmolytes. *Physiological reviews*, 71(4), 1081-1115.
- Gonzalez, A., Mannen, T., Çağatay, T., Fujiwara, A., Matsumura, H., Niesman, A. B., Brautigam, C. A., Chook, Y. M., & Yoshizawa, T. (2021). Mechanism of karyopherin-β2 binding and nuclear import of ALS variants FUS(P525L) and FUS(R495X). *Scientific reports*, 11(1), 3754. https://doi.org/10.1038/s41598-021-83196-y
- Guo, L., Kim, H. J., Wang, H., Monaghan, J., Freyermuth, F., Sung, J. C., O'Donovan, K., Fare, C. M., Diaz, Z., Singh, N., Zhang, Z. C., Coughlin, M., Sweeny, E. A., DeSantis, M. E., Jackrel, M. E., Rodell, C. B., Burdick, J. A., King, O. D., Gitler, A. D., . . . Shorter, J. (2018). Nuclear-Import Receptors Reverse Aberrant Phase Transitions of RNA-Binding Proteins with Prion-like Domains. *Cell*, 173(3), 677-692.e620. https://doi.org/10.1016/j.cell.2018.03.002
- Harel, A., & Forbes, D. J. (2004). Importin beta: conducting a much larger cellular symphony. *Molecular cell*, 16(3), 319-330.
- Harreman, M. T., Hodel, M. R., Fanara, P., Hodel, A. E., & Corbett, A. H. (2003). The auto-inhibitory function of importin α is essentialin vivo. *Journal of biological chemistry*, 278(8), 5854-5863.

- Hoelz, A., Debler, E. W., & Blobel, G. (2011). The Structure of the Nuclear Pore Complex. *Annual Review of Biochemistry*, 80(1), 613-643. https://doi.org/10.1146/annurev-biochem-060109-151030
- Hoffmann, E. K., Lambert, I. H., & Pedersen, S. F. (2009). Physiology of cell volume regulation in vertebrates. *Physiological reviews*, 89(1), 193-277.
- Hogan, P. G., Chen, L., Nardone, J., & Rao, A. (2003). Transcriptional regulation by calcium, calcineurin, and NFAT. *Genes & development*, 17(18), 2205-2232.
- Irarrazabal, C. E., Gallazzini, M., Schnetz, M. P., Kunin, M., Simons, B. L., Williams, C. K., Burg, M. B., & Ferraris, J. D. (2010). Phospholipase C-gamma1 is involved in signaling the activation by high NaCl of the osmoprotective transcription factor TonEBP/OREBP. *Proc Natl Acad Sci U S A*, 107(2), 906-911. https://doi.org/10.1073/pnas.0913415107
- Irarrazabal, C. E., Liu, J. C., Burg, M. B., & Ferraris, J. D. (2004). ATM, a DNA damage-inducible kinase, contributes to activation by high NaCl of the transcription factor TonEBP/OREBP. *Proceedings of the National Academy of Sciences*, 101(23), 8809-8814.
- Ivic, N., Potocnjak, M., Solis-Mezarino, V., Herzog, F., Bilokapic, S., & Halic, M. (2019). Fuzzy Interactions Form and Shape the Histone Transport Complex. *Mol Cell*, 73(6), 1191-1203.e1196. https://doi.org/10.1016/j.molcel.2019.01.032
- Kalderon, D., Richardson, W. D., Markham, A. F., & Smith, A. E. (1984). Sequence requirements for nuclear location of simian virus 40 large-T antigen. *Nature*, 311(5981), 33-38.
- Kosugi, S., Hasebe, M., Entani, T., Takayama, S., Tomita, M., & Yanagawa, H. (2008). Design of Peptide Inhibitors for the Importin α/β Nuclear Import Pathway by Activity-Based Profiling. *Chemistry & biology*, 15(9), 940-949. https://doi.org/https://doi.org/10.1016/j.chembiol.2008.07.019
- Kumar, R., DuMond, J. F., Khan, S. H., Thompson, E. B., He, Y., Burg, M. B., & Ferraris, J. D. (2020). NFAT5, which protects against hypertonicity, is activated by that stress via structuring of its intrinsically disordered domain. *Proceedings of the National Academy of Sciences*, 117(33), 20292-20297. https://doi.org/doi:10.1073/pnas.1911680117
- Kutay, U., Izaurralde, E., Bischoff, F. R., Mattaj, I. W., & Görlich, D. (1997). Dominant-negative mutants of importin-β block multiple pathways of import and export through the nuclear pore complex. *The EMBO journal*, 16(6), 1153-1163. https://doi.org/https://doi.org/10.1093/emboj/16.6.1153
- Lang, F., Busch, G. L., Ritter, M., Volkl, H., Waldegger, S., Gulbins, E., & Haussinger, D. (1998). Functional significance of cell volume regulatory mechanisms. *Physiological reviews*, 78(1), 247-306.
- Li, Y., Chen, L., Han, Z., Na, J., Wang, R., Jing, T., & Zhao, B. (2022). Exploring the effects of mutations on NFAT5-DNA binding using molecular dynamics simulations and energy calculations. *International Journal of Quantum Chemistry*, 122(21), e26980. https://doi.org/https://doi.org/10.1002/qua.26980
- Macara, I. G. (2001). Transport into and out of the nucleus. *Microbiol Mol Biol Rev*, 65(4), 570-594, table of contents. https://doi.org/10.1128/mmbr.65.4.570-594.2001
- Matsuura, Y. (2016). Mechanistic Insights from Structural Analyses of Ran-GTPase-Driven Nuclear Export of Proteins and RNAs. *Journal of Molecular Biology*, 428(10, Part A), 2025-2039. https://doi.org/https://doi.org/10.1016/j.jmb.2015.09.025
- Mitrousis, G., Olia, A. S., Walker-Kopp, N., & Cingolani, G. (2008). Molecular basis for the recognition of snurportin 1 by importin beta. *J Biol Chem*, 283(12), 7877-7884. https://doi.org/10.1074/jbc.M709093200

- Molliex, A., Temirov, J., Lee, J., Coughlin, M., Kanagaraj, A. P., Kim, H. J., Mittag, T., & Taylor, J. P. (2015). Phase separation by low complexity domains promotes stress granule assembly and drives pathological fibrillization. *Cell*, *163*(1), 123-133.
- Morley, S. J., & Naegele, S. (2002). Phosphorylation of eukaryotic initiation factor (eIF) 4E is not required for de novo protein synthesis following recovery from hypertonic stress in human kidney cells. *Journal of biological chemistry*, 277(36), 32855-32859.
- Nagoshi, E., Imamoto, N., Sato, R., & Yoneda, Y. (1999). Nuclear Import of Sterol Regulatory Element–binding Protein-2, a Basic Helix-Loop-Helix–Leucine Zipper (bHLH-Zip)–containing Transcription Factor, Occurs through the Direct Interaction of Importin β with HLH-Zip. *Molecular biology of the cell*, 10(7), 2221-2233.
- Ni, S.-H., Sun, S.-N., Zhou, Z., Li, Y., Huang, Y.-S., Li, H., Wang, J.-J., Xiao, W., Xian, S.-X., Yang, Z.-Q., Wang, L.-J., & Lu, L. (2020). Arctigenin alleviates myocardial infarction injury through inhibition of the NFAT5-related inflammatory phenotype of cardiac macrophages/monocytes in mice. *Laboratory Investigation*, 100(4), 527-541. https://doi.org/10.1038/s41374-019-0340-8
- Odeh, H. M., Fare, C. M., & Shorter, J. (2022). Nuclear-Import Receptors Counter Deleterious Phase Transitions in Neurodegenerative Disease. *J Mol Biol*, 434(1), 167220. https://doi.org/10.1016/j.jmb.2021.167220
- Palmeri, D., & Malim, M. H. (1999). Importin β can mediate the nuclear import of an arginine-rich nuclear localization signal in the absence of importin α . *Molecular and Cellular Biology*, 19(2), 1218-1225.
- Pumroy, R. A., Nardozzi, J. D., Hart, D. J., Root, M. J., & Cingolani, G. (2012). Nucleoporin Nup50 stabilizes closed conformation of armadillo repeat 10 in importin α5. *J Biol Chem*, 287(3), 2022-2031. https://doi.org/10.1074/jbc.M111.315838
- Qin, X., Li, C., Guo, T., Chen, J., Wang, H.-T., Wang, Y.-T., Xiao, Y.-S., Li, J., Liu, P., Liu, Z.-S., & Liu, Q.-Y. (2017). Upregulation of DARS2 by HBV promotes hepatocarcinogenesis through the miR-30e-5p/MAPK/NFAT5 pathway. *Journal of Experimental & Clinical Cancer Research*, 36(1), 148. https://doi.org/10.1186/s13046-017-0618-x
- Renault, L., Nassar, N., Vetter, I., Becker, J., Klebe, C., Roth, M., & Wittinghofer, A. (1998). The 1.7 Å crystal structure of the regulator of chromosome condensation (RCC1) reveals a seven-bladed propeller. *Nature*, 392(6671), 97-101. https://doi.org/10.1038/32204
- Robbins, J., Dilwortht, S. M., Laskey, R. A., & Dingwall, C. (1991). Two interdependent basic domains in nucleoplasmin nuclear targeting sequence: identification of a class of bipartite nuclear targeting sequence. *Cell*, 64(3), 615-623.
- Rollenhagen, C., Mühlhäusser, P., Kutay, U., & Panté, N. (2003). Importin beta-depending nuclear import pathways: role of the adapter proteins in the docking and releasing steps. *Mol Biol Cell*, *14*(5), 2104-2115. https://doi.org/10.1091/mbc.e02-06-0372
- Soniat, M., & Chook, Y. M. (2015). Nuclear localization signals for four distinct karyopherin-β nuclear import systems. *Biochemical Journal*, 468(3), 353-362.
- Soniat, M., & Chook, Yuh M. (2016). Karyopherin-β2 Recognition of a PY-NLS Variant that Lacks the Proline-Tyrosine Motif. *Structure*, 24(10), 1802-1809. https://doi.org/https://doi.org/10.1016/j.str.2016.07.018
- Su, Q., Mehta, S., & Zhang, J. (2021). Liquid-liquid phase separation: Orchestrating cell signaling through time and space. *Molecular cell*, 81(20), 4137-4146. https://doi.org/https://doi.org/10.1016/j.molcel.2021.09.010

- Su, X., Ditlev, J. A., Hui, E., Xing, W., Banjade, S., Okrut, J., King, D. S., Taunton, J., Rosen, M. K., & Vale, R. D. (2016). Phase separation of signaling molecules promotes T cell receptor signal transduction. *Science*, *352*(6285), 595-599.
- Theodore, M., Kawai, Y., Yang, J., Kleshchenko, Y., Reddy, S. P., Villalta, F., & Arinze, I. J. (2008). Multiple nuclear localization signals function in the nuclear import of the transcription factor Nrf2. *J Biol Chem*, 283(14), 8984-8994. https://doi.org/10.1074/jbc.M709040200
- Tong, E. H. Y., Guo, J.-J., Huang, A.-L., Liu, H., Hu, C.-D., Chung, S. S. M., & Ko, B. C. B. (2006).
 Regulation of Nucleocytoplasmic Trafficking of Transcription Factor OREBP/TonEBP/NFAT5
 *. Journal of biological chemistry, 281(33), 23870-23879.
 https://doi.org/10.1074/jbc.M602556200
- Vetter, I. R., Arndt, A., Kutay, U., Görlich, D., & Wittinghofer, A. (1999). Structural view of the Ran–importin β interaction at 2.3 Å resolution. *Cell*, 97(5), 635-646.
- Wing, C. E., Fung, H. Y. J., & Chook, Y. M. (2022). Karyopherin-mediated nucleocytoplasmic transport.

 Nature Reviews Molecular Cell Biology, 23(5), 307-328. https://doi.org/10.1038/s41580-021-00446-7
- Wippich, F., Bodenmiller, B., Trajkovska, M. G., Wanka, S., Aebersold, R., & Pelkmans, L. (2013). Dual specificity kinase DYRK3 couples stress granule condensation/dissolution to mTORC1 signaling. *Cell*, 152(4), 791-805.
- Xu, S., Wong, C. C., Tong, E. H., Chung, S. S., Yates, J. R., 3rd, Yin, Y., & Ko, B. C. (2008). Phosphorylation by casein kinase 1 regulates tonicity-induced osmotic response element-binding protein/tonicity enhancer-binding protein nucleocytoplasmic trafficking. *J Biol Chem*, 283(25), 17624-17634. https://doi.org/10.1074/jbc.M800281200
- Yancey, P. H., Clark, M. E., Hand, S. C., Bowlus, R. D., & Somero, G. N. (1982). Living with water stress: evolution of osmolyte systems. *Science*, 217(4566), 1214-1222.
- Yoshizawa, T., Ali, R., Jiou, J., Fung, H. Y. J., Burke, K. A., Kim, S. J., Lin, Y., Peeples, W. B., Saltzberg, D., Soniat, M., Baumhardt, J. M., Oldenbourg, R., Sali, A., Fawzi, N. L., Rosen, M. K., & Chook, Y. M. (2018). Nuclear Import Receptor Inhibits Phase Separation of FUS through Binding to Multiple Sites. *Cell*, 173(3), 693-705.e622. https://doi.org/10.1016/j.cell.2018.03.003
- Yoshizawa, T., & Guo, L. (2021). Karyopherin-βs play a key role as a phase separation regulator. *J Biochem*, 170(1), 15-23. https://doi.org/10.1093/jb/mvab072
- Zhao, G., Aghakeshmiri, S., Chen, Y. T., Zhang, H. M., Yip, F., & Yang, D. (2021). NFAT5-Mediated Signalling Pathways in Viral Infection and Cardiovascular Dysfunction. *Int J Mol Sci*, 22(9). https://doi.org/10.3390/ijms22094872
- Zhou, R., Tian, K., Huang, J., Duan, W., Fu, H., Feng, Y., Wang, H., Jiang, Y., Li, Y., Wang, R., Hu, J., Ma, H., Qi, Z., & Ji, X. (2022). CTCF DNA-binding domain undergoes dynamic and selective protein–protein interactions. *iScience*, *25*(9), 105011. https://doi.org/https://doi.org/10.1016/j.isci.2022.105011
- Zhou, X. (2016). How do kinases contribute to tonicity-dependent regulation of the transcription factor NFAT5? *World J Nephrol*, 5(1), 20-32. https://doi.org/10.5527/wjn.v5.i1.20
- Zhou, X., Gallazzini, M., Burg, M. B., & Ferraris, J. D. (2010). Contribution of SHP-1 protein tyrosine phosphatase to osmotic regulation of the transcription factor TonEBP/OREBP. *Proceedings of the National Academy of Sciences*, 107(15), 7072-7077. https://doi.org/doi:10.1073/pnas.1002795107